This is to certify that the

dissertation entitled

TOWARD AN "INTERRUPTED σ-BOND":
ION BINDING STUDIES OF DIA- AND PARAMAGNETIC
TRIARYLPROPELLER IONOPHORES

presented by

Scott J. Stoudt

has been accepted towards fulfillment
of the requirements for

Ph.D. degree in Chemistry

Major professor

Date 17 Aug, 1995

TOWARD AN "INTERRUPTED σ-BOND": ION BINDING STUDIES OF DIA- AND PARAMAGNETIC TRIARYLPROPELLER IONOPHORES

By

Scott J. Stoudt

A DISSERTATION

Submitted to
Michigan State University
in partial fulfillment of the requirements
for the degree of

DOCTOR OF PHILOSOPHY

Department of Chemistry

1995

ABSTRACT

TOWARD AN "INTERRUPTED σ-BOND":
ION BINDING STUDIES OF DIA- AND PARAMAGNETIC
TRIARYLPROPELLER IONOPHORES

By

Scott J. Stoudt

The ion binding properties of tris(2-methoxyphenyl)-Z (Z = $C^{\bullet}$, N) propellers and a related triarylborane (Z = B) species were probed to gain an understanding of the relationship between structure and magnetic coupling within pairs of these subunits. To promote pairing of the ligands about a metal ion, two triarylamine moieties were tethered to make a covalently-linked diamine complexant. Studies of the free diamagnetic ligands and their metal complexes, using NMR, X-ray crystallography, ESR, and computational methods, provided detailed information on stoichiometries, energetics, and geometrical nature of metal ion binding by these systems. Although the studies validated the ion binding strategy for self-assembly of these triarylpropeller ionophores, ESR investigations failed to reveal evidence of ion binding by tris(2-methoxyphenyl)methyl radical or a biradical analogue.

To my parents

TABLE OF CONTENTS

LIST OF TABLES

Table

LIST OF FIGURES

Figure

CHAPTER 1

INTRODUCTION

The research described herein is motivated by the challenge of designing organic magnetic materials. Our strategy is to "turn on" magnetic interactions between simple organic paramagnets with the structurally well-defined relationships enforced by metal ion complexation. Ultimately, extended chains of organic radicals strung together via metal ions offer the possibility of a designed molecular solid with unique magnetic properties.

In order to design extended systems of interacting subunits, it is desirable to examine the behaviors of the individual subunits, and their simple pairwise interactions, to gain an understanding of the relationship between structure and magnetic interactions within pairs of simple paramagnets. Given two weakly interacting electrons, one ultimately needs to know which forces favor the low-spin singlet state and which favor the much rarer high-spin coupled triplet state, which promises the most interesting magnetic behaviors. By designing dia- and paramagnetic molecular models of substructures within the potential extended system, it is possible to individually characterize the structural and magnetic coupling components of the system.

This thesis deals with spectroscopic and structural studies of ion binding by dia- and paramagnetic triarylpropeller ionophores. Because of the highly interdisciplinary nature of the project, I shall begin Chapter 1 by introducing the concepts of self-assembly and pairwise electron coupling; these two overviews, respectively, are primarily based on reviews by Lindsey[1] and Rajca.[2] Detailed rationale and description of the project are presented at the end of Chapter 1. The use of metal ion complexation to assemble triarylpropeller ligands requires a detailed description of the ion

binding properties of the triarylpropeller framework. Chapters 2 and 3 describe studies of ion binding by diamagnetic systems; this work is extended in Chapter 4 to paramagnetic triarylpropeller ligands. Lastly, Chapter 5 provides detailed information on experimental procedures.

1.1. Self-Assembly

Self-assembly is the spontaneous formation of a well-defined, higher-ordered structure from a given set of components under specific conditions. The term "self-assembly" is often used loosely in the literature; for use in a strict sense, the assembly process must be reversible and the product stable at thermodynamic equilibrium. All information for assembly is contained within the subunits or precursor molecules, and neither additional factors nor energy input are required for assembly to occur.[1] The self-assembly of a given architecture involves three stages: *recognition* between the components, correct *orientation* so as to allow growth, and *termination* of the process leading to a discrete, finite species.[3] In this dissertation, the term self-assembly is viewed as applying only to those processes, as defined above, in which *three or more* separate components are brought together through multiple molecular recognition events.

Many components of biological systems contain the information for their own assembly. From a structural vantage point, formation of specific three-dimensional objects occurs because only those molecules having the correct positioning of functional groups can fit together to form the maximum number of bonding interactions.[4] Biological assembly not only affords a level of specificity and architectural control without parallel in

chemical synthesis, but does so with great efficiency under ambient conditions. Well-known examples of self-assembling biological systems include oligomers of DNA, microtubules,[5] and tobacco mosaic virus.[6] The self-assembly of the latter system from RNA and protein subunits is portrayed in Figure 1.1.

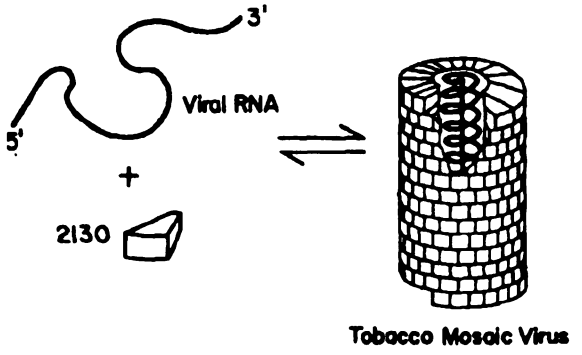

Figure 1.1. Self-assembly of tobacco mosaic virus. Reproduced with permission from ref 1. Copyright 1991 Gauthier-Villars.

Although the concepts of self-assembly are rooted in biology, they are also found in chemistry. For example, crystallization of molecular solids is self-assembly practiced by chemists on a daily basis. Crystal formation involves rapid and efficient generation of highly structured entities under a wide variety of conditions, and gives rise to assemblies having long-range three-dimensional order. Since the molecular packing patterns are determined by noncovalent, intermolecular interactions, one can view the process of crystal formation as a molecular recognition process at the surface of the crystal; repeated recognition events involving subsequent molecules ultimately gives an ordered solid. Crystallization thus provides a useful precedent for contemplating the use of self-assembly in materials chemistry.

Constructing complex structures via self-assembly processes, rather than by tedious bond-by-bond syntheses, is certainly an attractive idea. But beyond "mere" self-assembly lies the prospect of *designed self-assembly*—fitting molecules together in an arrangement predetermined by the chemist. When applied to the design of molecular solids, this is referred to as crystal engineering. The ability to predict crystal structure based on molecular structure would be invaluable for designing crystals that exhibit nonlinear optical properties,[7] electrical conductivity,[8] or ferromagnetic behavior.[9] Each of these solid-state properties is influenced by solid-state structure: the component molecules must have both the requisite molecular structure and the correct orientation with respect to one another in the crystal lattice.[10]

Rational control and predictability of molecular self-assembly processes are critical for directed crystal engineering, but control of molecular orientation in supramolecular structure is difficult and is recognized as a major obstacle in materials design. The problem lies in the weakness of intermolecular forces, which do not always align molecules in their equilibrium positions before they are trapped in the growing solid phase. Attempts at crystal engineering have explored such forces as charge-transfer,[8a] electrostatic,[8d,e] and halogen•••halogen[11] interactions, but hydrogen bonds have been the most utilized.

Considerable effort has been devoted to the study of molecular association via hydrogen bonds in solution, especially for cases involving the formation of dimeric species.[12] This important work has delineated some of the fundamental features of molecular recognition, and has demonstrated

that a full appreciation of the recognition properties of the individual components is needed to predict the shapes of larger aggregates.

Hydrogen bonds are moderately strong (1–5 kcal/mol) and directional,[13] and are thus more likely to enforce orientation than charge-charge or van der Waals interactions. In solid-state studies, Etter,[14] Leiserowitz,[15] Taylor and Kennard,[16] and others[17] have systematically characterized hydrogen bonding interactions and hydrogen bonding patterns occurring commonly between specific functional groups.

Work benefitting from the studies above has shown that complementary components can be brought together to create solid-state superstructures exhibiting desirable properties. Of particular interest is Veciana's use of hydrogen bonding in appropriately substituted nitronyl nitroxide radicals to obtain molecular solids with high dimensional organization.[18] Moreover, this fundamental work shows that hydrogen bonding between open-shell molecules can be used to prepare solids exhibiting ferromagnetic behavior. Finally, a wonderful example of designed self-assembly was reported by Wuest. Self-assembly of a rigid tetrapyridone produces a dimondoid network with large chambers, as illustrated in Figure 1.2. This network selectively enclathrates guest molecules present during crystallization.[19] The use of tetrahedrally disposed pyridones to control molecular aggregation is particularly elegant since Wuest *predicted* the three-dimensional structure based on knowledge of the hydrogen-bonding motifs preferred by dipyridones.

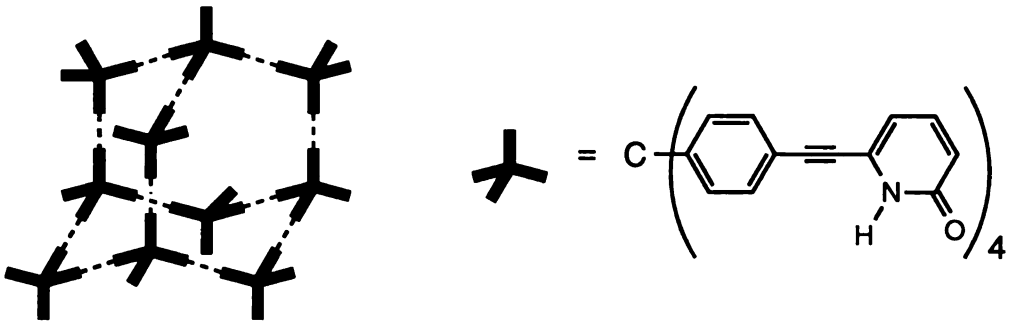

Figure 1.2. A schematic drawing of the three-dimensional dimondoid network of hydrogen bonds formed by a rigid tetrapyridone host. Adapted from ref 17c.

Coordinate bonds involving metal ions and organic ligands have been used in the self-assembly of inorganic superstructures. As with other molecular recognition processes, multiple binding sites are usually required for structural recognition since binding energies at any one site are small compared to those provided by covalent bonds. More data are available concerning the roles of bonding and structure (ring size, number of rings, steric factors, ligand basicity, etc.) in determining the stabilities of metal chelates than for any other self-assembling system.[20]

Crown ethers[21] and especially their three-dimensional cryptand[22] or spherand-type[23] derivatives have been developed to an extraordinary degree of refinement for the selective binding of metal ions. The hydrophilic, electronegative cavities of these ligands are ideally suited for complexation of alkali metal and alkaline earth metal cations according to their size.[24] The relationship between ligand cavity and cation radius is readily apparent in the crystal structures of crown ether complexes. The structure of a classical crown ether complex is typified by the symmetrical array of oxygen atoms.

These atoms contact the cation which lies exactly in the center of the ring, as seen in the structure of the 18-crown-6•KSCN complex[25] (Figure 1.3a). Self-assembly of crown ether complexes may result from a drastic size discrepancy between the cavity and the metal ion, as illustrated in Figures 1.3b and 1.3c. In cases where the metal ion is too big to fit in the cavity, *sandwich* complexes of 2:1 stoichiometry are formed, as found for [12-crown-4]$_2$•NaCl•5H_2O,[26] [12-crown-4]$_2$•NaOH•8H_2O,[27] [15-crown-5]$_2$•$BaBr_2$•2H_2O.[28] and [benzo-15-crown-5]$_2$•KI.[29] When the metal ion is too small to fill the cavity, binuclear metal complexes of 1:2 stoichiometry can be formed. Examples include dibenzo-24-crown-8•2Na(*o*-dinitrophenolate),[30] dibenzo-24-crown-8•2KSCN,[31] dibenzo-30-crown-10•2NaSCN,[32] and numerous complexes of transition metal ions with bis-chelating macromonocyclic ligands.[33]

It should be emphasized that although the cavity-metal ion size relationship is significant, it is a gross oversimplification to attribute all ion binding specificity to this factor alone. Many factors influence the self-assembly of a complex and its resulting structure, including ligand substituents and topology, choice of solvent, and the anion involved. Infrared spectroscopic studies have revealed that benzo-15-crown-5 forms a sandwich complex with Na^+ (which could smoothly fit into the cavity), if the anion is BPh_4^-.[34] Evidently this is due to the inability of the anion to provide donor atoms for the Na^+ ion which thus requires a second crown for sufficient coordination.

Macropolycyclic ligands possessing binding sites for several metal ions also may self-assemble to generate inorganic superstructures. Binuclear

transition metal complexes with macrobicyclic cryptands[35] and cylindrical macrotricycles[36] have been described.[37]

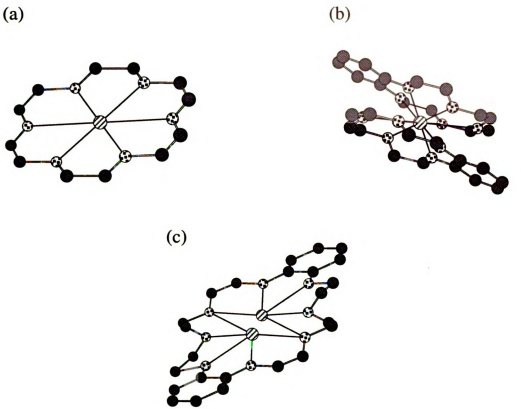

Figure 1.3. Illustration of various cation/ligand arrangements in crystalline crown ether complexes: (a) 18-crown-6•KSCN;[25] (b) [benzo-15-crown-5]$_2$•KI;[29] and (c) dibenzo-24-crown-8•2KSCN.[31] X-ray coordinates were obtained from the Cambridge Structural Database.

The ordering of metal ions and organic ligands into defined arrays presents intriguing prospects for the development of molecular materials and devices.[38] To this end, the controlled generation of novel types of arrays is of utmost interest. In these self-assembly processes, the ligands must contain the steric program that is "read" by the metal ions following the "algorithm" represented by their coordination geometry.[3] A beautiful demonstration of

this concept is provided by self-assembling inorganic helices. Addition of Cu(I) ions to ligand strands consisting of three bipyridine units results in the spontaneous assembly the double-stranded helicate, as illustrated in Figure 1.4. In the complex, two ligand strands are wrapped around each other with three Cu(I) ions holding them together.[39] The double-helix structure results from the tetrahedral-like coordination imposed by each $Cu(bpy)_2^+$ site, and from the design of the ligand which disfavors binding to only one strand. These two features make up, respectively, the recognition process (the "algorithm") and the molecular steric "program" that leads to preferential formation of the double-helical structures. Of particular interest is that binding of one metal ion facilitates the binding of subsequent ions (positive cooperativity),[39] and that a given ligand forms a double-helix preferentially with an identical strand if a mixture of ligands is used (self-recognition).[39] Constable and coworkers have shown that double-helical structures are formed when the metal ion is too small for the cavity in the planar (bipyridine) ligand configuration, and that π-stacking interactions play a critical role in the stability of the double-helical geometry.[40]

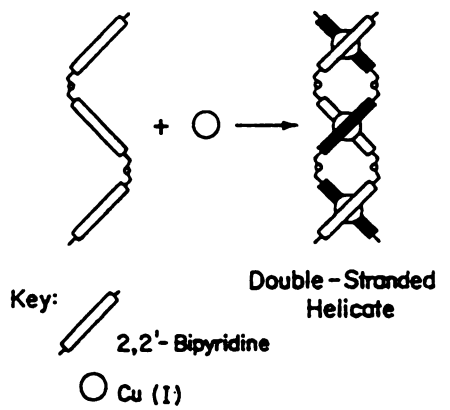

Figure 1.4. Self-assembly of a double-stranded helicate. Reproduced with permission from ref 1. Copyright 1991 Gauthier-Villars.

Using suitably designed ligands and selected metal ions, the self-assembly of several types of architectures has been described for double[38,41] and triple[42] helical complexes, as well as circular,[3] capped,[43] cylindrical,[3] grid-like,[44] and rack-type[45] multi-component species. An important aspect of this work is that inorganic superstructures can indeed be generated on the basis of the structural design envisioned by the chemist.

From a coordination chemistry perspective, helicates are polynuclear complexes containing a string of metal ions. Although these systems exhibit all of the essential features of a strict self-assembly process, a disadvantage is that the size of the architecture formed depends on the size of the oligobipyridine strand, the length of which is dictated by covalent bonds. A more practical approach to materials involves the use of multidentate ligands and appropriate metal ions to generate coordination polymers, where coordinate bonds are responsible for both the assembly process and the size of the superstructure. This kind of approach has been applied to the preparation of conducting materials, albeit with varied success. Metal derivatives of 1,5-diformyl-2,6-dihydroxynaphthalene[46] are reported to have conductivities on the order of 10^{-2} (ohm cm)$^{-1}$, but these are exceptional cases. Recently, Fox et al. have investigated the effect of perturbed ligand structure on the stability of several possible redox levels accessible to nickel-phosphine complexes.[47] Their studies involving mono- and bimetallic model complexes **1** and **2** ultimately led to the preparation of a semiconductive coordination polymer **3** from 1,2,4,5-tetrakis(dimethylphosphino)benzene and $NiCl_2 \cdot 6H_2O$.[48]

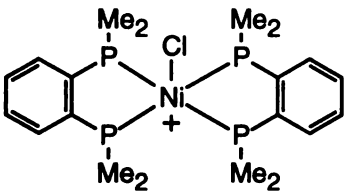

1

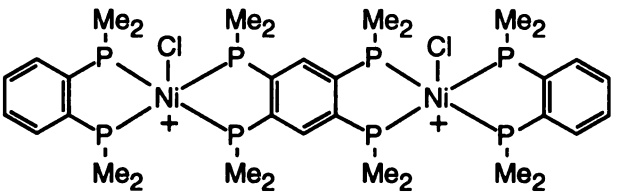

2

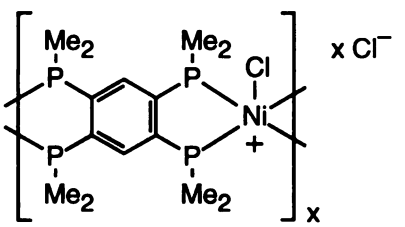

3

1.2. Electron Spin Coupling: The Pairwise Interaction

A pair of electrons can couple to give a total spin (S) of either $S = 0$ ("antiparallel spins") or $S = 1$ ("parallel spins"). These spin values correspond to singlet and triplet spin states, respectively, and reference can be made to either antiferromagnetic ($S = 0$) or ferromagnetic ($S = 1$) spin coupling. The energy difference between the two spin states (ΔE_{ST}) measures the strength of the coupling (neglecting spin-orbit coupling). In a sense, antiferromagnetic coupling may be considered as a weak chemical bond, with ΔE_{ST} being a measure of the bond strength. The challenge is to achieve and understand ferromagnetic coupling, which is antithetical to bonding.

In considering the simple case of pairwise electron coupling, a question that arises is: What factors dictate the preference for one spin state

over the other? To answer this question requires explicit consideration of the effects of electron repulsion.

Because electrons are indistinguishable, the Pauli principle requires that the wave function for an atom or a molecule must be antisymmetric to electron interchange. The determinantal wave function that ensures this antisymmetry gives rise to two types of two-electron integrals.[49] The first is the Coulomb integral (J_{ab}); it is the electrostatic repulsion between two electrons in orbitals a and b. The second is the exchange integral (K_{ab}), an interaction that has no classical analogue. It is defined as the energy of repulsion of the overlap charge density with an identical overlap charge density.[50] The physical interpretation is complicated, but essentially K_{ab} is a measure of the degree to which electrons in different orbitals "feel" each other's presence. Since this interaction is electrostatic in nature, K_{ab} is intrinsically positive. Its size depends on the compactness versus diffuseness of the overlap density, and on the value of the one-electron overlap integral (S_{ab}).[51] The ΔE_{ST} depends on K_{ab} and S_{ab}, as well as the one-electron energy difference between the two orbitals. The interplay of K_{ab} and S_{ab} in determining the lowest spin state is described below for examples in which the two electrons are in two degenerate (or nearly degenerate) orbitals.

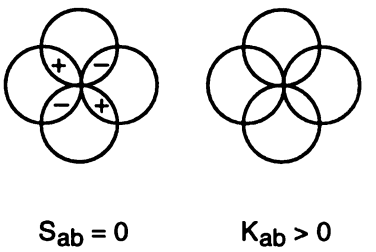

Figure 1.5. Orthogonal p-orbitals illustrating S_{ab} and K_{ab} regions.

The triplet ground state of atomic C results from ferromagnetic coupling of the two electrons in the half-occupied, orthogonal p-orbitals. In this case $S_{ab} = 0$ because the regions of positive orbital overlap cancel the regions of negative overlap. However, the two p-orbitals are partially coextensive in space (as defined by the overlap density) and so cancellation of K_{ab} does not occur—its magnitude is quite substantial. Pictorial representations of S_{ab} and K_{ab} are presented in Figure 1.5. The driving force for ferromagnetic coupling of spins is the Pauli principle, which allows electrons of like spin to avoid each other and therefore minimize electron repulsion. This is the physical significance of the K_{ab} term. Electrons of opposite spin (singlet state) are free to occupy the "exchange region" and therefore experience a greater destabilizing electron repulsion. In accord with Hund's rule, the triplet state is thus lower in energy than the singlet.

When $S_{ab} \neq 0$, it usually becomes the dominant term in determining spin orientations, leading to spin pairing. For H_2 the singlet is the ground state, even at very large internuclear distances where one has an essentially degenerate pair of NBMOs. As the two orbitals get further apart, S_{ab} is greatly reduced. However, the K_{ab} term falls off more rapidly, approximately as $(S_{ab})^2$.[51] Since the orbitals share a decreasing region of overlap in which the Pauli principle can operate, the electrostatic advantage of parallel spin alignment is outweighed by the attractive interaction of the electron of one nucleus with the other nucleus, favoring the singlet state. This description of the bonding in H_2, which is based on MO theory, provides a reasonable picture of why the singlet is the ground state at small internuclear separations. However, it fails to predict that the singlet is preferred at large internuclear distances. The problem is that the MO wave

function is constructed by placing the pair of electrons in a σ-bonding orbital without considering the fact that the electrons would attempt to avoid each other (electron correlation). Consequently, the MO wave function tends to exaggerate the ionicity of H_2. This effect is significant at large distances where the atoms are essentially independent and should be described by separate, localized wave functions; in this situation the triplet is incorrectly predicted by MO theory to be the lowest spin state.

The fact that the singlet is the ground state for H_2 at all separations is better addressed by a valence bond (VB) description. The VB wave function is such that each electron in the electron-pair bond between the two hydrogen atoms tends to "reside" on its "own" atom. In considering electron interchange, the VB approach overemphasizes electron correlation, placing less weight (than the MO approach) on the ionic terms in the wave function. As a result, VB theory better describes H_2 at large separations where the *isolated* atoms provide an extreme case, whereas MO theory is better at small distances where the *combined* atoms provide the extreme case.

The preceding paragraphs have described the importance of electron repulsion in determining the state ordering in simple two-electron systems. Based on these considerations, a prescription for obtaining a triplet ground state is for the two electrons to occupy the same regions of space (i.e. substantial overlap density) but have a net overlap (overlap integral S_{ab}) near 0. An obvious strategy leading to ferromagnetic interaction between two spin carriers A and B is to arrange them so that the two SOMOs a and b are orthogonal (or nearly so).[52,53] Unfortunately, the orthogonality condition is difficult to impose on the SOMOs of neighboring molecules. Moreover, it is

not always sufficient to provide ferromagnetic interaction;[54] significant overlap density is required. Thus far, this approach has only been intentionally achieved by controlling the geometry through the use of bridges connecting the spin carriers, as described below.

Alternant hydrocarbons (AHs) are a class of molecules comprised of conjugated rings with even numbers of carbon atoms and linear conjugated chains. Compounds **4–8** are common examples of AHs. The connectivities of **4–6** make drawing Kekulé structures for these molecules imposible. This type of connectivity (called odd-alternant) for biradicals **4–6** gives rise to two degenerate, singly-occupied NBMOs. Conversely, Kekulé molecules **7** and **8** (called even-alternant) are closed-shell species and therefore do not possess NBMOs.

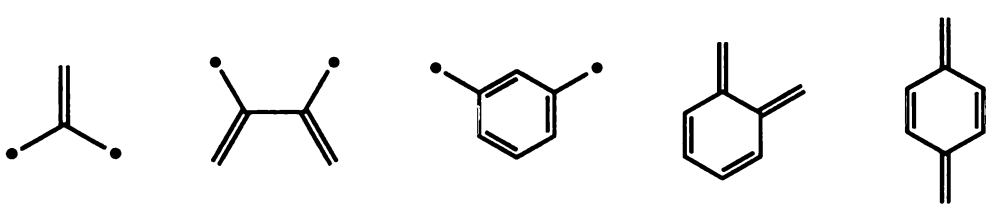

4 **5** **6** **7** **8**

In the case of odd-alternant systems, the half-filled NBMOs may be confined to separate atom sets in the molecule so they do not span any common atoms (disjoint MOs). In these systems the K_{ab} term, which corresponds to the simultaneous occupation of the same AO and destabilizes the singlet state, is insignificant. Consequently, the singlet and triplet states for a disjoint system are nearly degenerate. Thus, predictions for the lowest

energy state are problematic, as in the case of tetramethyleneethane (**5**).[55] On the other hand, the MOs may be orthogonal (so that $S_{ab} = 0$) and coincident at one or more atomic sites (non-disjoint MOs), resulting in strong ferromagnetic coupling (since K_{ab} is significant). The simplest and best studied non-disjoint AH is trimethylenemethane (**4**). Spectroscopic studies suggest a triplet ground state,[56] and ab initio calculations predict $\Delta E_{ST} \approx 15$ kcal/mol.[57] Compound **4** may be viewed as two methyl radicals connected to the same end of ethylene (1,1-connection). Alternatively, connecting two methyl radicals to opposite ends of ethylene gives butadiene, a closed-shell (Kekulé) molecule (and therefore a ground state singlet) with $\Delta E_{ST} = -74.3$ kcal/mol.[58] In a simplistic way, the ethylene moiety can be thought of as a ferromagnetic coupling unit (bridge) when 1,1-connected, and as an antiferromagnetic coupling unit when 1,2-connected. A large body of spectroscopic work indicates that *m*-benzoquinodimethane (**6**), a non-disjoint AH, has a triplet ground state[59]; ab initio calculations predict $\Delta E_{ST} \approx 10$ kcal/mol.[60] In contrast, its *o*-[61] and *p*-isomers[62] **7** and **8**, respectively, are closed-shell (Kekulé) molecules having singlet ground states. Thus a *meta*-connected benzene moiety is a ferromagnetic coupling unit, whereas *ortho*- and *para*-linked benzenes are antiferromagnetic couplers. The important observation here is that simple connectivities (bridges) that produce non-disjoint NBMOs give ferromagnetically coupled systems. In particular, *meta*-linkage of spin centers to a benzene ring has been realized as a powerful paradigm for designing and synthesizing high-spin molecules.[63]

One of the main drawbacks to biradicals such as **4** and **6** is their high reactivity and poor stability; neither of these molecules is isolable. To

prepare more robust biradicals, work has focused on linking stable monoradicals via a spin coupling unit. *Meta*-connection of two diphenylmethyl moieties to a benzene ring corresponds to the Schlenk hydrocarbon (**9**),[64] which is almost completely oligomerized at room temperature. Heating a solution of oligomerized **9**, followed by rapid cooling, gives an ESR signal at 77 K; Curie studies suggest that a minor species possesses a triplet ground state.[65] It is well-known that triphenylmethyl itself is highly associated in solution, dimerizing in a head-to-tail fashion to a methylenecyclohexadienylidene structure.[66] The use of suitably bulky substituents, especially at the positions *para* to the benzylic site, helps to improve the biradical's stability and limits (or prevents) association in solution.[67] Examples include biradicals **10–16**,[68] all of which give triplet ESR spectra in frozen solutions.

Spin centers can also be connected via multiple coupling units. Sequential linkage of *meta*-connected benzenes apparently leads to ferromagnetically coupled systems despite the disjoint nature of this connection. Weak ferromagnetic coupling is claimed in **17**[69]; ESR Curie studies on impure samples give $\Delta E_{ST} \approx 0.3$ kcal/mol. Biradical derivatives are also known that are based on sequential *para*-connection of benzene units. Ground state singlets are found for Thiele's hydrocarbon (**18**),[70] a close relative of **5**; Chichibabin's hydrocarbon (**19**);[70,71] and the Müller hydrocarbon (**20**).[72] It is important to point out that the lowest spin state is often difficult to predict in these "stretched out" systems since coupling is generally weak, and because structural or medium effects may be significant.[2,73]

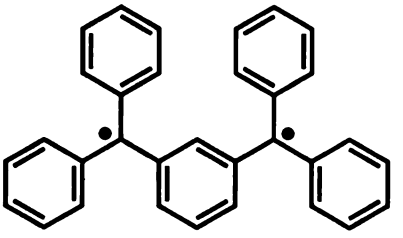

9

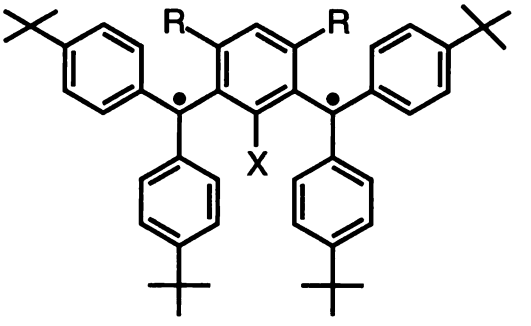

10 R = H, X = H
11 R = Me, X = H
12 R = *i*-Pr, X = H
13 R = Me, X = Me
14 R = CF_3, X = H

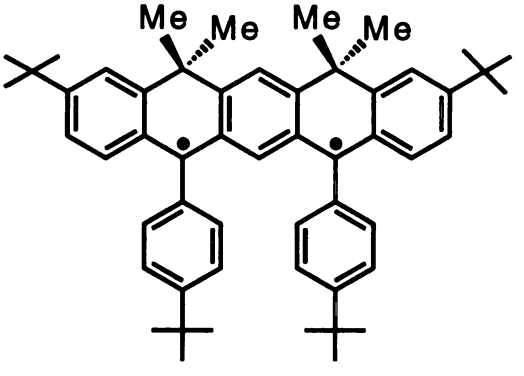

15

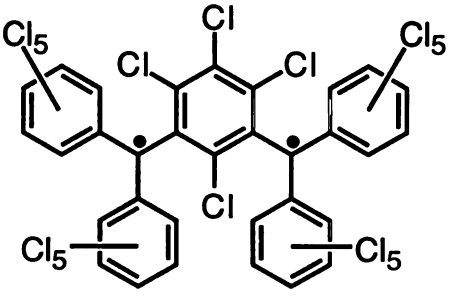

16

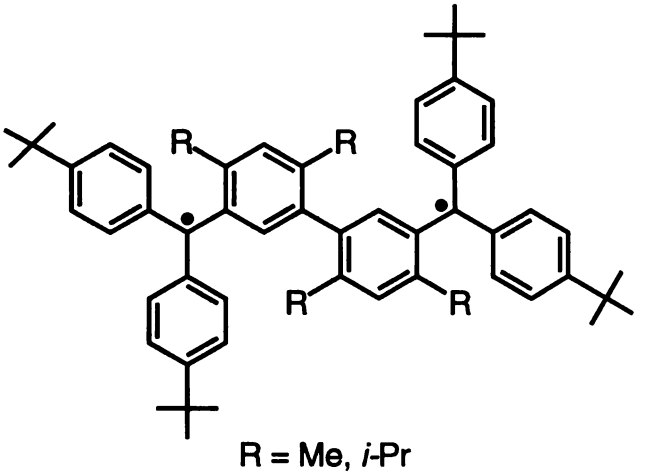

R = Me, *i*-Pr

17

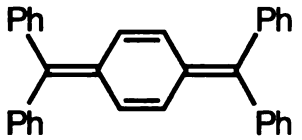

18

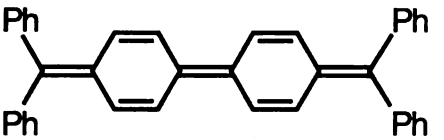

19

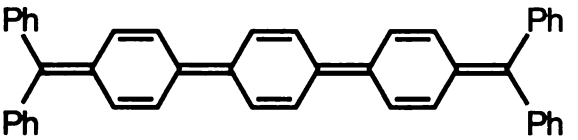

20

An example illustrating the use of single-atom bridges to link radical centers is 1,3-cyclobutanediyl (**21**), a molecule that has been shown by Dougherty[74] to have a triplet ground state. The cause of the triplet ground state in **21** is thought to be through-bond coupling,[75] mediated by the "bridging" CH_2 groups. The through-space overlap of the radical p-orbitals is substantial ($S_{ab} > 0$), and would produce a large HOMO–LUMO gap which favors a singlet ground state. However, the CH_2 groups of **21** have filled orbitals of π symmetry that can mix with the p-orbitals, but only with the symmetric combination (the HOMO). This through-bond interaction of the radical p-orbitals raises the energy of the HOMO to a level that, by coincidence, is nearly degenerate with the LUMO. Thus, the energetic consequences of overlap between the radical p-orbitals are cancelled, but K_{ab} remains large, favoring a triplet ground state.[76] This through-bond spin coupling mechanism is analogous to the inorganic "superexchange" model.[77]

The complex $CuVO(fsa)_2en{\bullet}CH_3OH$ (**22**)[78] is a bimetallic system that somewhat resembles biradical **21**. The X-ray structure[79] of **22** is shown in Figure 1.6. In this complex the magnetic orbitals are orthogonal due to molecular symmetry, and so $S_{ab} = 0$. The unpaired electron of Cu (II) ($S = 1/2$) occupies the $d_{x^2-y^2}$ orbital, while the unpaired electron of V(IV) ($S = 1/2$) occupies the d_{xy} orbital. Here K_{ab} is very large because the 2p orbitals of the bridging oxygen atoms give both σ overlap with a d_{xy} orbital on Cu and π overlap with a $d_{x^2-y^2}$ orbital on V. This results in an appreciable overlap density and therefore a large value of K_{ab}. Compound **22** is thus a ground state triplet with a large $\Delta E_{ST} = 118\ cm^{-1}$.[80]

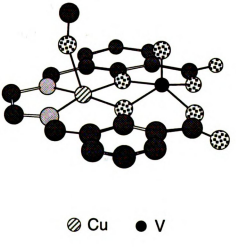

Figure 1.6. X-ray structure of **22**.[79] X-ray coordinates were obtained from the Cambridge Structural Database.

A very interesting approach to "linking" two radical centers through bridging units involves coordination of nitroxide ligands to a transition metal ion.[81] The coordination chemistry of these ligands has been reviewed.[82]

The nature of the coupling of a nitroxide directly bound to a metal ion can be rationalized on the basis of orbital overlap considerations. The unpaired electron of a free nitroxyl radical occupies a π^* orbital shared by the oxygen and nitrogen atoms. Metal orbitals of appropriate symmetry include the d_{x2-y2}, d_{xz}, and d_{z2} orbitals[83] shown in Figure 1.7 for axially bound nitroxides. Ferromagnetic coupling is expected when this orbital and the d_{x2-y2} orbital of the metal are orthogonal ($S_{ab} = 0$), as depicted in Figure 1.7a; this occurs when the M–O–N angle is 180°. An example of a complex having this geometry is $Cu(hfac)_2(NITPh)_2$.[84] Decreasing the M–O–N angle in this situation results in greater overlap, which favors antiferromagnetic coupling. Shortening of the M–O distance is expected to make any interaction, either ferro- or antiferromagnetic, more intense; the nature of the interaction just depends on the relative orientation of the interacting orbitals.

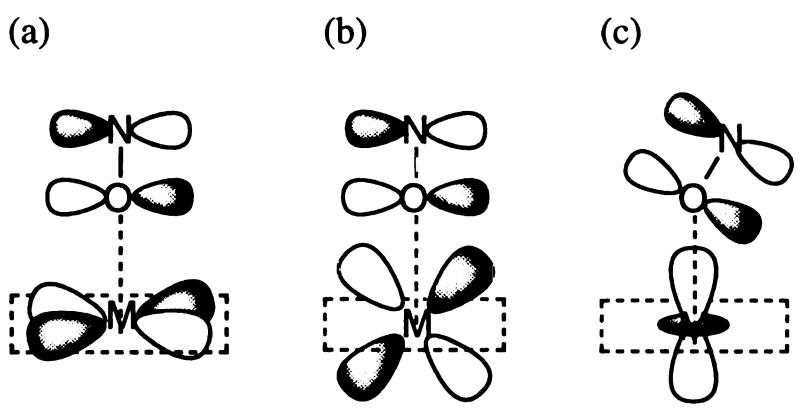

Figure 1.7. Possible orbital interactions between a nitroxide radical and a transition metal ion: (a) π^*–d_{x2-y2}; (b) π^*–d_{xz}; and (c) π^*–d_{z2}. Adapted from ref 81.

Antiferromagnetic coupling requires nonzero overlap ($S_{ab} > 0$) of the π^* orbital of the radical and one or more magnetic orbitals of the metal ion.

Figures 1.7b and 1.7c are relevant to nitroxide complexes of Ni(II), Co(II), and Mn(II), and they invariably lead to antiferromagnetic coupling. Thus, the ground states of $Ni(hfac)_2(proxyl)_2$,[83] $Co(hfac)_2(proxyl)_2$,[83] and $Mn(hfac)_2(proxyl)_2$[85,86] have zero, one, and three unpaired electrons, respectively. These spin states are due to antiferromagnetic coupling of the nitroxyl spins ($S = 1/2$) with the metal-based unpaired spins ($S = 1$ (Ni), $S = 3/2$ (Co), and $S = 5/2$ (Mn)).

In a recent overview,[52] Kollmar and Kahn describe various strategies for the design of ferromagnetically coupled systems, and summarize the work as follows:

"To conclude, we would like to stress that the through-space interactions on which we have focused in this Account are generally weak except when p atomic orbitals belonging to adjacent molecules point to each other. A way to increase the interaction is by linking the molecular units by closed-shell bridges. Such an approach also allows one to control the relative orientations of the units and therefore to impose the relative symmetries of the interacting orbitals."

1.3. The "Tripod Ether" Approach to Electron Coupling

We are working to achieve and understand electron coupling in radical pairs or higher oligomers designed so that electron interactions are mediated and enforced by metal cations. By "inverting" the concepts of Cram, Lehn, and others—preorganization of an ion's full complement of Lewis basic sites and careful choice of cavity size—we seek to control the self-assembly of organic free radical ionophores.

Tris(2,6-dimethoxyphenyl)methyl (**23**), originally synthesized by Martin et al., is a remarkably stable free radical.[87] It is monomeric and air-stable, presumably by virtue of its D_3 propeller conformation in which the central carbon bearing the lone electron is protected from above and below by tripods of methoxy groups. Studies on open-chain polyether ligands[88] suggest that these ether oxygen "tripods" can serve as binding sites for metal ions. Two molecules of **23** can self-assemble about a metal cation, fixing the radicals' relative orientation which, in turn, dictates electron coupling. Scheme 1.1 portrays the proposed coupling in "interrupted σ-bonds"—radical pairs **24** or oligomers **25** in which metal cations mediate electron interactions. For radicals like **23** which may bind metals on two faces, alternating radical/metal cation stacks are anticipated; such chains would center around linear arrays of one-electron carbon-centered p-orbitals interacting through metal ions. Figure 1.8 shows an illustration of the radical-metal ion-radical dimer **24** as calculated by molecular mechanics.

Scheme 1.1.

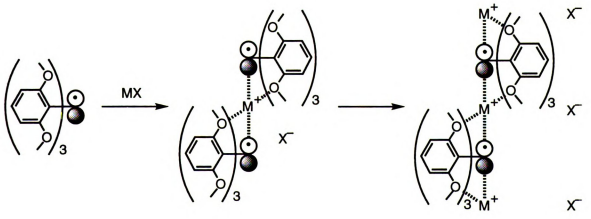

23 **24** **25**

Figure 1.8. Optimized structure of dimer **24** as calculated by Molecular mechanics.

This work is concerned with the ion binding capabilities of dia- and paramagnetic triaryl-Z propeller (Z = B, C$^{\bullet}$, N) analogues of radical **23**. The triaryl-Z frameworks are new to the ion binding field, so their complexation abilities have been studied using a variety of techniques, including NMR, X-ray crystallography, ESR, and computational methods. Detailed information has been obtained on the stoichiometry, energetics, and geometrical nature of metal ion binding by these tripod ionophores. We have found that the complexing abilities of the ether tripods depend strongly upon solvent, metal cation, and counterion identities. In many cases, binding is limited to one tripod per metal ion, as opposed to the hoped-for pairing of tripods about the metal ion as in **24**. To enhance their complexing abilities, and to examine specifically the relationship induced between a pair of tripods when they do coordinate about a single metal ion, we have tethered two tripods to make a covalently-linked diamine ligand. Characterization of simple 1:1 and 2:1 complexes between tripods and metal ions has provided a basic picture of aggregation in extended structures, and has allowed us to probe the requirements for the design of molecular solids with long-range structure. Ion binding by the diamagnetic triaryl-Z tripods (Z = B, N) has

revealed the possibility of controlled assembly of paramagnetic tripod ionophores ($Z = C^{\bullet}$) whose pairwise electron interactions may then be turned on by the binding event. Both a monoradical and a biradical analogue of **23** have been prepared, and ESR studies pursued to evaluate ion binding by these systems.

CHAPTER 2

TRIARYL-Z PROPELLERS (Z = B, N)

2.1. Background

Establishing the ion binding potential of polydentate triarylmethyl radicals is critical to the development of our approach. The structural basis for ion complexation by these substrates is exemplified by the propeller-like (helical) conformations adopted by per-*ortho*-substituted triaryl-Z compounds (Z = B, C, N, or P). Surprisingly, radical **23** adopts an unusual conformation in the solid state (Figure 2.1); one aryl ring is twisted out of the central methyl carbon plane by only 12° while the other rwo rings are twisted by 61°.[89] This structure represents a point well along the way to the transition state for the two-ring flip racemization pathway,[90] and its large deviation from the D_3 ground state is unprecedented for triaryl-Z propellers. The distorted "binding site" in solid **23** seems a poor representation of its solution conformation, which is D_3 in symmetry on the ESR timescale.[87] The tripod binding site is more realistically shown by the X-ray structure of carbocation **26**. In contrast to radical **23**, the more nearly D_3 propeller conformation of **26** positions the methoxy groups in such a way as to form a pair of nucleophilic oxygen pockets in which the lone pairs project toward the center of a small cavity. The crystal structure of **26**•BF_4 is shown in Figure 2.2 alongside the calculated (MMP2) structure of radical **23**.

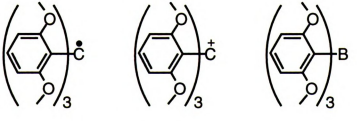

23 **26** **27**

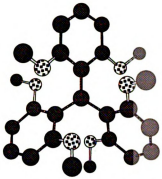

Figure 2.1. X-ray structure of **23**.[89]

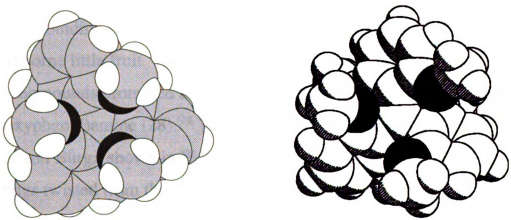

Figure 2.2. Space-filling views of "tripod" binding sites: calculated (MMP2) structure of **23** (left) and X-ray structure[89] of **26**•BF_4 (right, BF_4^- counterion not shown).

The structural similarity to podands[88] suggests that these "tripod ethers"[91] can serve as hosts for metal cations. According to the principle of preorganization,[92] the smaller the conformational changes in host and guest required for complexation, the stronger the binding. Although the racemization barrier for **23** is predicted to be quite low,[93] the symmetrical substitution in all six *ortho* positions maintains the integrity of the ether tripods. Thus **23** and its analogues are expected to require little reorganization by the metal ion. With only three Lewis basic sites to offer an

ion, these substrates are not expected to be powerful ion complexants. Their structures, however, appear to optimize the cavities they do exhibit.

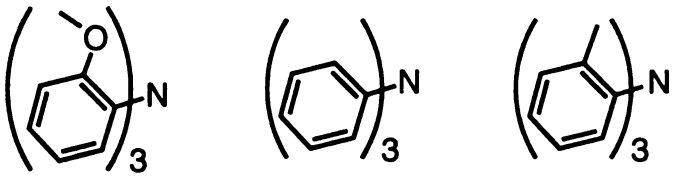

28 **29** **30**

Ion binding studies involving radical **23** and the isostructural borane **27** had borne little fruit. The various difficulties and limited success with these compounds prompted a study of the known tris(2-methoxyphenyl)amine (**28**).[94] The X-ray structure[95] of **28** reported by Müller and Bürgi, shown in Figure 2.3, reveals a C_3 geometry with the three aryl rings twisted from the C_3 axis by ca. 45°. The nitrogen is slightly pyramidalized to allow the methoxy substituents to move away from each other, forming a nucleophilic pocket. This "binding conformation" is apparently quite favorable despite the low rotational barriers observed for tris-*ortho*-substituted triaryl-Z compounds,[96] and the presence of only one tripod binding site precludes formation of oligomeric chains.

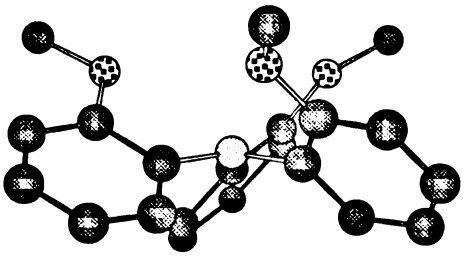

Figure 2.3. X-ray structure of **28**.[95] X-ray coordinates were obtained from the Cambridge Structural Database.

2.2. Ion Binding Studies of Triarylpropeller Ionophores

Compound **28** was prepared (70%) by a copper-catalyzed Ullmann-type condensation of *o*-anisidine with 2-iodoanisole under phase-transfer[97] conditions. The ability of amine **28** to bind metal ions was initially studied in $CDCl_3$ solution by comparing the ^1H NMR spectra in the absence and presence of added salts. Unexpectedly, addition of excess solid $Mg(ClO_4)_2$ to **28** immediately produced an orange solution that exhibited broadening of the methoxy proton resonance and coalescence of the aromatic multiplet, as shown in Figure 2.4. These spectral changes could not be attributed to the presence of excess solid since broadening persisted after filtration of the sample (Figure 2.4d). Similarly, addition of excess $LiBF_4$ to **28** also gave an orange solution that showed analogous spectral changes; the unbroadened ^1H NMR spectrum of **28** was recovered upon addition of D_2O. In a control experiment, a solution of triphenylamine (**29**) in the presence of $Mg(ClO_4)_2$ instantly turned aqua-blue in color; the ^1H NMR spectrum of the sample revealed considerable line-broadening of the aromatic proton resonances. The unbroadened ^1H NMR spectrum of **29** was obtained on shaking the sample with D_2O. In contrast, a solution of triphenyl*methane* treated with excess $Mg(ClO_4)_2$ did not change color or exhibit the NMR line-broadening phenomenon.

The observations recounted above suggested that both **28** and **29** were being oxidized to their respective radical cations. A $CDCl_3$ solution of **28** (or **29**) gave an unresolved ESR signal (no fine structure) when treated with either $Mg(ClO_4)_2$ or $LiBF_4$. *A paramagnetic species was detected only when the Mg^{2+} or Li^+ salt was present with the amine—neither amines nor salts*

Figure 2.4. 300 MHz ^1H NMR spectra of **28** in $CDCl_3$: (a) with no added salt; (b) with excess $Mg(ClO_4)_2$ at t = 0; (c) at t = 22 h; and (d) after filtration of sample (c) to remove excess solid.

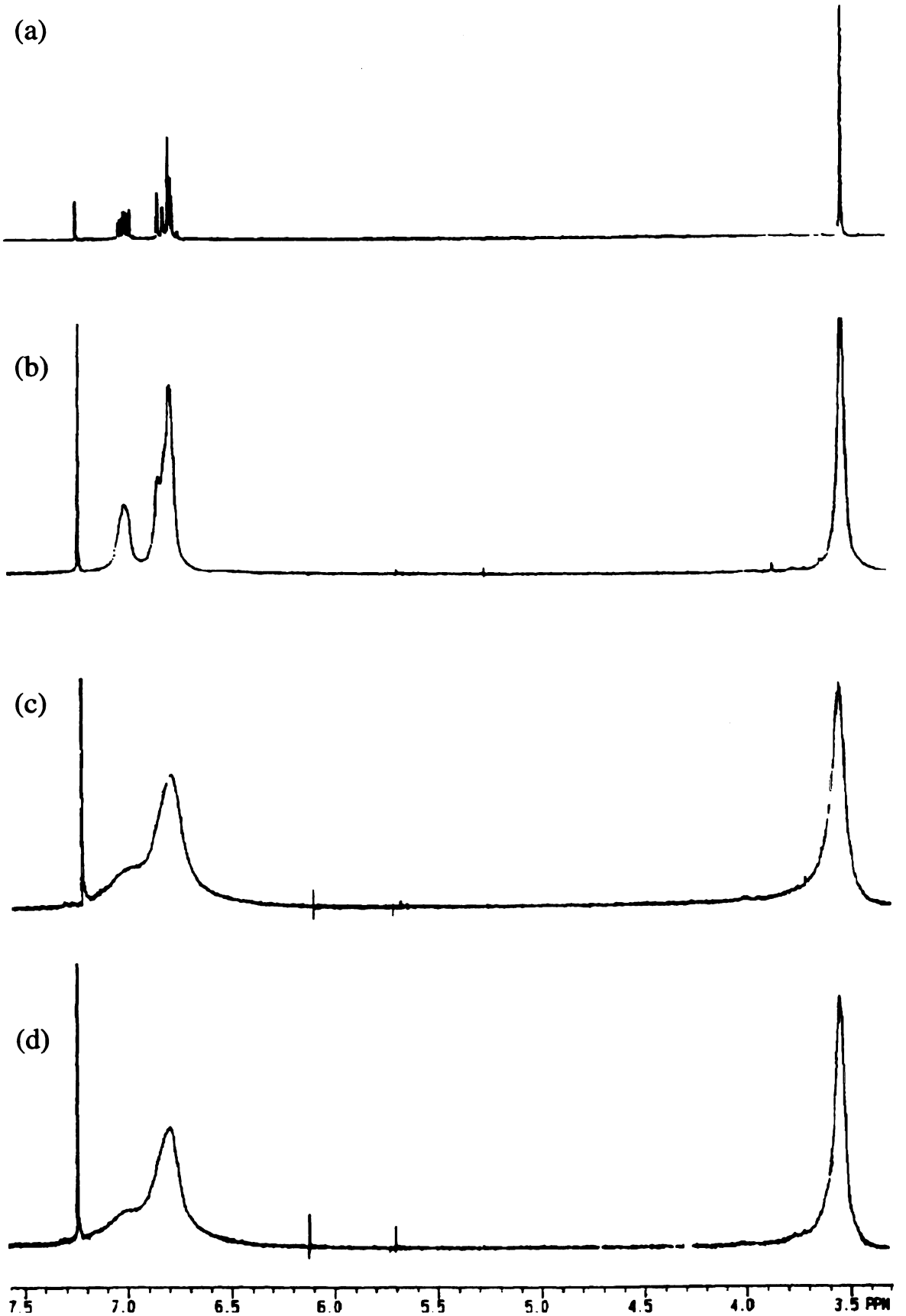
(a)
(b)
(c)
(d)
7.5
7.0
6.5
6.0
5.5
5.0
4.5
4.0
3.5 PPM

alone in $CDCl_3$ generated a radical species. It is interesting that tris(2-methylphenyl)amine (**30**) and triethylamine do not undergo this oxidation process. This may be a reflection of their higher oxidation potentials (E_{ox} = 1.01[98] and 1.15 V[99] vs. SCE, respectively) compared to those of **28** (E_{ox} = 0.80 V vs. SCE)[97] and **29** (E_{ox} = 0.92 V vs. SCE).[100]

It is known that the radical cations of both **28** and **29** (**28**$^{+\bullet}$ and **29**$^{+\bullet}$) undergo facile self-reaction to form *p*-benzidines **31**[98] and **32**,[100,101] respectively, as shown in Scheme 2.1. From electrochemical studies performed in acetonitrile, the bimolecular rate constant for benzidine formation is $6.0 \pm 0.5 \times 10^1$ L mol^{-1} sec^{-1} in the case of **28**$^{+\bullet}$, and $2.4 \pm 0.5 \times 10^3$ L mol^{-1} sec^{-1} for **29**$^{+\bullet}$.[98] In our experiments, however, solutions of the amines in the presence of $Mg(ClO_4)_2$ or $LiBF_4$ remain colored for a week or more, giving strong ESR signals. The ^{1}H NMR spectra of these samples never showed any evidence of a *p*-benzidine product, even after "quenching" the radical species with D_2O. Earlier work has shown that, when **29** is oxidized with I_2, the ESR spectrum of the more stable **32**$^{+\bullet}$ is observed.[101] Additionally, it has been observed that electrolysis of **29** initially gives the ESR spectrum of **29**$^{+\bullet}$, which is soon replaced by the spectrum of **32**$^{+\bullet}$ formed in the follow-up reaction.[100] The absence of fine structure in our ESR spectra does not allow us to directly address this issue. However, for the oxidation of both **28** and **29**, our failure to observe compounds **31** and **32** by NMR suggests that benzidine formation is not appreciable, if it occurs at all.

Scheme 2.1.

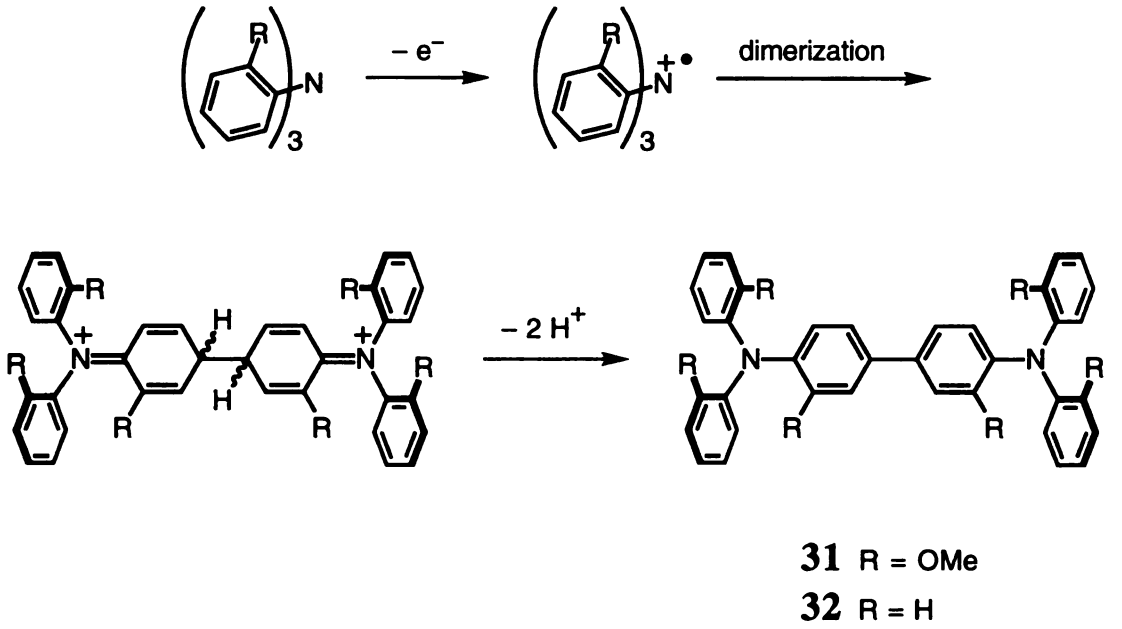

In trying to determine the identity of the oxidizing species, O_2 was ruled out as the oxidant by the following experiment: Solutions of **28** were prepared under argon in a glove-box using rigorously degassed (freeze-pump-thaw cycles) $CDCl_3$; treatment of the solutions with either $Mg(ClO_4)_2$ or $LiBF_4$ still resulted in oxidation of the amine, as confirmed by ESR. Several other salts were also found to effect the oxidation process, including $LiClO_4$, $LiPF_6$, and $MgBr_2$. The likelihood of the anions playing a key role in the oxidation process seemed small, especially since BF_4^- and PF_6^- are used in electrochemistry as redox inactive counterions.[102] However, the presence of a metal ion appears important, since neither **28** nor **29** is oxidized when treated with *n*-Bu_4NBF_4.

A salient result was the observation that a solution of **28**, in the presence of excess LiI, remained colorless and did not give an ESR signal.

Figure 2.5. 300 MHz ^1H NMR spectra of **28** in $CDCl_3$: (a) with no added salt; (b) with excess LiI; and (c) after treatment of (b) with D_2O.

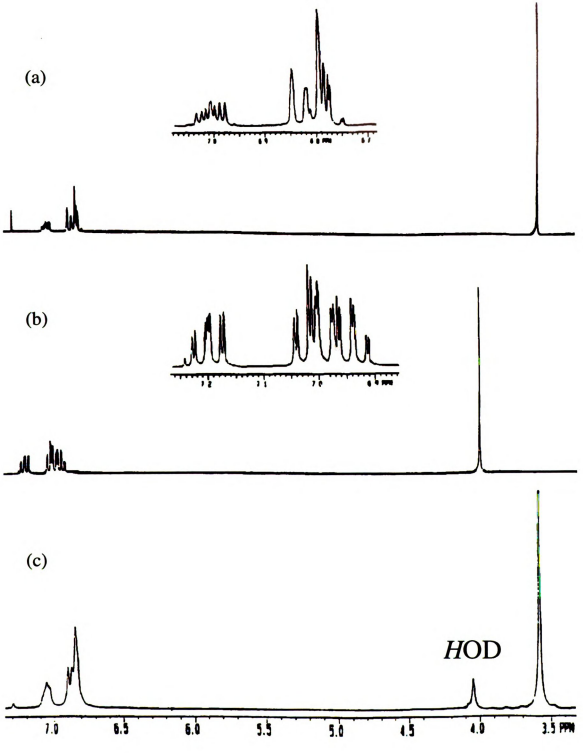
(a)
(b)
(c)
HOD
7.0
6.5
6.0
5.5
5.0
4.5
4.0
3.5 PPM

The ^1H NMR spectrum of this sample is well-resolved and reveals significant changes: The methoxy proton resonance is markedly shifted downfield ($\Delta\delta = 0.47$ ppm) and the splitting pattern of the aromatic multiplet has changed, as shown in Figure 2.5b. These spectral changes are not due to a chemical transformation of the amine since the ^1H NMR spectrum of "unchanged" **28** is obtained upon addition of D_2O (Figure 2.5c). Additionally, treatment of **29** in $CDCl_3$ with excess LiI did not produce an ESR signal, nor significant shifting nor line-broadening in the ^1H NMR spectrum.

It appears that the oxidant is the $CDCl_3$ solvent. This notion is supported by the observation that experiments carried out in CD_2Cl_2 also produce amine radical cations, but in poor electron-accepting media like acetone, acetonitrile, benzene, or pyridine, oxidation is not observed. Oxidation of **28** or **29** in the presence of counterions such as ClO_4^- and BF_4^- is interpreted as the inability of these anions to reduce the amine radical cation once it is formed. For the purposes of NMR studies, the use of I^- salts effectively protects against the oxidation process: Evidently I^- is sacrificed to make I_2 instead of allowing the amine to be oxidized. Indeed, these samples eventually show the yellow color characteristic of I_2 in $CDCl_3$ solution. We have also found that oxidation is not a problem with BPh_4^- as the counterion, although the reason for this is not understood. In any event, complications arising from the oxidation of **28** can be surmounted by judicious choice of anions.

Triarylamine radical cations are of interest since they have been proposed as building blocks for the preparation of bulk magnetic materials.

Recently, Stickley and Blackstock[103] have shown that two- and three-electron oxidation of **33**, a *m*-quinodimethane analogue, gives a triplet diradical dication and a quartet triradical trication, respectively. In the long run, the oxidation "difficulty" described above may give access to an interesting new group of tripod paramagnets in the guise of the remarkably long-lived amine radical cations we have observed.

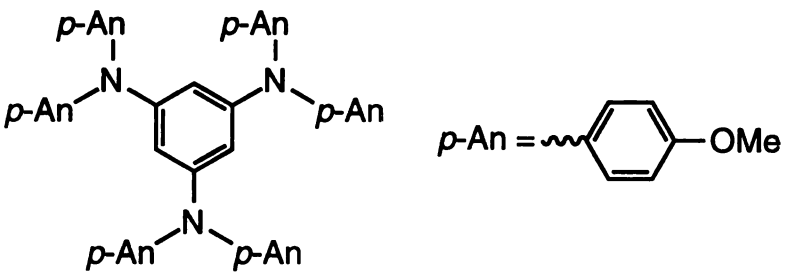

33

The striking changes observed in the ^{1}H NMR spectrum of **28** after addition of excess LiI (vide supra) provides strong evidence for Li^+ complexation. The different splitting pattern of the aromatic multiplet, compared to that of the free host, is attributed to conformational reorganization during complexation. Marked changes in the ^{13}C NMR spectrum of **28** are also observed upon addition of excess LiI, most notably the methoxy ^{13}C resonance (for which $\Delta\delta = 2.56$ ppm). Confirmation of Li^+ complexation is provided by ^{7}Li NMR spectroscopy. Attempts to obtain a ^{7}Li signal of LiI in $CDCl_3$ foundered due to the insolubility of LiI in this solvent. However, when excess LiI was added to a solution of **28** in $CDCl_3$, a ^{7}Li resonance was observed at 2.11 ppm (relative to a 0.3 M LiCl/MeOH

external reference). A 1:1 complex stoichiometry (**28**•LiI) was determined by comparing its ^{1}H (OCH_3) and ^{7}Li NMR integrals to those of a $LiBPh_4$•3glyme reference sample; details are given in Chapter 5. Amine **28** cannot compete with H_2O for LiI—hence the recovery of the "free" amine ^{1}H NMR spectrum on shaking the sample with D_2O. In $CDCl_3$, compound **28** binds other salts as well; details of these binding studies are described in Chapter 3.

The association of **28** with LiI in $CDCl_3$ involves a rapid exchange process. Fast exchange rates are favored by ligand flexibility and low complex stability.[104] The methoxy proton resonance of **28** (3.54 ppm) was shifted to 3.62, 3.90, and 3.85 ppm on addition of ca. 0.5, 1.0, and 4.0 equivalents of LiI, respectively. Line-broadening of the methoxy proton resonance and the aromatic multiplet was also observed (no ESR signals). Equilibration of these samples over 4 days revealed further changes: The methoxy signal had again shifted downfield (to 3.64, 4.01, and 4.03 ppm, respectively), and all of the resonances had sharpened considerably. A $CDCl_3$ solution of **28** treated with LiI (0.5 equivalents) was examined by variable temperature (VT) NMR. Decoalescence of the methoxy resonance was observed between –20 and 0 °C, giving two signals at 3.54 and 4.04 ppm (ca. 1:1 by integration) which correspond to free and complexed host, respectively. Broadening of the signals is due to the rapid exchange (on the NMR timescale) of free and bound tripod ligands, which results in a population-average signal. Unfortunately, we have been unable to determine the molecularity of this exchange process since the kinetics are complicated by the insolubility of LiI in $CDCl_3$ (in the absence of **28**).

While ion binding in the relatively nonpolar chlorocarbon solvents is interesting, we wished to measure binding constants and stoichiometries in a solvent which could dissolve both host and guest. The solvents mentioned previously—acetonitrile, acetone, and pyridine—are obvious candidates, but studies with **28** have shown that evidence for ion binding is not readily apparent in these media. These solvents, which have Gutmann donor numbers[105] of 14.1, 17, and 33.1, respectively, effectively compete with **28** for metal ions.

Nitromethane was selected for binding studies because of its low donor number (2.7)[105] and relatively high dielectric constant (35.9). As observed in $CDCl_3$, the exchange between free and complexed **28** in nitromethane is fast on the NMR timescale. Again, only a single, population-average signal is observed regardless of the amount of **28** or metal salt present. Binding constants were determined from tandem ^1H and ^7Li (^{23}Na) NMR titrations. The salt (guest) concentration was held constant, and the concentration of the host was incrementally changed to span a host to guest ratio between 0 and 9. Complexation constants (K_f's) were obtained from plots of the ^1H and ^7Li (^{23}Na) chemical shift variation as a function of the host/guest mole ratio; details of the experimental procedure and the data treatment are given in Chapter 5.

Information obtained from the nonlinear least-squares curve-fits is summarized in Table 2.1. The inflections in the binding isotherms are indicative of 1:1 complex formation. Essentially the same K_f value is obtained for **28**•Li^+ with the I^- and ClO_4^- salts. Both LiI and $LiClO_4$ form contact ion pairs in nitromethane,[106] but this seems to have a negligible

effect on complex formation. The **28**•Li^+ complexes are ion-paired with the anions, as evidenced by the anion dependence of the calculated ^7Li chemical shifts. Interestingly, the calculated ^7Li shift for **28**•LiI is nearly identical to that seen in $CDCl_3$ solution for this complex. The calculated methoxy proton chemical shift for **28**•LiI (3.93 ppm) is also close to that observed for this complex in $CDCl_3$ solution.

Table 2.1. Formation Constants and Chemical Shift Data for Alkali Metal Complexes of **28** in CD_3NO_2 Obtained from Tandem $^1H/^7Li$ (^{23}Na) NMR Titrations[a]

	K_f (M^{-1})	δ (OCH_3, ppm)	δ (M^+, ppm)
LiI	1.6×10^4	3.92 (3.57)[b]	2.51[c] (1.29)[c,d]
$LiClO_4$	4.4×10^4	3.92	2.10[c] (0.84)[c,d]
$NaBPh_4$	6.9×10^2	3.65	−8.94[e] (−12.9)[e,d]

[a]$[M^+] = 5 \times 10^{-3}$ M. [b]Chemical shift of 0.05 M **28** in CD_3NO_2. [c]Referenced to 0.30 M LiCl/MeOH. [d]Chemical shift in the absence of **28**. [e]Referenced to 0.30 M NaCl/H_2O.

In contrast to LiI and $LiClO_4$, $NaBPh_4$ is completely dissociated in nitromethane.[107] The K_f value obtained for **28**•Na^+ is nearly two orders of magnitude smaller than that of **28**•Li^+, indicating that Na^+ is not complexed as strongly as Li^+. It is interesting to note that the data suggest a 1:1 complex stoichiometry, but crystals of the 2:1 complex between **28** and $NaBPh_4$ are obtained on slow evaporation of a nitromethane solution (vide infra). The calculated methoxy proton chemical shift for **28**•$NaBPh_4$ (3.65 ppm) is significantly different from what is found in $CDCl_3$ (3.14 ppm), for which a 2:1 complex is indicated (vide infra). In accord with this observation, the

calculated ^{23}Na chemical shift for **28**•$NaBPh_4$ differs from that seen in $CDCl_3$ for **28**$_2$•$NaBPh_4$ (–5.5 ppm), which is described in the next chapter.

To determine the importance of the ether tripod of **28** to ion binding, the ligand properties of triarylamines **34** and **35** were studied in $CDCl_3$. Compound **34** was synthesized (18%) from aniline and 2-iodoanisole using the method described for **28**, and **35** was similarly prepared (70%) from diphenylamine and 2-iodoanisole.

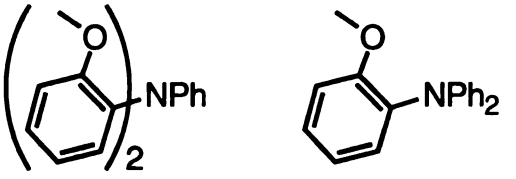

34 **35**

When a solution of **34** was shaken with excess LiI, the complex **34**•LiI was formed. The ^1H NMR spectrum of **34**•LiI may be compared to that of the free host: The methoxy resonance is shifted downfield ($\Delta\delta$ = 0.40 ppm) and the appearance of the aromatic region has changed. The ^{13}C NMR spectrum also exhibits significant changes, most notably the downfield shift of the methoxy signal ($\Delta\delta$ = 2.1 ppm). A ^7Li resonance is observed at δ 2.74 ppm, which is considerably shifted (downfield) from that of **28**•LiI. Addition of D_2O to a solution of **34**•LiI recovers the ^1H and ^{13}C spectra of the free amine. No salt uptake is observed (^1H NMR) with NaI, $NaBPh_4$, KB(4-ClPh)$_4$, KI, $RbBPh_4$, RbI, CsI, or $CsBPh_4$.

In contrast to **34**, no changes are observed in the ^1H or ^{13}C NMR spectra of **35** on addition of excess LiI, even after monitoring the sample over several days. Furthermore, no salt uptake is observed (^1H NMR) with NaI, $NaBPh_4$, $KB(4\text{-}ClPh)_4$, KI, $RbBPh_4$, RbI, CsI, or $CsBPh_4$. Apparently an ether tripod is not required for ion binding by these triarylpropeller systems, but only one methoxy ether oxygen is not sufficient for complexation. Not surprisingly, ion binding *is not observed* (^1H, ^{13}C, and ^7Li or ^{23}Na NMR) with any of the aforementioned salts when methoxybenzene (anisole) or 1,3-dimethoxybenzene is the host in $CDCl_3$.

It should be mentioned that both **34** and **35** are oxidized to amine radical cations by $Mg(ClO_4)_2$ or $LiBF_4$ in $CDCl_3$, giving light-blue and emerald-green solutions, respectively. However, these oxidations appear to be slower than those of **28** and **29**, only producing ESR signals and line-broadened ^1H NMR spectra after ca. 1 day.

It is well-known from carbohydrate chemistry that, even in H_2O, as few as three neutral oxygen atoms in a molecule suffice to form well-defined and reasonably stable complexes with metal ions, provided that the oxygen donors are suitably disposed. The 1:1 Li^+ complex formation observed with **34** (and lack thereof with **35**) suggested participation of the central nitrogen as a third donor atom. The ion binding ability of tris(2-methoxyphenyl)methane (**36**)[108] was investigated to test this notion, but no evidence of Li^+ binding was found. A plausible interpretation is that the methine hydrogen atom of **36** projects into the ether tripod, blocking complex formation. The analogous tris(2-methoxyphenyl)borane, which would be a more appropriate test system, turned out to be too sensitive for

isolation and use as an ion binding probe. Evidence suggests that this compound is indeed formed, but decomposes during workup.

It was reasoned that since both borane **27** and trimesitylborane (**37**)[109] are fairly stable compounds, tris(2-methoxy-6-methylphenyl)borane (**38**) should be as well. The compound was in fact prepared (65%) by addition of 2-methoxy-6-methylphenylmagnesium iodide to BF_3•Et_2O at 0 °C. Stoichiometry determinations indicate that, like **28**, this "one-faced" tripod ether binds LiI in a 1:1 complex in $CDCl_3$. The ^{1}H NMR spectra of **38** and **38**•LiI are presented in Figure 2.6. No evidence (^{1}H NMR) of complex formation was obtained with $LiClO_4$ or $NaBPh_4$. While the results described above are not direct proof of the nitrogen's participation in complexes of **28** and **34**, they do show that the ether tripod alone is sufficient to bind a metal ion.

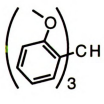

36

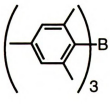

37

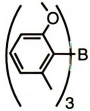

38

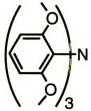

39

Tris(2,6-dimethoxyphenyl)amine (**39**), the nitrogen analogue (Z = N) of radical **23**, was synthesized (vide infra) to examine the ion binding properties of a "two-faced" triarylpropeller ionophore. Shaking a $CDCl_3$ solution of **39** with excess LiI gives a ^{1}H NMR spectrum considerably different from the free host: The methoxy signal is shifted downfield

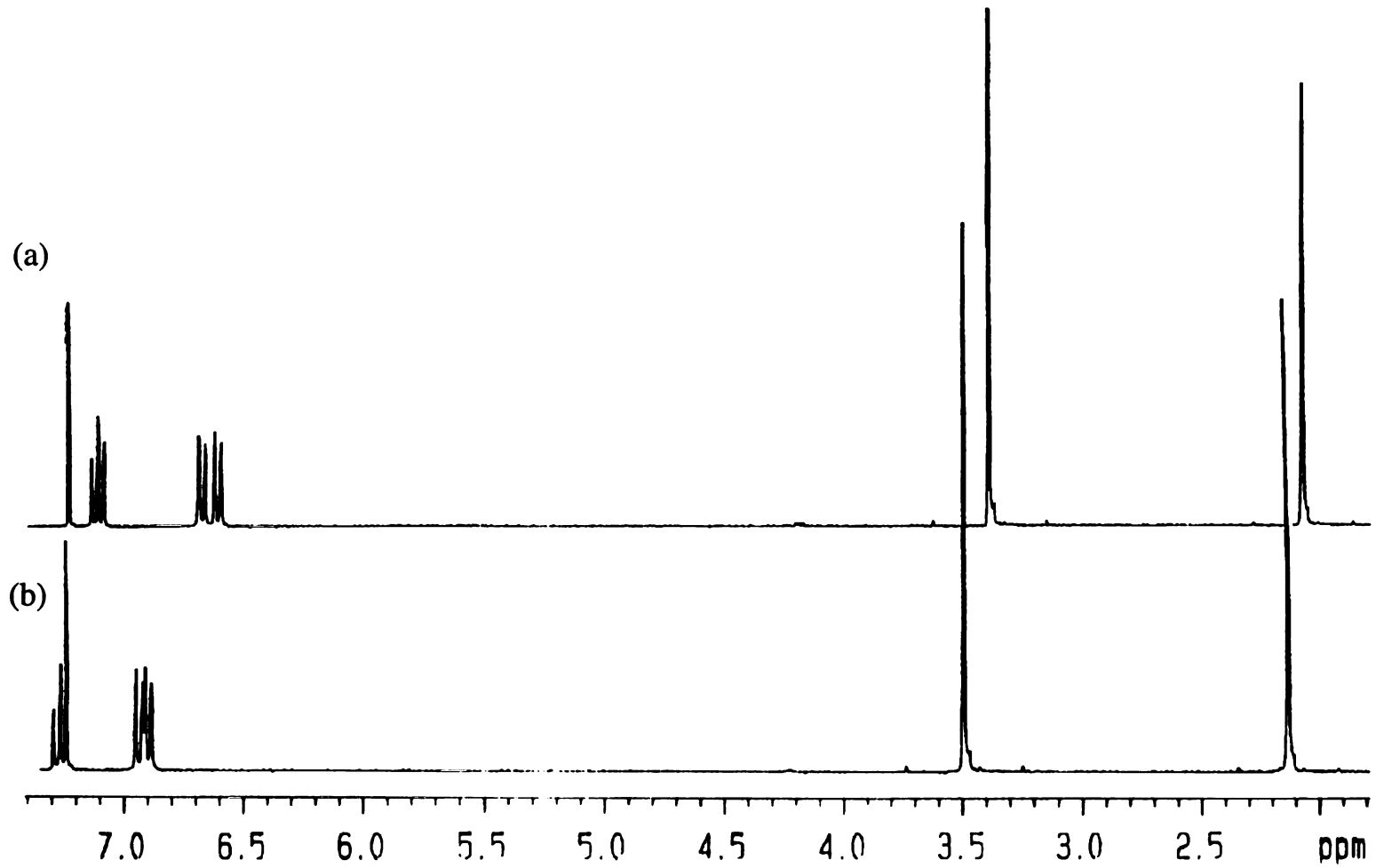

Figure 2.6. 300 MHz ^{1}H NMR spectra of (a) **38** and (b) **38**•LiI in $CDCl_3$.

($\Delta\delta$ = 0.32 ppm), as well as the *meta*- ($\Delta\delta$ = 0.35 ppm) and *para*- ($\Delta\delta$ = 0.35 ppm) ring proton resonances. A stoichiometry determination indicates that a 1:2 complex is formed between **39** and LiI, suggesting that one LiI is bound per tripod unit of **39**. The **39**•2LiI complex is the only example to date in which two metal ions are bound to a "simple" triarylpropeller ligand.[110] In stark contrast, no ion complexation of any kind is seen with $NaBPh_4$.

Unfortunately, the LiI complexes mentioned in the preceding paragraphs appear to be stable only in solution. Attempts to crystallize these complexes under various conditions have been unsuccessful. The following section describes X-ray crystallographic studies of free ligands aimed at structural characterization of tripod binding sites in the solid state.

2.3. Crystallographic Studies of Tripod Binding Sites

As mentioned earlier in this chapter, the free radical **23** was prepared by J. C. Martin et al.; their ESR spectrum, obtained at –80 °C, indicated a D_3 propeller structure with the three aryl rings twisted 45-50° out of the coordination plane of the central carbon.[87] CPK models of this species show tripods of methoxy oxygens above and below the plane of the radical carbon; these substructures call to mind the paired oxygen tripods which surround alkali metal cations in Lehn's [2.2.2] cryptates.[111]

As part of our binding site analysis, we reported X-ray structures of **23**, **27**, and **26**•BF_4.[89] It was noted that the crystal geometry of radical **23** is remarkably unsymmetrical, showing one ring nearly coplanar with the carbon coordination plane, while the other two are steeply twisted (see Table

2.2). To gain insight into the geometrical preferences of per-*ortho*-substituted Ar_3Z propellers, we have synthesized and structurally characterized three related tripod ethers, **39**, **38**, and **26**•I_3. Crystallographic data for these compounds are in Table 2.3, and the fractional coordinates can be found in Tables 2.4A–2.6A in the Appendix. Amine **39** completes the isosteric series Ar_3Z, shown in Figure 2.7, where Z = B, C•, N; borane **38** is a structural intermediate between **27** and the known trimesitylborane (**37**); and the salt **26**•I_3[112] may be compared to **26**•BF_4 previously described. The new structures, **39**, **38**, and **26**•I_3, are displayed in Figure 2.8.

Tris(2,6-dimethoxyphenyl)amine (**39**) was synthesized by the copper-catalyzed Ullmann coupling of 2,6-dimethoxyaniline with 2,6-dimethoxyiodobenzene under phase-transfer[97] conditions. Intramolecular congestion, which apparently blocks the formation of tris(2,6-dimethylphenyl)amine and trimesitylamine by the usual condensation methods,[113] evidently does not prohibit triarylamine formation in this system. However, prolonged reaction times did result in formation of the cyclized amine **40**; similar ring closures have been used to prepare 9-(2,6-dimethoxyphenyl)-1,8-dimethoxyxanthydrol and sesquixanthydrol from tris(2,6-dimethoxyphenyl)methanol.[114]

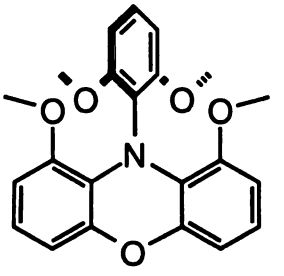

40

Table 2.3. Crystallographic Data for Compounds **39**, **38**, and **26•I_3**

	39	**38**	**26•I_3**
formula	$C_{24}H_{27}NO_6$	$C_{24}H_{27}BO_3$	$C_{25}H_{27}I_3O_6$
fw	425.49	374.29	804.20
$F(000)$	904	800	768
space group	$C2/c$	$P2_1/n$	$P2_1/c$
crystal system	monoclinic	monoclinic	monoclinic
Z	4	4	2
a, Å	10.813(2)	9.437(1)	7.40(2)
b, Å	20.540(3)	15.364(2)	11.114(3)
c, Å	9.982(2)	14.573(2)	16.682(2)
β, deg	98.80(1)	92.55(1)	96.82(1)
V, Å^3	2190(1)	2110.8(8)	1362(4)
D_c, g cm^{-3}	1.290	1.178	1.960
μ(Mo K$_\alpha$), cm^{-1}	0.87	0.70	34.38
$2\theta_{max}$, deg	55	50	45
final R^a	0.057	0.079	0.057
final $R_w{}^b$	0.076	0.093	0.067

$^aR = ||F_o| - |F_c||/\Sigma|F_o|$. $^bR_w = \{\Sigma w(|F_o| - |F_c|)^2/\Sigma w|F_o|^2\}^{1/2}$; $w = 1/\sigma^2(|F_o|)$.

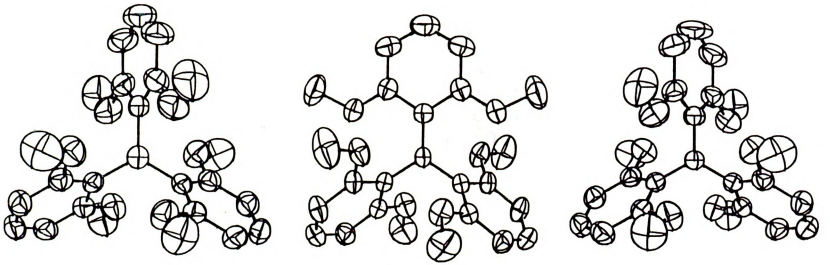

27 (Z = B) **23** (Z = C•) **39** (Z = N)

Figure 2.7. X-ray structures of the homologous series tris(2,6-dimethoxyphenyl)-Z (Z = B, C•, N), showing the near D_3 symmetric structures of the borane **27** (left) and the amine **39** (right), for comparison with the unsymmetrical structure of radical **23** (center).

The X-ray structure of **39** is similar to that of perchlorotriphenylamine.[113] The molecule occupies a crystallographic site of C_2 symmetry; the three C–N bond lengths (1.418, 1.416, and 1.416 Å), the three C–N–C bond angles (119.6, 120.2, and 120.2°), and the three aryl ring twist angles (62.0, 61.0, and 61.0°) are all very similar. Thus, the crystal geometry of **39** deviates only slightly from the ideal propeller shape (D_3 symmetry), as found for the isostructural borane **27**.[89]

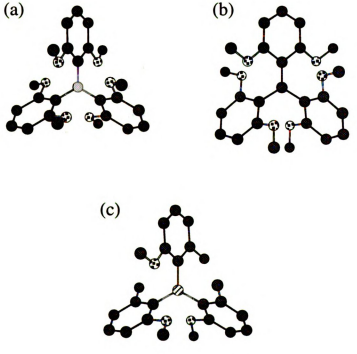

Figure 2.8. X-ray structures of (a) amine **39**, (b) cation **26**•I_3 (I_3^- counterion not shown) and (c) borane **38**.

The X-ray structure of **38** reveals two methoxy groups on one face; the third is on the other face. Consistent with this finding, the ^{1}H NMR resonances for the methoxy and the methyl groups of **38** split into 1:2 pairs at low temperature. A variable temperature NMR study yielded ca. 9.7

kcal mol^{-1} for the barrier to site interconversion. We attribute this barrier to the coupled aryl ring rotations found by Mislow et al. for the related dimesitylaryl boranes, which show barriers of 10–16 kcal mol^{-1}.[115]

Table 2.2. Ring Twists in Hexamethoxytriphenyl-Z Propellers and Related Species

Compound		Θ_1[e]	Θ_2[e]	Θ_3[e]	Θ_{AM1}[e]	Comments
23[a]	**Z = C•**	12.2(2)	61.0(1)	[61.0]	48.9[f]	C_2 Axis
27[a]	**Z = B**	62.8(2)	64.2(2)	[64.2]	56.8	C_2 Axis
39	**Z = N**	62.0(1)	61.0(1)	[61.0]	51.6	C_2 Axis
26•BF_4[a]	**Z = C^+**	32.6(2)	46.1(2)	48.9(2)	43.4[g]	General
26•I_3	**Z = C^+**	35.8(2)	46.5(2)	[46.5]	43.4[g]	C_2 Axis
38	**Z = B**	57.3(3)	58.4(3)	61.6(3)	66.2, 64.5, 63.2[h]	General
37[b]	**Z = B**	51.1	49.6	[49.6]	57.8	C_2 Axis
41[c]	**Z = B**	25.8	52.9	56.3	27.0, 64.0, 64.0	General
44[d]	**Z = C**	4.3(6)	62.3(6)	65.5(6)	—	General

[a]Ref 89.
[b]Ref 112.
[c]Ref 117.
[d]Ref 121.
[e]Twist angles (degrees) of mean aryl ring planes out of central atom's three-carbon plane; coplanar = 0.0°; square brackets enclose symmetry-defined twists.
[f]Radical AM1 calculations used the half-electron method[120]; UHF gives 46.4°.
[g]Cation AM1 calculations were run without counterion.
[h]X-ray and AM1 values of Θ for the three unique aryl rings in **38** are listed in parallel order. They may be labeled as Θ_3 = unique (OCH_3 "up"), Θ_2 = pair (OCH_3 "down"; ring toward unique's OCH_3 side), Θ_1 = pair (OCH_3 "down"; ring toward unique's CH_3 side).

The series of boranes **27**,[89] **38**, **37**,[115,116] shows average twist angles of 63.7°, 59.1°, and 50.1°, respectively. Significantly, the twist angles become smaller as the methoxy groups are replaced by methyl groups.

Resonance between the π-donor methoxy groups and the boron center should favor flatter structures. Most measures of steric bulk find methyl groups to be larger than methoxy groups, again suggesting that the steeper twists should be found in **37**. Thus, the opposite trend might be expected on grounds of both resonance and steric effects.

An interesting case in which, as in **23**, one aryl ring prefers a geometry coplanar with the central ZC_3 plane is the $Li^+(12\text{-crown-}4)_2$ salt of **41**, obtained by deprotonation of a *para*-methyl group in trimesitylborane.[117] Here, the twist angles of the neutral rings are 52.9 and 56.3°, while the quinoid ring remains 25.8° out of the central coordination plane despite the driving force for charge delocalization by π-overlap with the central boron.

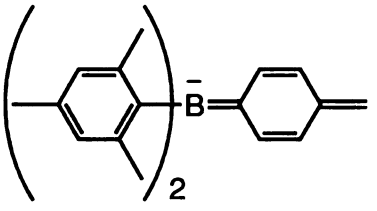

41

Does the geometry of **23** reflect the radical's intrinsic chemistry or is it merely a statistical outlier in the normal range of planar triaryl-Z ring twists? It is clear that the unsymmetrical geometry of **23** is not simply due to its paramagnetic nature. Of the few known triarylmethyl radical structures,[89,118] the trimesitylborane radical anion,[116] and the tris(p-biphenylyl)aminium radical cation,[119] none show such extreme deviations

from threefold symmetry. However, the small number of Ar_3Z structures (where Z = B, C, N) prevents the use of purely structural arguments to answer this question. In Martin's original report and our own work, X-band EPR (ca. 10 GHz frequency) of **23** shows three equivalent aromatic rings down to –100 °C; if **23** is unsymmetrical, this finding places an upper bound of 3–4 kcal mol^{-1} on its ring equivalencing processes. Furthermore, two structural comparisons hint that the propeller geometries are not grossly affected by environmental influences: The twist angles in amine **39** closely match those in borane **27**; and in carbocations **26**, the twist angles show little variation between the BF_4^- and the I_3^- salts. Taken together, the above observations make it seem unlikely that the strange geometry of **23** could arise from packing forces alone.

If an electronic effect intrinsic to **23** produced this radical's unsymmetrical geometry, one might reasonably expect it to be reflected in molecular orbital calculations. In fact, AM1 calculations[120] on compounds **23**, **27**, **39**, and **26** result in threefold symmetric structures in all cases, even when the calculations begin at highly unsymmetrical structures or at the crystal geometries; for comparison purposes, the computed twist angles are included in Table 2.2. We have also computationally explored the energetic cost of constraining the aryl ring twists in **23** to the twist angles (12.2°, 61.0°, 61.0°) seen in the crystal structure. The AM1 method finds that such a distorted geometry is only 2.9 kcal mol^{-1} higher in energy than the D_3 form. Thus, we believe that the solution structure of **23** is a threefold symmetric propeller, but that a distortion of the type seen in the crystal structure is easily accessed at room temperature.

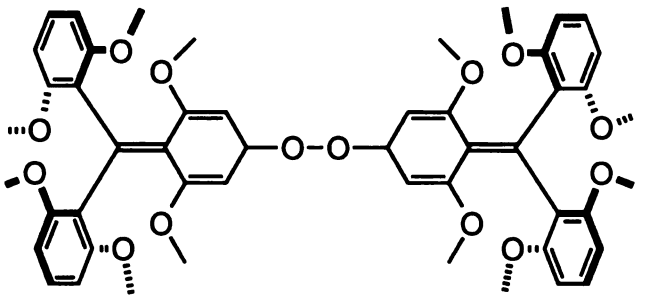

42

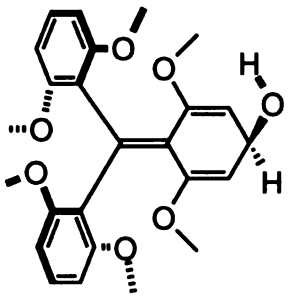

43

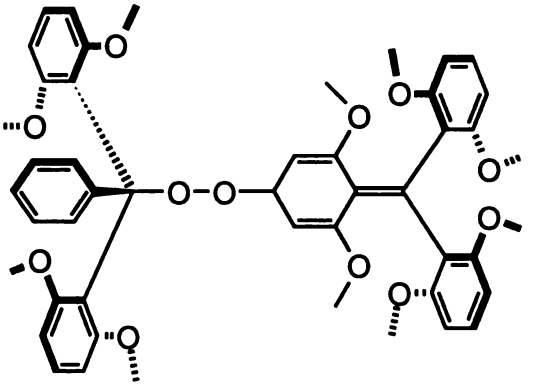

44

A possible explanation for the apparently distorted crystal geometry of **23** was suggested by the discovery that oxygen slowly reacts with **23** to form peroxide **42** and alcohol **43**. As in **41**, these two compounds should have double bonds between the oxidized aryl ring and the erstwhile radical carbon; thus the cyclohexadienylidene ring should be nearly coplanar with the central carbon. The X-ray structure of the closely related peroxide **44** (Table 2.2) shows just such an unsymmetrical arrangement.[121] Both **42** and **43** are much less soluble than radical **23**; it therefore seems reasonable that these species could seed the crystallization of **23**, inducing the radicals to adopt contorted shapes.

CHAPTER 3

ION-BEARING PROPELLERS

3.1. Background

Metal ion complexation by tripod ethers is a new motif for self-assembly of molecular systems.[122] Recent work from these labs has probed the structural,[89] dynamic,[112] and electronic[110b] characteristics of tripod ethers and their complexes. Our approach to organic molecular magnetic materials rests on the abilities of paramagnetic tripod ethers (e.g. **23**) to self assemble by ion binding as in **24**, putting the unpaired electrons into magnetic communication in extended chains. This self-assembly strategy has necessitated a detailed investigation of the ion binding properties achievable within the tripod ether framework. Here we report detailed NMR and X-ray structural studies of ion binding by tripod ether systems using stable, diamagnetic analogues of **23**.

As mentioned earlier, tris(2-methoxyphenyl)amine (**28**) is a useful diamagnetic model for **23**; it can offer only one tripod binding site, precluding chain formation, and it crystallizes in a C_3 geometry, placing the three methoxy groups on one face of the propeller.[95] Complex $\mathbf{28}_2$•Na^+ then mimics a radical-metal-radical subunit of **24**. In the double tripod ligand 1,2-bis[{2-bis(2-methoxyphenyl)aminophenoxy}]ethane (**45**), covalent linkage of two molecules of **28** further promotes pairing of tripod sites about a metal cation to form **45**•M^+. Vögtle and co-workers have examined three-armed "open-chain cryptands"[123] related to **28** and **45**, but to our knowledge, no triarylamine propeller based complexes have been structurally characterized; in particular, tris(2-benzyloxyphenyl)amine, a close analogue of **28**, did not yield crystalline complexes with alkali or alkaline-earth salts.[110a] The NMR and X-ray studies reported here for **28**, **45**, and related complexes validate

the ion binding strategy for self-assembly of tripod ethers. As detailed below, the ion binding ability of ligand **45** augurs well for the use of biradical **46** to probe pairwise metal cation-mediated radical-radical coupling. Details concerning the synthesis of compound **45** are given in Chapter 5.

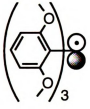

23

28

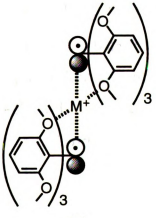

24

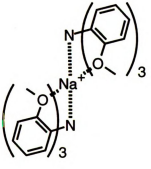

28$_2$•Na^+

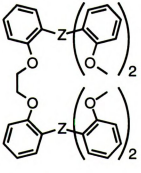

45 (Z = N)
46 (Z = $C^{\bullet}$)

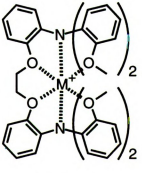

45•M^+

3.2. Ion Binding Studies

Treatment of $CDCl_3$ solutions of **28** with LiI, $LiBPh_4$, or $NaBPh_4$ in excess leads to stoichiometric uptake of these otherwise insoluble salts, as revealed by ^1H, ^{13}C, and alkali metal (^7Li, ^{23}Na) NMR spectra. Stoichiometries and key NMR data are summarized in Table 3.1 and in Chapter 5. With LiI and $LiBPh_4$, 1:1 ligand:salt ratios are found; $NaBPh_4$, however, yields *a 2:1 ligand:salt stoichiometry*, our first finding of twofold complexation of a metal cation by a tripod ether. No salt uptake is seen in $CDCl_3$ with NaI, KI, $KBPh_4$, $KB(4\text{-}ClPh)_4$, $RbBPh_4$, CsI, or $CsBPh_4$. Analogous studies of **45** show stoichiometric uptake of LiI, $LiBPh_4$, NaI, $NaBPh_4$, and $KB(4\text{-}ClPh)_4$. With LiI, a 1:2 ligand:salt ratio is found; it appears that, as in **28**, one tripod of **45** binds one equivalent of LiI (vide infra). However, the other salts investigated—$LiBPh_4$, NaI, $NaBPh_4$, and $KB(4\text{-}ClPh)_4$—show 1:1 stoichiometries upon complexation. No complexation of KI, $KBPh_4$, $RbBPh_4$, CsI, or $CsBPh_4$ by ligand **45** was observed in $CDCl_3$.

Beyond the above simple stoichiometries, solution structures of the complexes may be inferred from detailed analysis of the ^1H, ^{13}C, and alkali metal NMR spectra. For **28**•LiI, time-averaged C_3 symmetric coordination of the Li^+ ion in the ether tripod is indicated by a single methoxy ^1H resonance and seven ^{13}C signals. The narrow ^7Li linewidth ($\Delta\nu_{1/2}$ = 1.0 Hz) suggests a symmetrical environment about Li^+.[124] In a poorly solvating medium like $CDCl_3$, the complex is most likely intimately ion-paired with the I^- counterion,[125] as seen in the recently reported structure of the LiI complex of tris(2-pyridylmethyl)amine;[126] an MNDO-calculated structure

of **28**•LiI is presented in Figure 3.1a. Analogous complexation of an equivalent of LiI in each tripod moiety of **45** is supported by ^{1}H, ^{13}C, and ^{7}Li (δ, $\Delta\nu_{1/2}$) data which are similar to those observed for **28**•LiI. Thus, the methoxy ^{1}H and ^{13}C shifts for **28** and **45** are nearly identical, both in the free ligands (^{1}H: 3.54 and 3.51 ppm; ^{13}C: 55.7 and 55.8 ppm, respectively) and in the resulting LiI complexes (^{1}H: 4.02 and 4.01 ppm; ^{13}C: 58.3 and 58.3 ppm), while the ^{7}Li shifts are more variant (2.11 and 1.85 ppm).

For **28**•$LiBPh_4$, symmetrical coordination of Li^+ by the three oxygen atoms of the ligand is again suggested by ^{1}H (Figure 3.2) and ^{13}C NMR. However, the methoxy ^{1}H, ^{13}C, and ^{7}Li resonances of this complex are shifted upfield from their counterparts in **28**•LiI. Like the latter complex, **28**•$LiBPh_4$ can be envisioned as an intimate ion pair in which the BPh_4^- ion completes the coordination sphere of the tripod-bound Li^+ ion. In related work, the ion pair formation constants in 1,2-dichloroethane solution are reported to be 1660 M^{-1} and 7400 M^{-1} for dibenzo-18-crown-6•$LiBPh_4$ and triphenylphosphine oxide•$LiBPh_4$, respectively.[127]

Figure 3.1b shows the structure of **28**•$LiBPh_4$ as calculated by MNDO. The upfield chemical shifts above can be understood as resulting from ring current effects due to the BPh_4^- phenyl groups. This view is strongly supported by two additional findings: the ^{7}Li resonance is much broader in **28**•$LiBPh_4$ than in **28**•LiI ($\Delta\nu_{1/2}$ = 41 Hz vs. 1 Hz), and the BPh_4^- *ortho* protons are shifted roughly 0.2 ppm downfield compared to their chemical shifts in **45**•$LiBPh_4$, **45**•$NaBPh_4$, and **28**$_2$•$NaBPh_4$, complexes in which the metal cation is shielded from direct contact with the BPh_4^- counterion (vide infra). Analogous time-averaged interactions

Table 3.1. NMR Data for **28**, **45** and Related Li^+, Na^+, and K^+ Complexes in $CDCl_3$ at 20 °C

Species	$\delta(OCH_3$, ppm)	$\delta(OCH_2$, ppm)	$\delta(M^+$, ppm)	k_{ex} (s^{-1})	$\Delta G^{\ddagger}$ (kJ mol^{-1})
Free ligand **28**	3.54				
28•LiI	4.02		2.11[a]	333 (283 K)[b]	
28•$LiBPh_4$	3.45		–0.08[a]		
$\mathbf{28}_2$•$NaBPh_4$	3.24		–11.9[c]		
$\mathbf{28}_2$•$NaB(4\text{-}ClPh)_4$	3.24		–10.3[c]		
Free ligand **45**	3.51	3.38			
45•2LiI	4.01	4.04	1.85[a]		
45•$LiBPh_4$	3.38	3.21	0.15[a]		
45•NaI	3.37, 3.06	3.84	d	d	d
45•$NaBPh_4$	3.14, 2.88	3.23, 2.95	–5.5[c]	0.96 ± 0.12	71.8 ± 0.3
45•$NaB(4\text{-}ClPh)_4$	3.23, 2.94	3.49, 3.39	–5.3[c]	1.02 ± 0.14	71.7 ± 0.3
45•$KB(4\text{-}ClPh)_4$	3.40, 3.13	3.23		7.40 ± 0.40	66.8 ± 0.1

[a]Referenced to external 0.30 M LiCl in methanol. [b]The coalescence rate constant k_c (coalescence temperature T_c) determined by dynamic NMR; this value is the rate of Li^+ exchange. [c]Referenced to external 3.0 M aqueous NaCl. [d]The low solubility of **45**•NaI in $CDCl_3$ precluded ^{23}Na and dynamic NMR measurements.

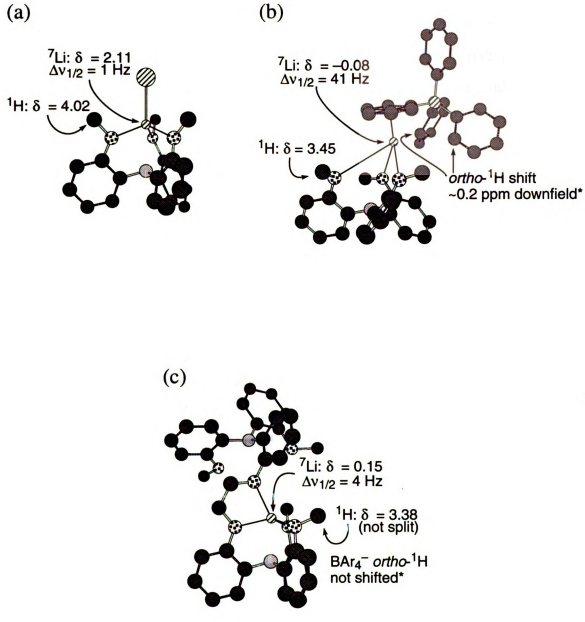

*Relative to any $NaBAr_4$ complex

Figure 3.1. MNDO-calculated structures of Li^+ complexes presented with salient NMR data obtained on $CDCl_3$ solutions: (a) **28**•LiI; (b) **28**•$LiBPh_4$; and (c) **45**•Li^+.

between Cs^+ ions and BPh_4^- *ortho* protons have been uncovered by Bauer in ^{133}Cs, ^1H HOESY (heteronuclear Overhauser and exchange spectroscopy) NMR studies of $CsBPh_4$ contact ion pairs in pyridine solution.[128] Unfortunately, our ^6Li, ^1H HOESY[129] NMR study of **28**•$^6LiBPh_4$ in $CDCl_3$ did not reveal any interactions between the complexed Li^+ ion and the BPh_4^- counterion.

In each of the three Li^+ complexes discussed above, the counterion caps a Li^+ ion bound in an ether tripod. The 1:1 ligand:salt stoichiometry found for complex **45**•$LiBPh_4$ implies a different binding motif, in which the Li^+ ion is sandwiched between the two triether tripods of **45**. Two additional comparisons lend support to this picture: First, the ^7Li linewidth of **45**•$LiBPh_4$ is narrow ($\Delta\nu_{1/2}$ = 4 Hz), indicating a more symmetrical ^7Li coordination sphere than that in **28**•$LiBPh_4$; second, as noted above, the *ortho* protons of the BPh_4^- phenyl rings do not exhibit the downfield shifting seen in **28**•$LiBPh_4$. Thus, the second tripod ether is preferred over the BPh_4^- counterion as a capping ligand when the triarylamine subunits are covalently linked. Consistent with this finding, the ^7Li $\Delta\delta$ between **45**•2LiI and **45**•$LiBPh_4$ (+1.70 ppm) is smaller than that between **28**•LiI and **28**•$LiBPh_4$ (+2.19 ppm). The ^1H NMR spectrum of **45**•$LiBPh_4$ is shown in Figure 3.3, and the MNDO-calculated structure of the complex is presented in Figure 3.1c.

Although Li^+ displays variable complex stoichiometries, Na^+ is only taken up by *pairs* of tripods. Complexes $\mathbf{28}_2$•$NaBPh_4$ and $\mathbf{28}_2$•$NaB(4\text{-}ClPh)_4$ are symmetrical on the NMR timescale, as shown by the simplicity of their ^1H and ^{13}C spectra; the ^1H NMR spectrum of $\mathbf{28}_2$•$NaBPh_4$ is shown

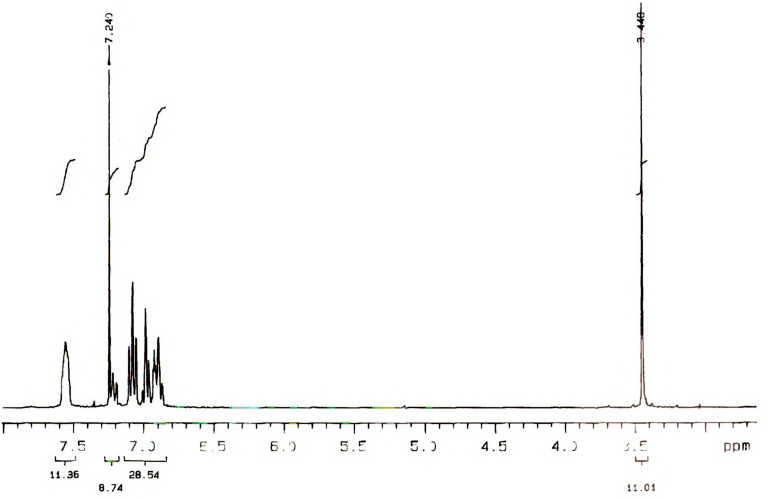

Figure 3.2. 300 MHz ^{1}H NMR spectrum of **28**•$LiBPh_4$ in $CDCl_3$.

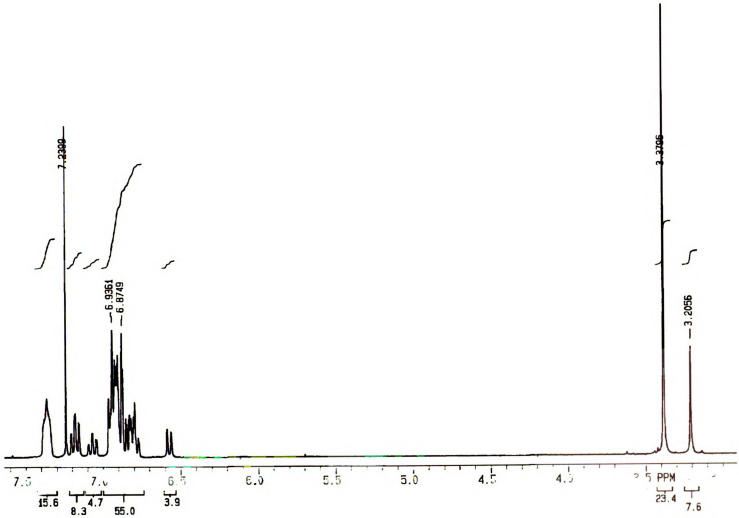

Figure 3.3. 300 MHz ^{1}H NMR spectrum of **45**•$LiBPh_4$ in $CDCl_3$.

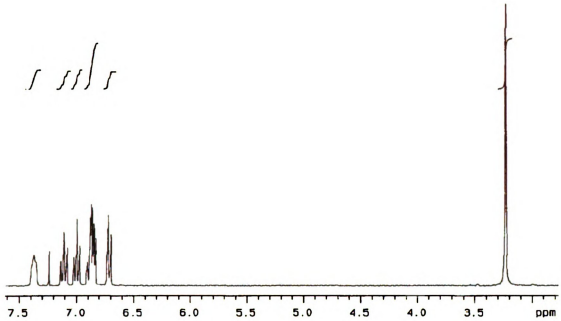

Figure 3.4. 300 MHz ^{1}H NMR spectrum of **28**$_2$•$NaBPh_4$ in $CDCl_3$.

in Figure 3.4. As in the complexes of **45** with $NaBPh_4$, $NaB(4\text{-}ClPh)_4$, and NaI, their methoxy ^{1}H resonances shift upfield relative to that of free ligand. In the **45**•Na^+ complexes, the ^{23}Na chemical shifts are independent of the BAr_4^- counterion but are somewhat sensitive to the nature of the solvent. The ^{23}Na chemical shift for **45**•$NaBPh_4$ is –5 ppm ($\Delta\nu_{1/2}$ = 250 Hz) in $CDCl_3$/acetone-d_6 (7:1, v/v) and –5.9 ppm ($\Delta\nu_{1/2}$ = 160 Hz) in $CDCl_3$/acetone-d_6 (1:1, v/v). In the presence of excess $NaBPh_4$, two ^{23}Na signals are observed in $CDCl_3$/acetone-d_6 (7:1, v/v) at –5 ppm (complexed Na^+) and –10 ppm (solvated Na^+). A similar experiment in $CDCl_3$/acetone-d_6 (1:1, v/v), however, shows only a single, population-averaged signal. The ^{23}Na chemical shift for 0.03 M $NaBPh_4$ is –10.4 ppm ($\Delta\nu_{1/2}$ = 76 Hz) in $CDCl_3$/acetone-d_6 (7:1, v/v) and –7.4 ppm ($\Delta\nu_{1/2}$ = 14 Hz) in

$CDCl_3$/acetone-d_6 (1:1, v/v). In comparison, the ^{23}Na chemical shift for 0.03 M **28**$_2$•$NaBPh_4$ is –8.2 ppm ($\Delta\nu_{1/2}$ = 107 Hz) in $CDCl_3$/acetone-d_6 (7:1, v/v) and –7.6 ppm ($\Delta\nu_{1/2}$ = 14 Hz) in $CDCl_3$/acetone-d_6 (1:1, v/v). Addition of one equivalent of $NaBPh_4$ to each of these solutions results in a single, population-averaged signal at –8.4 ppm ($\Delta\nu_{1/2}$ = 120 Hz) and at –7.6 ppm ($\Delta\nu_{1/2}$ = 17 Hz), respectively. In $CDCl_3$ solution, the ^{23}Na shifts for **28**$_2$•$NaBPh_4$ and **45**•$NaBPh_4$ are –11.9 ppm ($\Delta\nu_{1/2}$ = 240 Hz) and –5.5 ppm ($\Delta\nu_{1/2}$ = 260 Hz), respectively (see Table 3.1 and Chapter 5).

It is generally observed that ^{23}Na chemical shifts move upfield both with decreased solvent donicity[130] and with lowered Na^+ coordination number by oxygen ligands.[131] Thus, the upfield changes in ^{23}Na chemical shifts from **45**•$NaBPh_4$ and **45**•NaB(4-ClPh)$_4$ to **28**$_2$•$NaBPh_4$ and **28**$_2$•NaB(4-ClPh)$_4$, and the greater dependence of the latter two on solvent composition, imply that **28** is, as expected, the weaker ligand. As will be seen below, X-ray structural data also support these ideas. Competition and extraction experiments also indicate stronger binding of Na^+ by **45** than by **28**. Ligand **45** is competitive with 18-crown-6 for $NaBPh_4$ in dry $CDCl_3$; similarly, a $CDCl_3$ solution of **45** extracts $NaBPh_4$ from D_2O almost quantitatively, as determined by ^1H NMR. Unlike **45**, ligand **28** is completely unable to compete with D_2O for $NaBPh_4$. Finally, neither **28** nor **45** is a strong enough ligand to compete with D_2O for LiI or $LiBPh_4$.

In complexes **45**•$NaBPh_4$, **45**•NaB(4-ClPh)$_4$, **45**•NaI, and **45**•KB(4-ClPh)$_4$, the methoxy resonances of **45** split into two equal intensity peaks; the methylene resonances split into an apparent AB quartet with $NaBPh_4$ (Figure 3.5) and NaB(4-ClPh)$_4$, but only broaden with NaI and

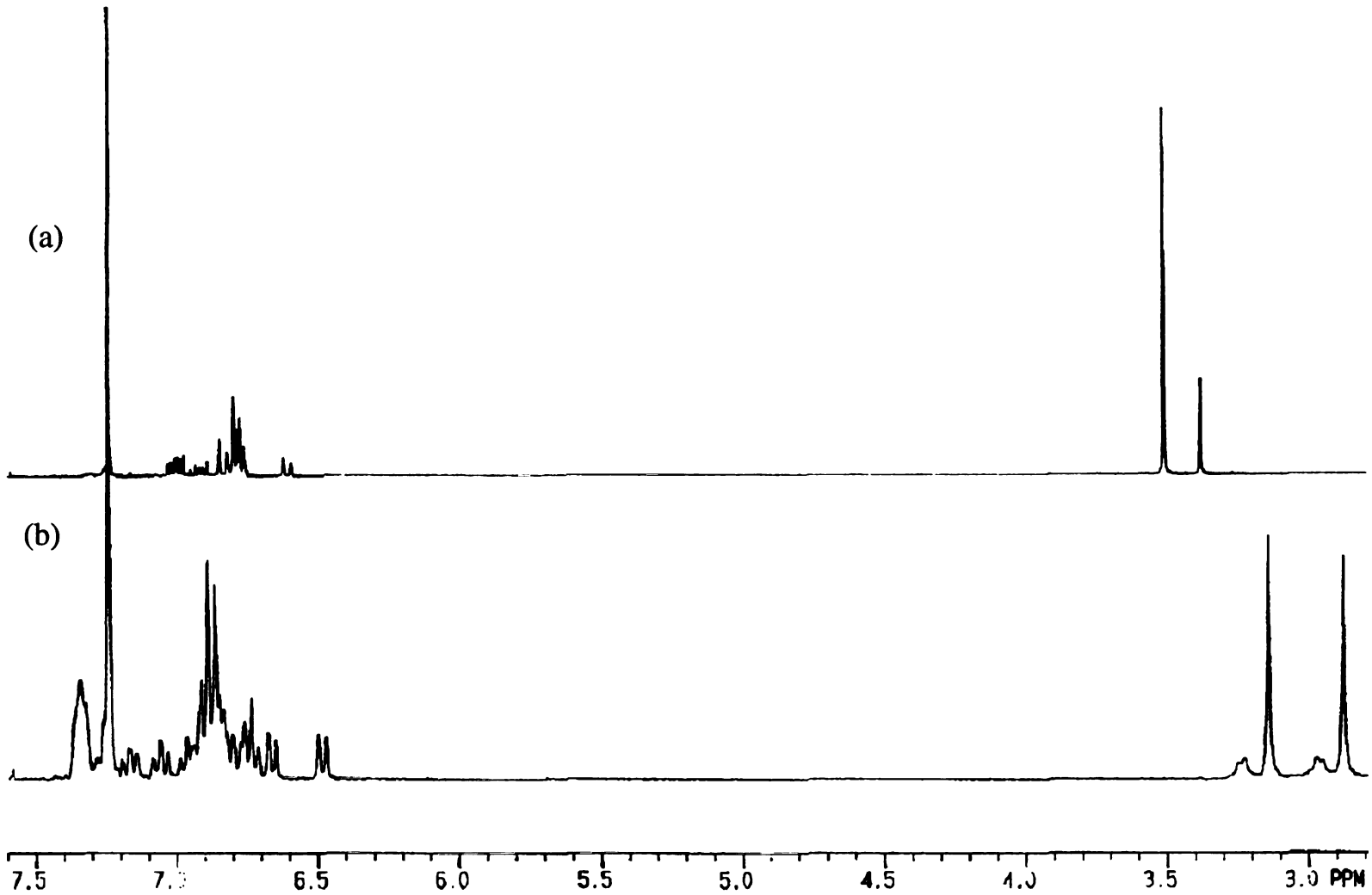

Figure 3.5. 300 MHz ^{1}H NMR spectra of (a) **45** and (b) **45**•$NaBPh_4$ in $CDCl_3$.

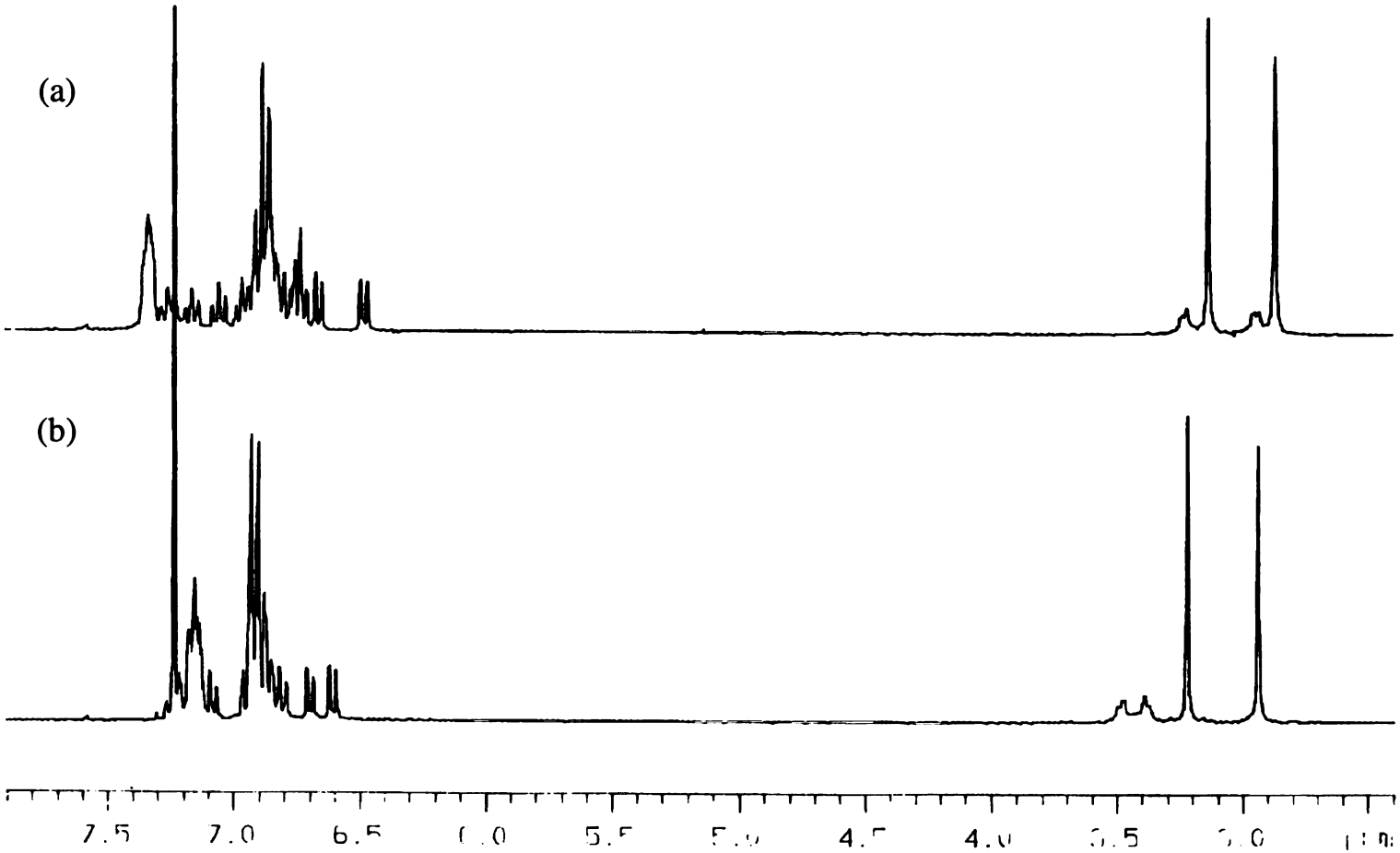

Figure 3.6. 300 MHz ^{1}H NMR spectra of (a) **45**•$NaBPh_4$ and (b) **45**•$NaB(4\text{-}ClPh)_4$ in $CDCl_3$.

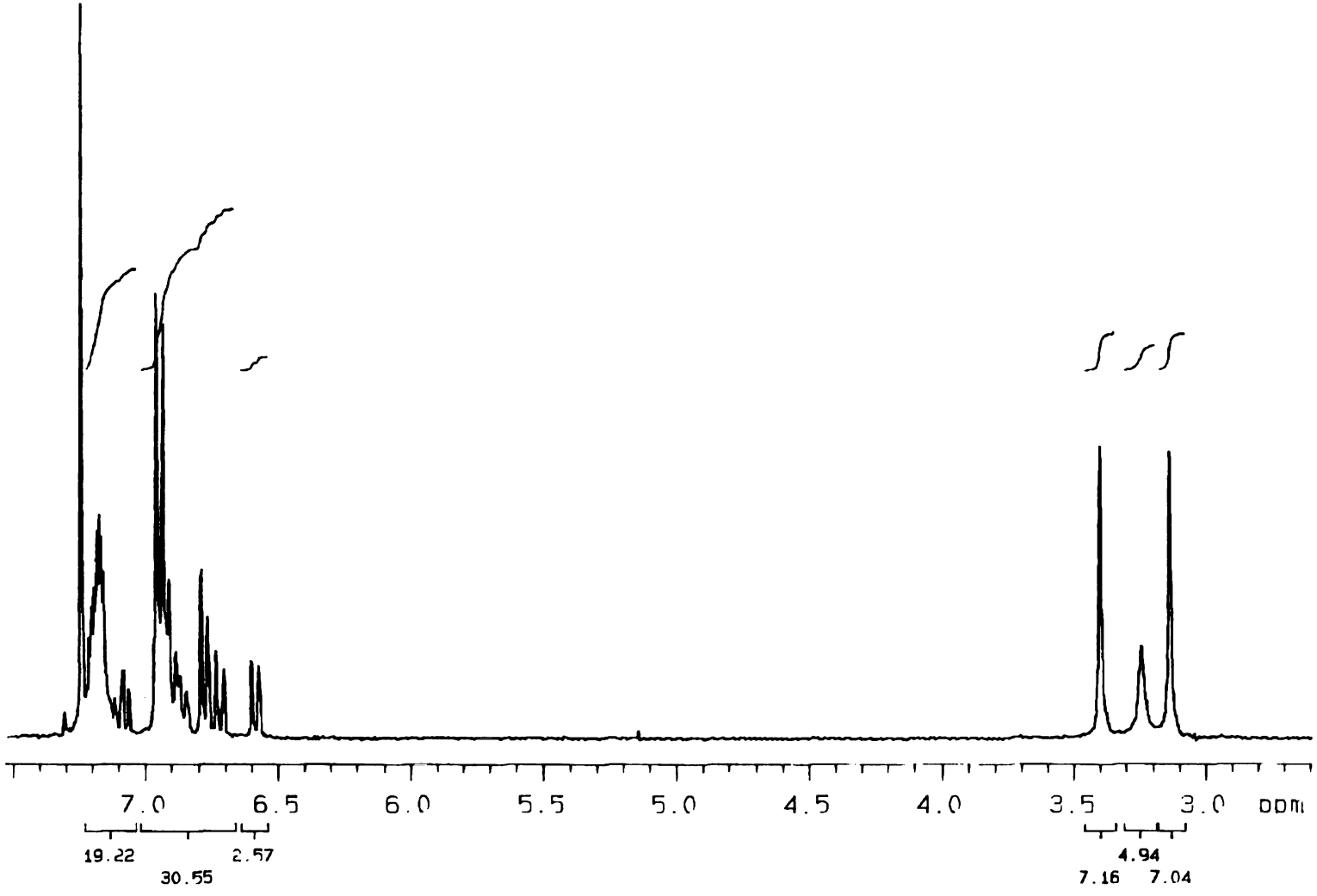

Figure 3.7. 300 MHz ^{1}H NMR spectrum of **45**•KB(4-ClPh)$_4$ in $CDCl_3$.

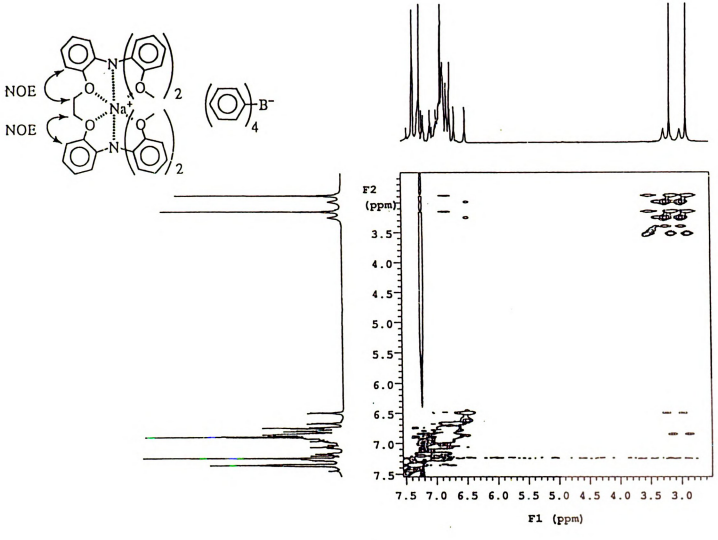

Figure 3.8. Contour plot of the 500 MHz ^{1}H ROESY spectrum of **45**•$NaBPh_4$ ($CDCl_3$, 0.03 M, 25 °C) which shows no interionic NOEs.

$KB(4\text{-}ClPh)_4$. These results suggest that Na^+ or K^+ binding locks the triarylamine subunits of **45** into propeller conformations, differentiating the methoxy sites into two sets on the NMR timescale at room temperature. Figure 3.6 shows the ^1H NMR spectra of **45**•$NaBPh_4$ and **45**•$NaB(4\text{-}ClPh)_4$, while the spectrum of **45**•$KB(4\text{-}ClPh)_4$ is displayed in Figure 3.7.

Lower limits on the binding energies of **45** with Na^+ and K^+ were obtained by measuring the rates of methoxy group site exchange (k_{ex}) in **45**•Na^+ and **45**•K^+ using the saturation spin transfer (SST) technique.[132] In $CDCl_3$ at 20 °C, the measured rate constants translate into $\Delta G^{\ddagger}$ values of 71.8 and 66.8 kJ mol^{-1}, respectively (see Table 3.1). The k_{ex} and $\Delta G^{\ddagger}$ values for complex **45**•Na^+ with BPh_4^- and $B(4\text{-}ClPh)_4^-$ counterions are equal within our uncertainties; evidently the site exchange barriers are not differentially affected by these anions despite differences in the ^1H NMR spectra shown in Figure 3.6. Unfortunately, although the ^1H NMR spectrum of **45**•NaI showed the methoxy group splitting characteristic of the other Na^+ complexes, its limited solubility precluded ^{13}C, ^{23}Na, and SST NMR measurements.

In $CDCl_3$ solution, all of the systems discussed here are expected to exist as tight ion pairs.[125,133] However, for the tripod ether complexes of Na^+ and K^+, variations in the counterions have negligible effects on the ^{13}C and ^{23}Na chemical shifts. The ^{13}C spectra for **45**•$NaBPh_4$ and **45**•$NaB(4\text{-}ClPh)_4$ show only minuscule differences, as do those for $\mathbf{28}_2$•$NaBPh_4$ and $\mathbf{28}_2$•$NaB(4\text{-}ClPh)_4$. As noted above, ^{23}Na spectra of **45**•Na^+ are insensitive to the BAr_4^- counterion, as are the rate constants for methoxy group site exchange. Excepting the case of **28**•$LiBPh_4$, evidence for ion interactions is

also lacking in the ^{1}H and ^{13}C spectra of the tetraarylborate anions, which are essentially unaffected by the nature of the complex cations (i.e. **28**$_2$•Na^+, **45**•Li^+, and **45**•Na^+ with BPh_4^-; **28**$_2$•Na^+, **45**•Na^+, and **45**•K^+ with $B(4\text{-}ClPh)_4)^-$).

The probes that should be most sensitive to ion pairing are the nuclei that make up the surfaces of groups around the "waist" of the ellipsoidal complex; here an anion can most closely approach the center of positive charge. Indeed, substantial variations are observed in the methoxy and especially the methylene ^{1}H chemical shifts for **45**•NaX (where X = I^-, BPh_4^-, $B(4\text{-}ClPh)_4)^-$). However, both one-dimensional NOE and two-dimensional ^{1}H ROESY[134] (rotating frame Overhauser effect spectroscopy) NMR experiments on **45**•$NaBPh_4$ failed to show interionic NOEs between the BPh_4^- counterion and the **45**•Na^+ core; the ^{1}H ROESY NMR spectrum is shown in Figure 3.8. Furthermore, the identical methoxy ^{1}H chemical shift values found in **28**$_2$•$NaBPh_4$ and **28**$_2$•$NaB(4\text{-}ClPh)_4$ indicate that interpretations of ion pairing should be made cautiously.

3.3. X-ray Studies of Metal Complexes

Crystals of **28**$_2$•$NaBPh_4$, **45**•$NaBPh_4$, **45**•$NaB(4\text{-}ClPh)_4$, **45**•$KB(4\text{-}ClPh)_4$•CH_3NO_2, and free **45** have been analyzed by X-ray diffraction; fractional coordinates for the compounds are given in Tables 3.2A–3.6A in the Appendix. Crystallographic data for these compounds can be found in Table 3.7, and selected geometrical information is compared in Table 3.8. Drawings with partial atom-labeling schemes (counterions omitted) for **28**$_2$•$NaBPh_4$; **45**•$NaB(4\text{-}ClPh)_4$ and **45**•$KB(4\text{-}ClPh)_4$•CH_3NO_2; and **45**

Table 3.7. Crystallographic Data for $\mathbf{28}_2$•$NaBPh_4$, **45**•$NaBPh_4$, **45**•$NaB(4\text{-}ClPh)_4$, **45**•$KB(4\text{-}ClPh)_4$•CH_3NO_2, and **45**

	28_2•$NaBPh_4$	45•$NaBPh_4$	45•NaB(4-ClPh)$_4$	45•KB(4-ClPh)$_4$•CH_3NO_2	45
formula	$C_{66}H_{62}BN_2NaO_6$	$C_{66}H_{60}BN_2NaO_6$	$C_{66}H_{56}BCl_4N_2NaO_6$	$C_{67}H_{59}BCl_4KN_3O_8$	$C_{42}H_{40}N_2O_6$
fw	1013.04	1011.02	1148.80	1225.96	668.80
$F(000)$	2160	1068	2392	1276	708
space group	$P2_1/c$	$P\bar{1}$	$P2_1/n$	Pn	$P\bar{1}$
crystal system	monoclinic	monoclinic	monoclinic	monoclinic	monoclinic
Z	4	2	4	2	2
a, Å	10.701(3)	12.157(1)	13.652(5	13.663(4)	8.068(1)
b, Å	37.593(3)	14.811(1)	18.75(1)	12.228(3)	14.599(2)
c, Å	13.774(2)	15.860(2)	22.80(5)	18.712(8)	16.475(3)
α, deg		105.400(8)			115.43(1)
β, deg	98.24(2)	91.594(9)	92.21(5)	91.45(3)	92.51(1)
γ, deg		95.354(8)			90.40(1)
V, Å^3	5483(3)	2737.(1)	5832(10)	3125(3)	1750.1(9)
D_c, g cm^{-3}	1.227	1.227	1.308	1.303	1.269
μ(Mo K$_\alpha$), cm^{-1}	0.79	0.79	2.62	3.10	0.79
$2\theta_{max}$, deg	50	55	47	47	55
final R[a]	0.056	0.108	0.051	0.055	0.102
final R_w[b]	0.057	0.132	0.056	0.061	0.101

[a]$R = ||F_o| - |F_c||/\Sigma|F_o|$. [b]$R_w = \{\Sigma w(|F_o| - |F_c|)^2/\Sigma w|F_o|^2\}^{1/2}$; $w = 1/\sigma^2(|F_o|)$.

Table 3.8. Selected Distances (Å), Angles (deg), and Torsion Angles (deg) in **28**$_2$•$NaBPh_4$, **45**•$NaBPh_4$, **45**•$NaB(4\text{-}ClPh)_4$, **45**•$KB(4\text{-}ClPh)_4$•CH_3NO_2, and **45**

	28_2•$NaBPh_4$	45•$NaBPh_4$	45•NaB(4-ClPh)$_4$	45•KB(4-ClPh)$_4$•CH_3NO_2	45
rN1···N2	5.25(1)	5.41(1)	5.316(5)	5.82(1)	7.91(1)
rM–N1	2.710(6)	2.682(8)	2.677(6)	2.95(1)	
rM–N2	2.677(7)	2.726(8)	2.685(6)	2.93(1)	
rM–O1	2.543(6)	2.524(8)	2.457(5)	2.654(9)	
rM–O2	2.516(6)	2.532(8)	2.428(5)	2.69(1)	
rM–O3	2.584(6)	2.490(8)	2.524(5)	2.792(9)	
rM–O4	2.521(6)	2.489(8)	2.491(5)	2.712(9)	
rM–O5	2.503(6)	2.453(8)	2.466(5)	2.78(1)	
rM–O6	2.726(6)	2.458(8)	2.485(5)	2.73(1)	
∠N–M–N	154.5(2)	178.6(3)	178.1(2)	164.5(5)	
τO3–C–C–O4		65.3(9)	62.29(6)	71.23(2)	84(1)
τM–N1–C_N–C_{O1}[a]	45.9(6)	32.9(5)	33.3(1)	–25.21(1)	–40(1)[b]
τM–N1–C_N–C_{O2}[a]	28.5(7)	29.4(5)	26.2(1)	–35.11(1)	–53(1)[b]
τM–N1–C_N–C_{O3}[a]	45.7(6)	48.2(5)	43.6(1)	–52.25(1)	–44(1)[b]
τM–N2–C_N–C_{O4}[a]	51.0(6)	48.5(5)	50.4(1)	–53.51(1)	47(1)[b]
τM–N2–C_N–C_{O5}[a]	23.7(7)	33.4(5)	30.0(1)	–33.14(1)	35(1)[b]
τM–N2–C_N–C_{O6}[a]	44.8(7)	34.2(5)	30.8(1)	–52.19(1)	47(1)[b]

[a]C_N and C_O are the N- and O-linked aryl carbons of interest. [b]For **45**, these values represent torsions relative to the pseudo threefold axis of the amine center, defined for each aryl ring as the average of two τC'_NN$C_N$$C_O$ angles, where C_N and C_O are the N- and O-linked aryl carbons of interest, and C'_N are the two other aryl carbons on the same nitrogen.

alone are given in Figures 3.9, 3.10, and 3.11, respectively. Complex **45**•$NaBPh_4$ is not displayed since its **45**•Na^+ core is visually indistinguishable from that in **45**•$NaB(4\text{-}ClPh)_4$.

In $\mathbf{28}_2$•$NaBPh_4$, the eight-coordinate Na^+ ion is sandwiched between two polyether tripods with Na–N distances of 2.677(7) and 2.710(6) Å and six Na–O distances averaging 2.565(6) Å. One Na–O distance is elongated (2.726(6) Å) relative to the other five (2.503(6)-2.583(6) Å; average = 2.533(6) Å), distorting the coordination sphere from an ideal bicapped octahedron. Excluding the long Na–O interaction, these distances are comparable to the Na–N (2.682(8) and 2.726(8) Å) and Na–O (2.453(8)-2.524(8) Å; average 2.491(8) Å) lengths found in **45**•$NaBPh_4$, and the Na–N (2.677(6) and 2.685(6) Å) and Na–O (2.428(5)-2.524(5) Å; average 2.475(5) Å) lengths in **45**•$NaB(4\text{-}ClPh)_4$. In light of the threefold crystallographic axis through the nitrogen atom in free ligand **28**,[95] the nearly linear N–Na–N angles in **45**•$NaBPh_4$ (178.6(3)°) and **45**•$NaB(4\text{-}ClPh)_4$ (178.1(2)°), and the NMR data discussed above, the low symmetry and bent (∠N–Na–N = 154.5(2)°) geometry of $\mathbf{28}_2$•$NaBPh_4$ are unexpected. The structures of $\mathbf{28}_2$•$NaBPh_4$, **45**•$NaBPh_4$, and **45**•$NaB(4\text{-}ClPh)_4$ are similar in having approximate C_2 symmetry and hence homochiral pitches for the two triarylamine propellers; for **45**•$NaBPh_4$ and **45**•$NaB(4\text{-}ClPh)_4$, this geometry is exactly as expected from the solution NMR data described above. The disposition of the basic atoms in $\mathbf{28}_2$•$NaBPh_4$, **45**•$NaBPh_4$, and **45**•$NaB(4\text{-}ClPh)_4$ is reminiscent of that seen in [2.2.2] cryptand•Na^+ (C222•Na^+) structures. For comparison to the above values, the average Na–N and Na–O distances in C222•NaI are 2.75 and 2.57 Å, respectively.[135] The six benzene rings in the tripod ether complexes enforce eclipsed N–C–C–O angles;

notably, the analogous torsions in C222•Na^+ can be nearly eclipsed,[136] although they are typically skewed.[137]

In contrast to **45**•$NaBPh_4$ and **45**•$NaB(4\text{-}ClPh)_4$, the K^+ complex of **45** crystallizes as a nitromethane solvate (**45**•$KB(4\text{-}ClPh)_4$•CH_3NO_2) which readily loses solvent on standing. The nitromethane molecule does not appear to interact with the **45**•K^+ complex. The eight-coordinate K^+ ion is bound between two polyether tripods with K–N distances of 2.93(1) and 2.95(1) Å, and six K–O lengths averaging 2.73(1) Å. Relative to the **45**•Na^+ complexes, this structure shows an increased O–C–C–O torsion angle (71.23(2)°) and a markedly bent N–K–N angle (164.5(5)°). Such differences are as expected based on the larger size of K^+ vs. Na^+, and hence the longer M^+–heteroatom distances in **45**•$KB(4\text{-}ClPh)_4$•CH_3NO_2 compared to those in **45**•$NaBPh_4$ and **45**•$NaB(4\text{-}ClPh)_4$. These distances are comparable to the average K–N and K–O lengths of 2.87 and 2.79 Å, respectively, found in C222•KI.[138]

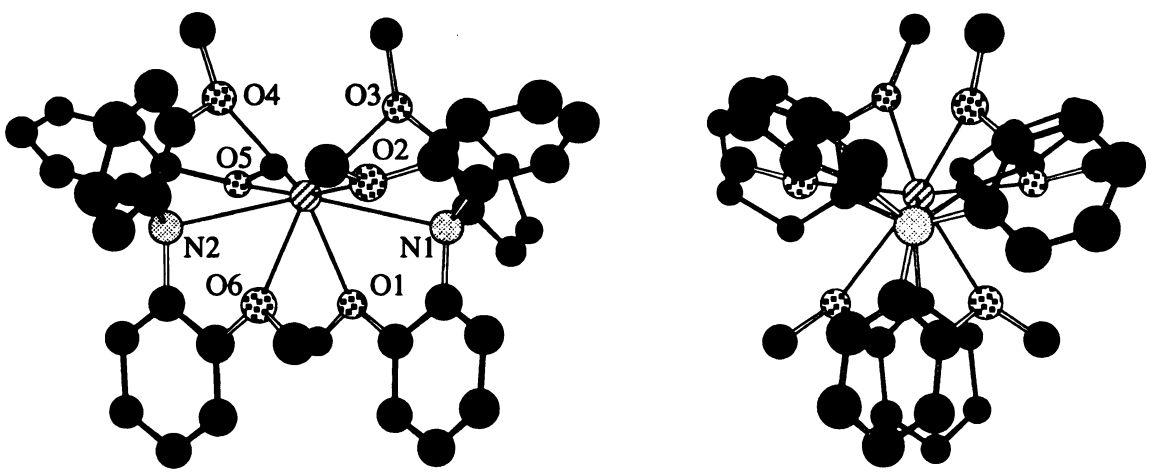

Figure 3.9. Side and end-on views of the X-ray structure of $\mathbf{28}_2$•$NaBPh_4$ (BPh_4^- counterion not shown).

(a)

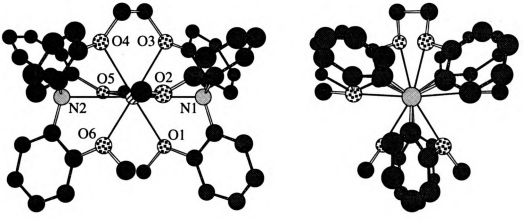

(b)

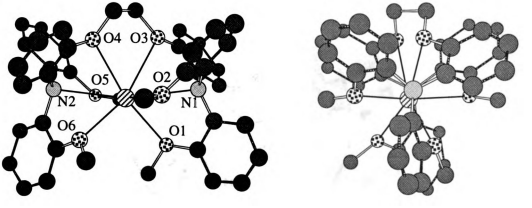

Figure 3.10. (a) Side and end-on views of the X-ray structure of **45**•NaB(4-ClPh)$_4$. (b) Side and end-on views of the X-ray structure of **45**•KB(4-ClPh)$_4$. For both structures, the B(4-ClPh)$_4^-$ counterion is not shown.

Free ligand **45** may be viewed as two linked molecules of **28** with similar aryl ring twist angles and nitrogen pyramidalization; as in **28**, each propeller's three alkoxy groups are on the same face.[95] Thus, the tripods of **45** represent convergent functionalities poised to encapsulate a suitable guest. Aryl methyl ethers ordinarily prefer a conformation with the methyl group and aryl ring coplanar, as seen for the methoxy groups of **28**,[95] **45**, and related *o*-methoxy substituted triaryl-Z propellers[139] described in Chapter 3. In anisole itself, the preference for a coplanar geometry has been estimated at 2-3 kcal/mol.[140] It is noteworthy, therefore, that the aryl-O bonds in the tether of **45** show large out-of-plane torsions ($\tau C_N–C_O–O–C_{H2}$ = 73.0° and 131.5°) which are relieved in **45**•M^+.

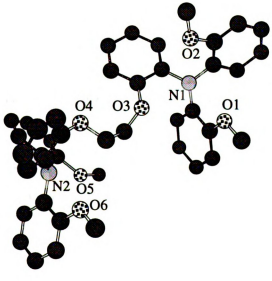

Figure 3.11. X-ray structure of **45**.

Although **45** is formally a podand,[88] it is a surprisingly strong ligand. As an open chain, six-fold benzannelated C222 analogue, **45** might be

expected to be a feeble ionophore, since bridge cleavage[88] and benzannelation[141] are both generally found to weaken the binding ability of C222.[142] However, scission of two bridges of C222 and benzannelation have opposite effects on the system's conformational flexibility. Two individually deleterious modifications thus offset each other, leaving **45** with substantial complexing ability.

When the last bridge in **45** is snipped, the now disconnected tripods **28** become much less effective complexants, as demonstrated above. These triarylamine propellers are free to rotate[96] to conformations in which the ether tripods are less ideally arranged than they appear in the crystal structure of **28**. Furthermore, the generally weak Lewis basicity of aryl substituted ethers[143] and amines[144] make the weak complexing ability of **28** unsurprising. What seems out of place is the strength of binding exhibited by **45**, since all of the above criticisms of **28** apply here as well. We can only surmise that in addition to the binding entropy decrease conferred by the tether, the complexation-induced strain relief suggested by the structures of free **45** and **45**•M^+ may also enhance binding. In any case, our observations indicate that biradical **46** should be an effective complexant, allowing further work to probe the effects of complexed metal ions on radical-radical interactions.

CHAPTER 4

TOWARD AN "INTERRUPTED σ-BOND"

We have made substantial progress toward a detailed understanding of the ion binding properties of our tripod ether systems. X-ray studies have yielded valuable structural characterization of the binding pocket in both free and complexed ligands, while NMR studies have examined the stoichiometries and dynamics of ion binding in solution. In the context of self-assembly, the modest success with amine **28** presents the possibilty of using radical **47** for the assemblage of a radical–metal ion–radical dimer structure like **24**. As noted in Chapter 3, the ion binding ability of amine **45** suggests that biradical **46** should be an excellent candidate to probe metal-ion-mediated pairwise electron coupling.

4.1. Syntheses of Paramagnetic Tripod Ether Ionophores

Triarylmethyl radicals are commonly generated by reduction of the corresponding triarylmethyl chlorides. Thus, **49** and **51** were sought as precursors to radical **47** and biradical **46**, respectively, as shown in Scheme 4.1.

Tris(2-methoxyphenyl)methanol (**48**)[108] was prepared (80%) by addition of methyl-2-methoxybenzoate to 2-methoxyphenylmagnesium bromide. Carbinol **48** in chloroform was treated with acetyl chloride, as described by Lund;[108] the results were as described, but the isolated product was a ~1:1 mixture of **49** and **48** (by ^{1}H NMR) which had the same melting point reported by Lund. Attempts to purify the desired chloride by fractional crystallization resulted in cocrystallization with carbinol **48**. Invariably, mixtures of **49** and **48** were obtained upon treatment of **48** with various halogenating agents under conditions that

have been used successfully in the preparation of other triarylmethyl halides.[145] Ishizu and coworkers mention the preparation of **49**—by treating **48** in methylene chloride with 2 equiv of $SOCl_2$—but no other details are given.[146] In our hands, this procedure affords not only chloride **49**, but also tris(2-methoxyphenyl)methane (**36**);[108] **48** is recovered. In contrast, reaction of **48** with $SOCl_2$ in benzene gave **49** as the major product, but with carbinol **48** as the impurity. Treatment of a benzene-d_6 solution of **48** with $SOCl_2$ and monitoring by ^{1}H NMR has shown that **48** is completely converted to **49** (Figure 4.1); however, evaporating the volatiles and then redissolving the residue in benzene-d_6 gives a mixture consisting of **49** and **48**. For our purposes, chloride **49** is best prepared, albeit as a mixture, by treating **48** in methylene chloride with ~10 equiv of $SOCl_2$. Using this procedure, a typical product mixture gives a **49/36** ratio of 31:1 by ^{1}H NMR (Figure 4.2). Although methane **36** is present as an impurity, it is diamagnetic, it shows no capacity for ion binding, and it should tolerate the reducing conditions used to prepare radical **47**.

Diol **50** was obtained (80%) by addition of 1,2-bis(2-carbethoxyphenyl)ethane to 2-methoxyphenylmagnesium bromide. As for the **48**→**49** transformation, difficulties were encountered in cleanly converting diol **50** to dichloride **51**. Saturation of a suspension of **50** in ether with anhydrous HCl gas, and standing overnight, gave a product mixture containing **51**, **50**, and the dimethane derivative **52**; presumably the latter product is formed by hydride abstraction from the solvent.[147] Reaction of **50** in methylene chloride with $SOCl_2$ gave an extremely complicated product mixture (by NMR), and no attempts were made to isolate and characterize these products. NMR experiments have shown that

Scheme 4.1.

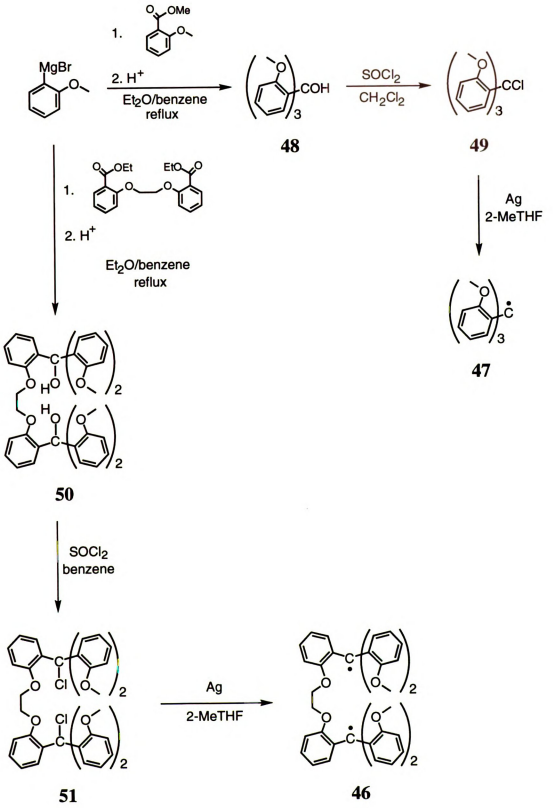
1.
OMe
MgBr
2. H+
Et2O/benzene
reflux
COH
3
48
SOCl2
CH2Cl2
CCl
3
49
Ag
2-MeTHF
C
3
47
1.
OEt
EtO
2. H+
Et2O/benzene
reflux
H
H
2
2
50
SOCl2
benzene
Cl
Cl
2
2
51
Ag
2-MeTHF
2
2
46

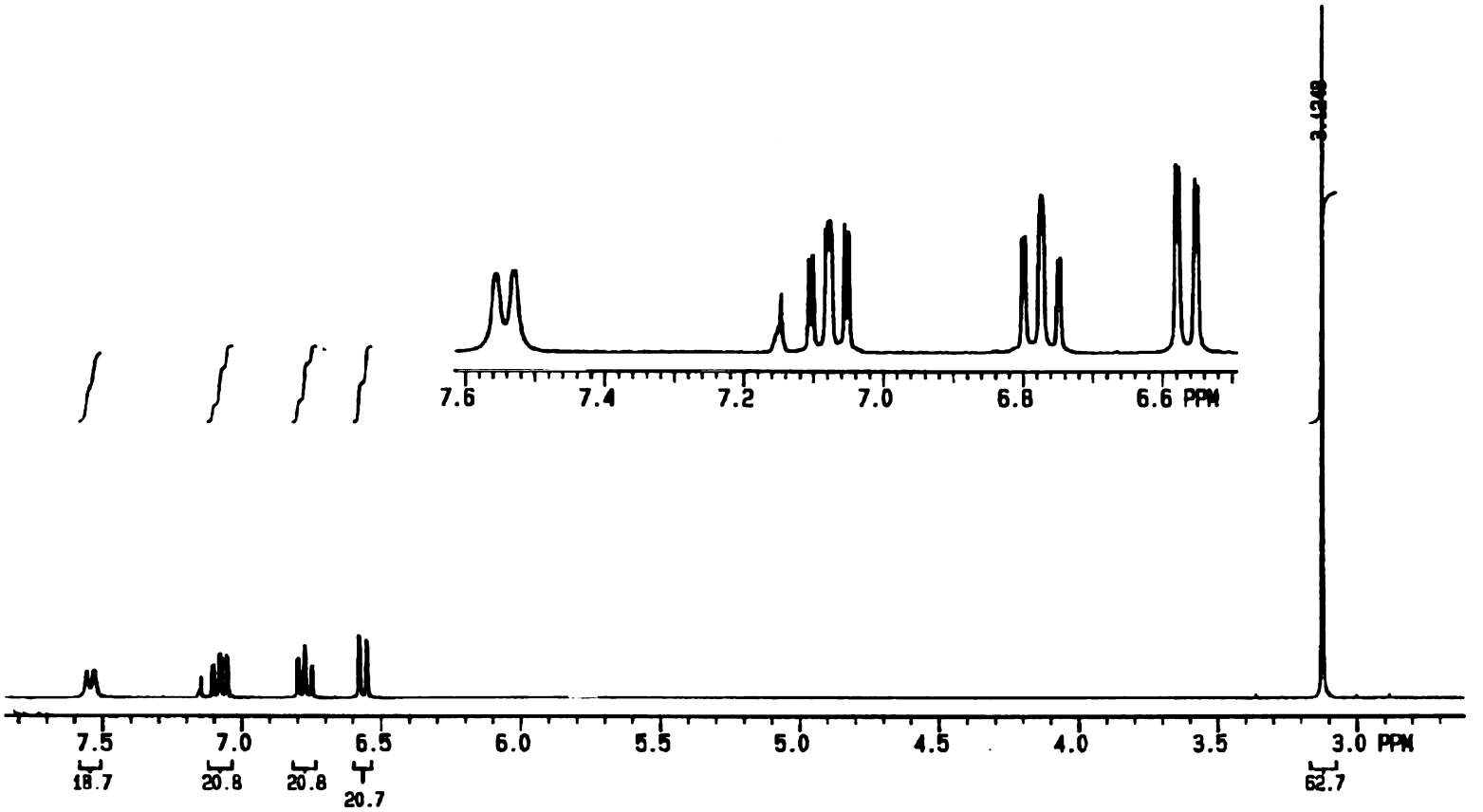

Figure 4.1. 300 MHz ^{1}H NMR spectrum of pure chloride **49** obtained on treatment of carbinol **48** in benzene-d_6 with excess $SOCl_2$ in an NMR tube.

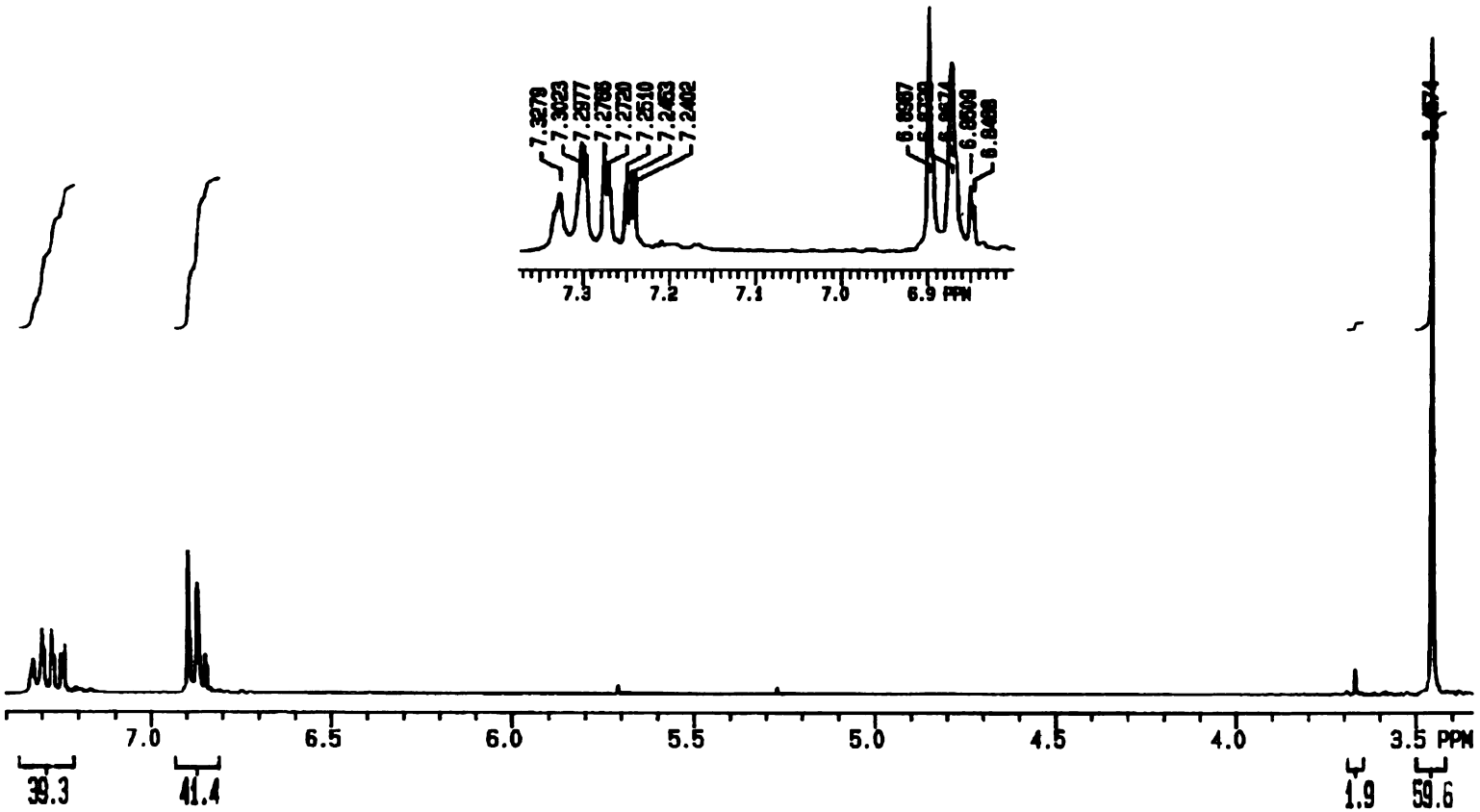

Figure 4.2. 300 MHz ^1H NMR spectrum ($CDCl_3$ solvent) showing the mixture of chloride **49** (major) and methane **36** (minor) obtained on treatment of carbinol **48** in CH_2Cl_2 with ~10 equiv of $SOCl_2$.

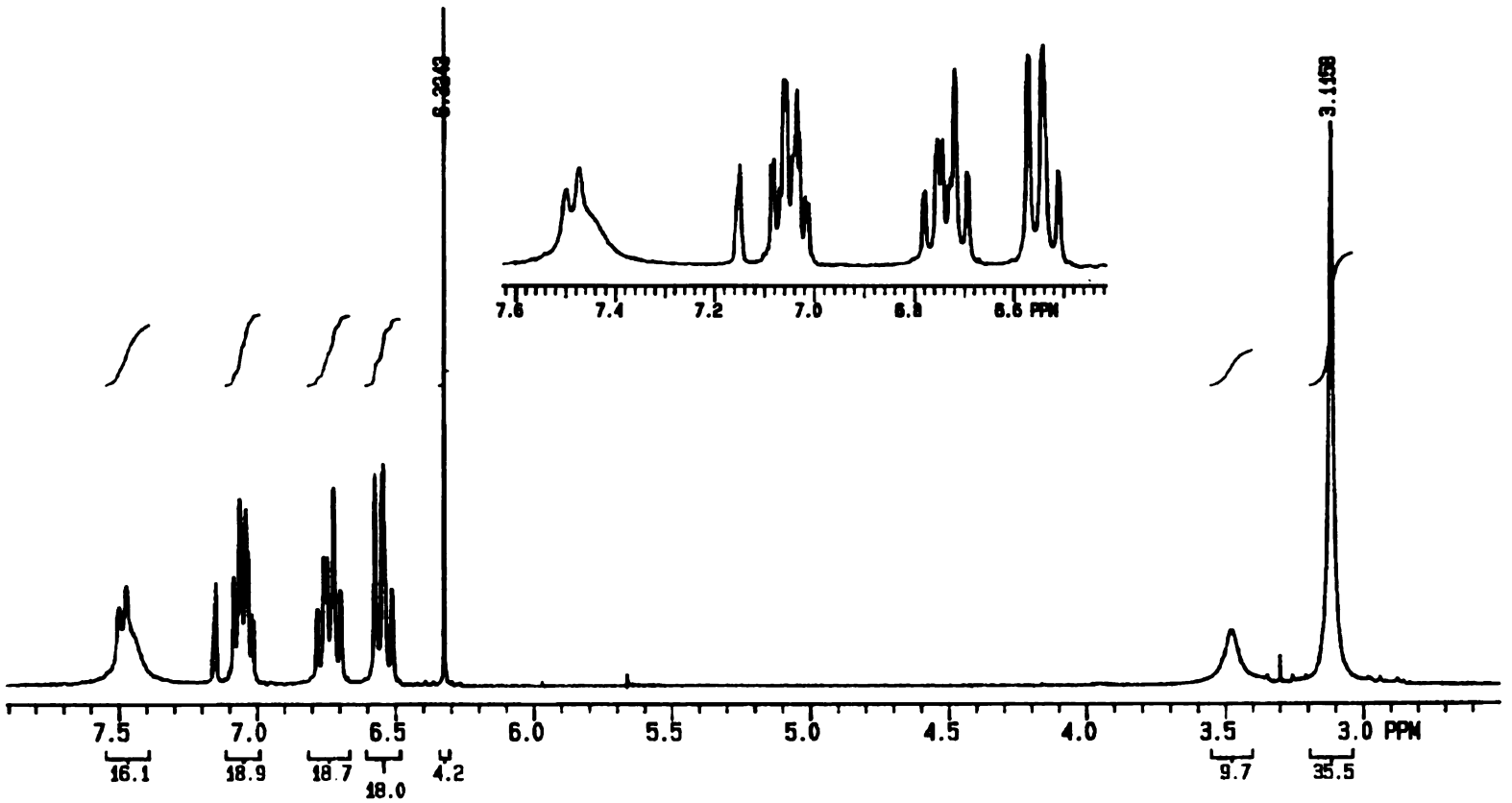

Figure 4.3. 300 MHz ^{1}H NMR spectrum of pure dichloride **51** obtained on treatment of diol **50** in benzene-d_6 with excess $SOCl_2$ in an NMR tube.

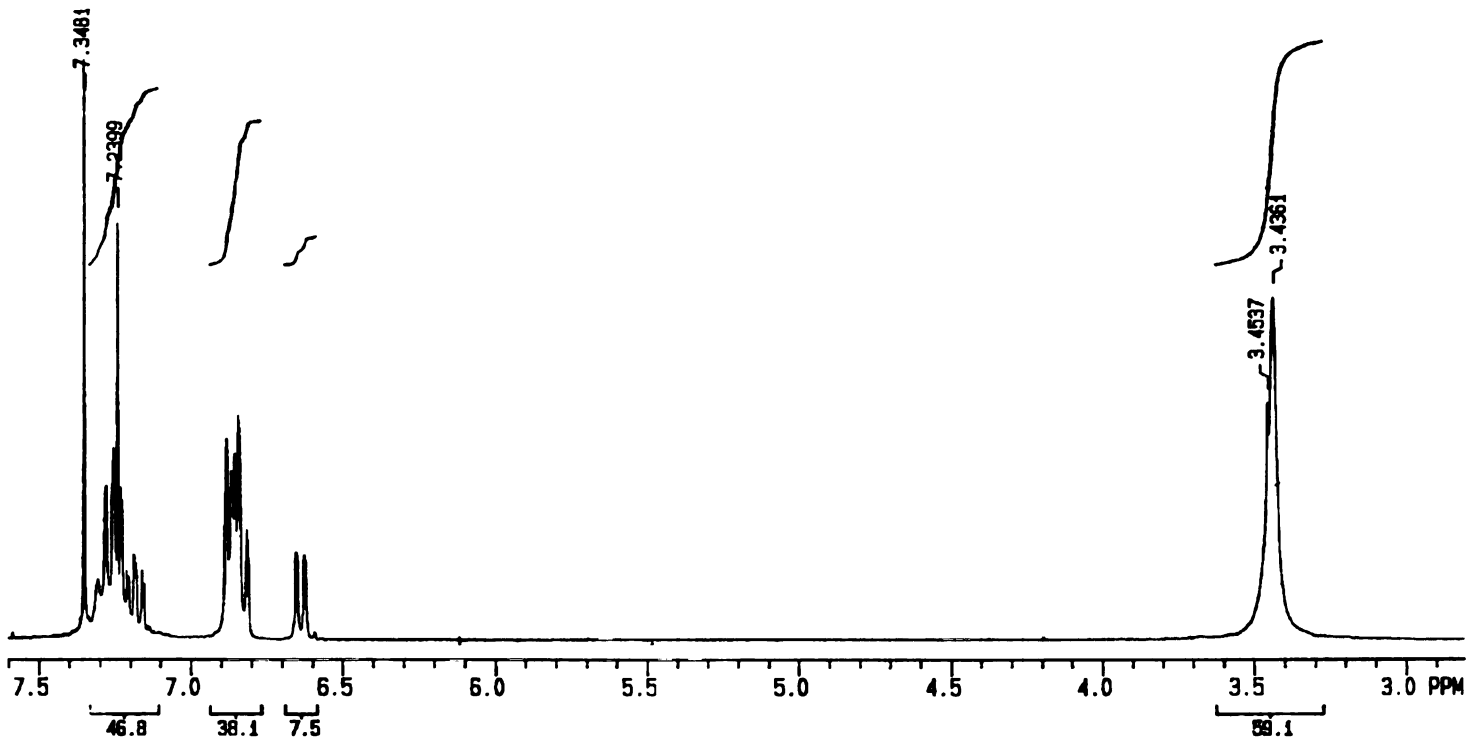

Figure 4.4. 300 MHz ^{1}H NMR spectrum ($CDCl_3$ solvent) of the mixture of dichloride **51** (major) and hydroxylic impurity (minor) obtained on treatment of diol **50** in benzene with ~20 equiv of $SOCl_2$.

diol **50** in benzene-d_6 is completely converted to dichloride **51** with $SOCl_2$ (Figure 4.3), but evaporation of the sample produces a mixture of **51** and **50**. We have found that dichloride **51** is best prepared, albeit as a mixture, by treating a benzene solution of **50** with ~20 equiv of $SOCl_2$; the product mixture consists of **51** (typically >95%), along with a small amount (<5%) of a hydroxlyic impurity (see Figure 4.4).

Treatment of chloride **49** or dichloride **51** with silver powder in dry, degassed 2-methyltetrahydrofuran (2-MeTHF) under argon produces a yellowish-orange solution of radical **47** or biradical **46**, respectively (Scheme 4.1); similar results are obtained in benzene, toluene, and chloroform. In contrast to radical **23**, both **47** and **46** are extremely oxygen sensitive and must be handled in the absence of air.

4.2. ESR Studies of Ion Binding

The room temperature ESR spectrum of **47** in 2-MeTHF is shown in Figure 4.5b; this spectrum shows excellent agreement with the simulated ESR spectrum (Figure 4.5a) that is generated using the proton hyperfine couplings[146] for **47** obtained from ENDOR measurements. For comparison, the room temperature ESR spectrum of **46** in 2-MeTHF is given in Figure 4.5c.

The $\Delta m_s = 1$ region of the ESR spectrum at 120 K for radical **47** in 2-MeTHF, shown in Figure 4.6a, is indicative of a doublet monoradical. In contrast, the $\Delta m_s = 1$ region of **46**, under the same conditions, consists of four symmetrical signals which are characteristic of a randomly oriented

Figure 4.5. (a) Simulated ESR spectrum of monoradical **47** generated with the proton hyperfine couplings[146] obtained from ENDOR measurements. (b) ESR spectrum of **47** in 2-MeTHF at room temperature. (c) ESR spectrum of biradical **46** in 2-MeTHF at room temperature.

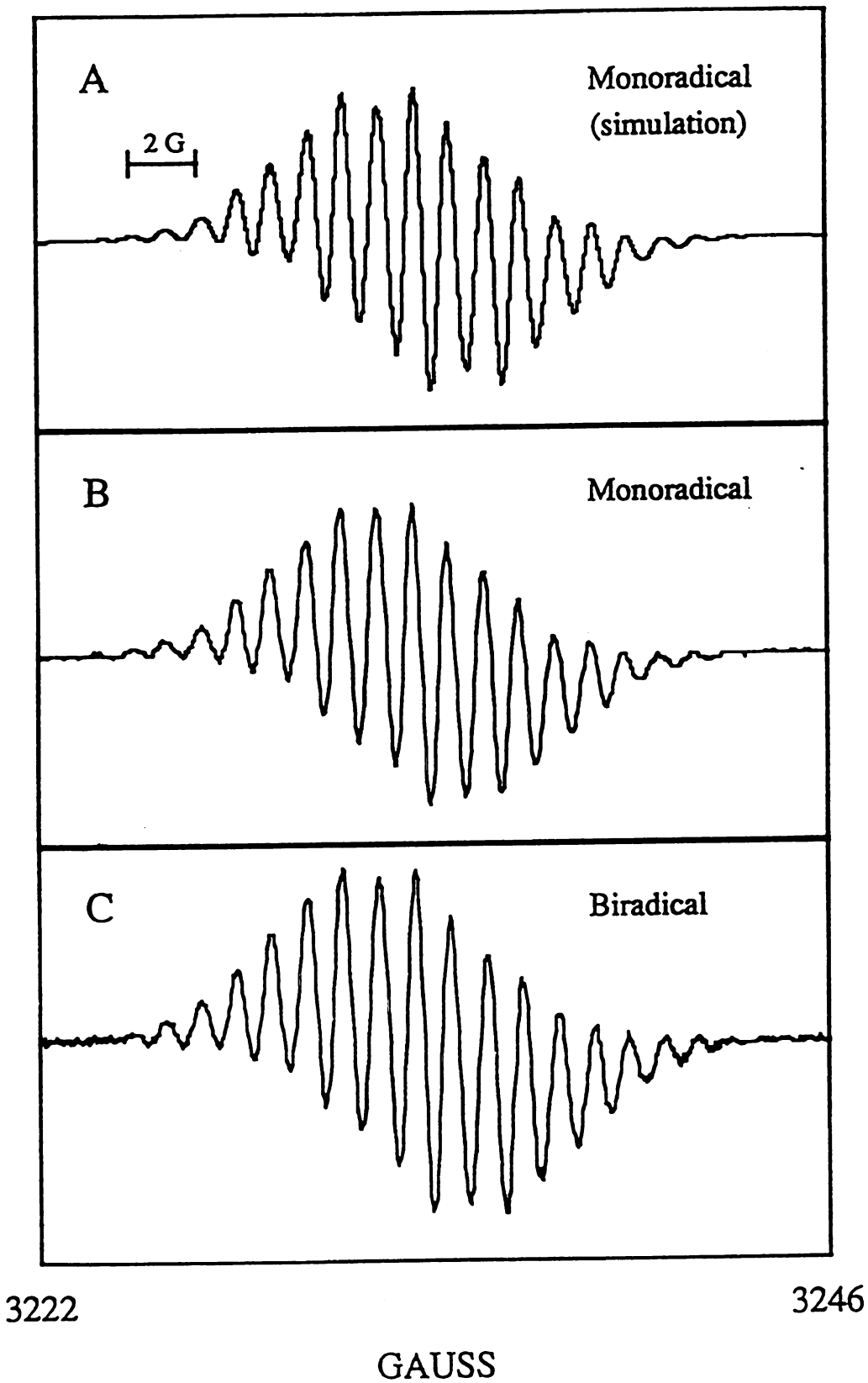
A
Monoradical
(simulation)
2 G
B
Monoradical
C
Biradical
3222
3246
GAUSS

triplet state (S = 1) biradical with the approximate zero-field degeneracy, $|E/hc| \approx 0$. The center peak in the spectrum corresponds to a doublet impurity, and is considerably more intense than the triplet peaks (Figure 4.7a). A half-field $\Delta m_s = 2$ transition is also observed, confirming the assignment of a triplet species. The other zero-field splitting parameter is $|D/hc| = 0.0051\ cm^{-1}$; within the point-dipole approximation, this D value corresponds to an average distance of ~8 Å between radical centers according to $R_{av}/Å = 1.375\ |D/cm^{-1}|^{-1/3}$.[148] Kurreck and coworkers have observed triplet ESR spectra for highly concentrated frozen solutions of tris(4-biphenylyl)methyl radical, and have interpreted these results as electron coupling between pairs of doublet monoradicals which form intermolecular D_3 π-complexes.[149] However, it seems unlikely that the triplet state observed for **46** is due to intermolecular spin coupling, since samples of monoradical **47** prepared at twice the concentration of **46** only show doublet spectra at 120 K. Finally, we note that the ESR spectrum of **46** at 120 K, both in frozen chloroform and frozen chloroform/acetone (7:1, v/v) solutions, shows a doublet signal in the $\Delta m_s = 1$ region; no half-field transition is detected in either case.

Samples of **47** and **46** in 2-MeTHF were treated with ~10 equiv of LiI, $NaBPh_4$, and $KB(4\text{-}ClPh)_4$. However, the ESR spectra of these homogeneous samples, either at room temperature or at 120 K, are essentially identical to those of **47** or **46** in the absence of added salt. The ESR spectrum of **47** in the presence of excess $NaBPh_4$ is displayed in Figure 4.6b, while the spectra of **46** in the presence of excess LiI, $NaBPh_4$, and $KB(4\text{-}ClPh)_4$ are presented in Figures 4.7b–d, respectively. Similarly, chloroform solutions of either **47** or **46** treated with the aforementioned

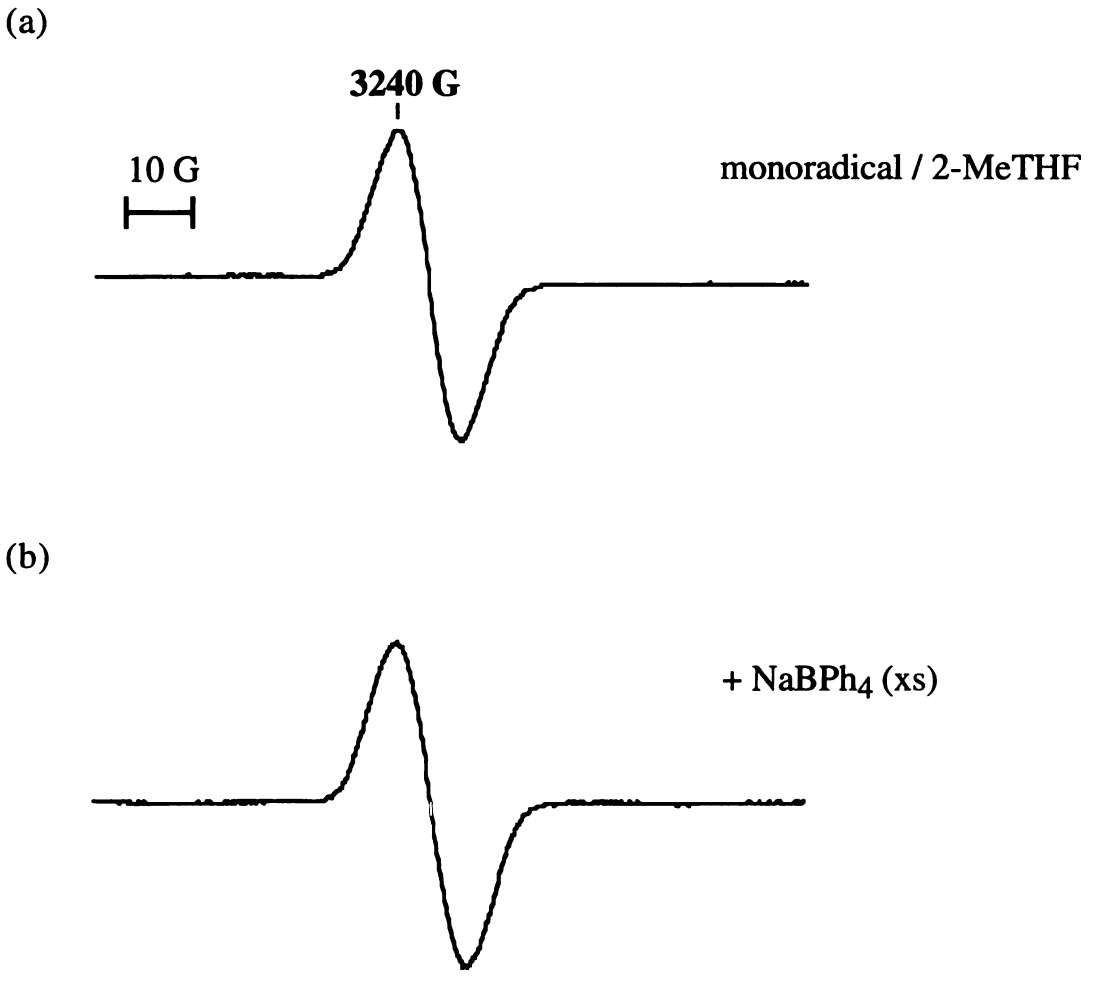

Figure 4.6. ESR spectra obtained on frozen 2-MeTHF solutions at 120 K: (a) monoradical **47** and (b) **47** with excess $NaBPh_4$.

salts also showed the same doublet ESR spectrum of **47** or **46** that is observed in the absence of salts. Additionally, these samples were filtered, evaporated in air, and the resulting residues were treated with D_2O. For both radical **47** and biradical **46**, no evidence of the Li^+ salt was found in the D_2O washing by ^7Li NMR, and no resonances attributable to the Na^+ or K^+ salt were observed by ^1H NMR. As found with 2-MeTHF as the

solvent, no changes were observed in the ESR spectra of **47** and **46** in chloroform/acetone (7:1, v/v) upon salt addition; in all cases, doublet spectra were obtained.

Lastly, we note that evidence for ion binding by **47** or **46** has not been detected in 2-MeTHF, chloroform, and chloroform/acetone (7:1, v/v) using the ESEEM (electron spin echo envelope modulation) technique.

The observations recounted above suggest that both radical **47** and biradical **46** are poorer ligands than we had expected. These results are quite surprising in light of the ion binding abilities exhibited by the diamagnetic model systems. The absence of any changes in the ESR spectra of **47** and **46** in both 2-MeTHF and chloroform/acetone (7:1, v/v) upon salt addition indicates that if pairwise electron coupling is present, it is less than kT. We have not been able to directly address whether ion binding is occurring in these solvents with either ligand, since UV–vis studies are hampered by the oxidation of both **47** and **46** upon salt addition to give intensely colored triarylmethyl cations, as previously observed with radical **23**. The situation is somewhat clearer for samples studied in chloroform. Indirect evidence (vide supra) suggests that **47** and **46** do not solubilize LiI, NaBPh4, or KB(4-ClPh)4, as previously observed with amines **28** and **45**.

Figure 4.7. ESR Spectra of biradical **46** obtained on frozen 2-MeTHF solutions at 120 K: (a) with no added salt; (b) with excess LiI; (c) with excess $NaBPh_4$; and (d) with excess $KB(4\text{-}ClPh)_4$.

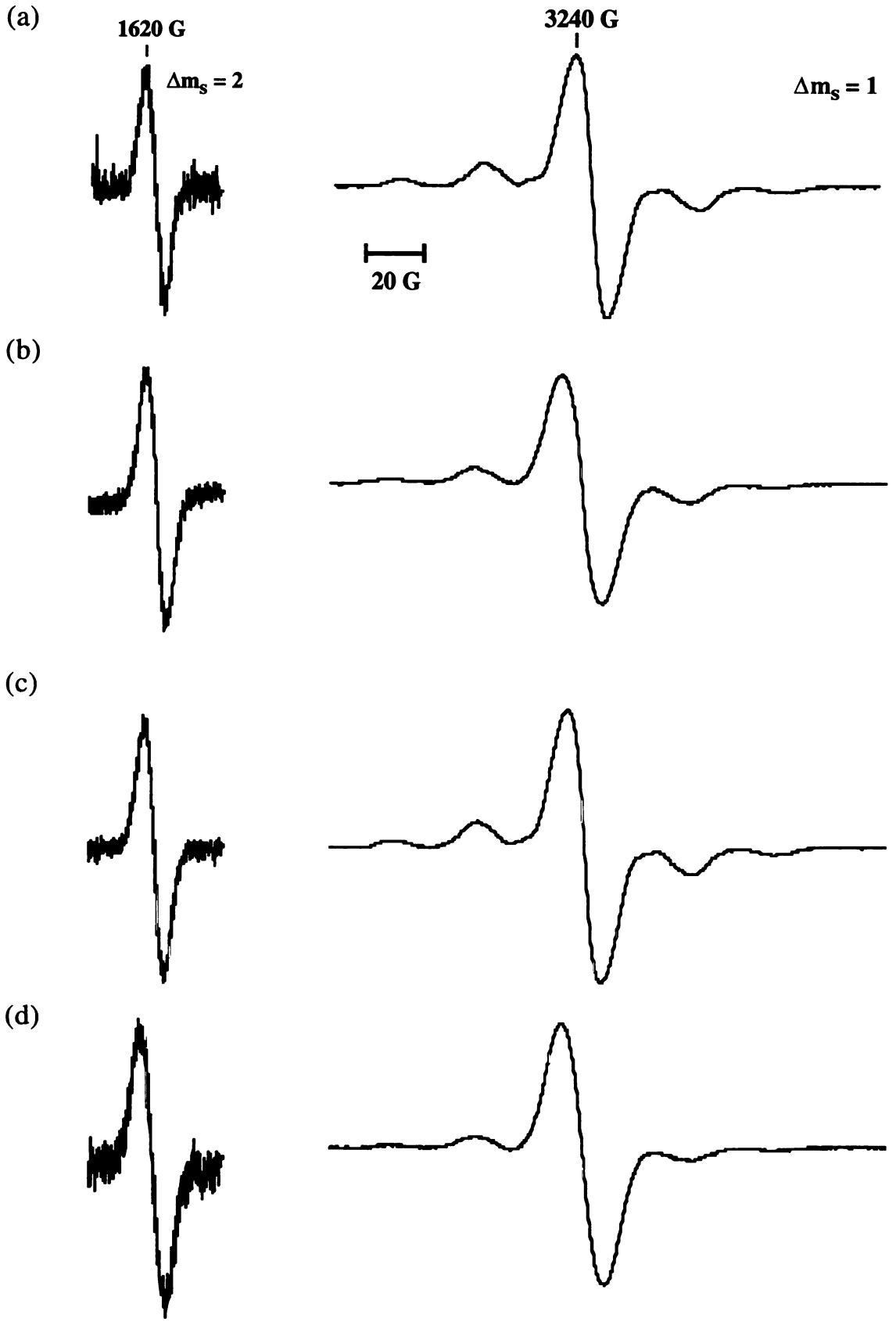
(a)
1620 G
$\Delta m_s = 2$
3240 G
$\Delta m_s = 1$
20 G
(b)
(c)
(d)

CHAPTER 5

EXPERIMENTAL SECTION

General Methods

Melting points were determined on a Thomas-Hoover apparatus and are uncorrected. Fourier-transform infrared (IR) spectra were obtained on a Nicolet IR/42 spectrophotometer; each sample was measured as a thin layer prepared by evaporating a $CHCl_3$ solution on a NaCl plate. Electron impact (EI) mass spectra were obtained on a Fisons VG Trio-1 mass spectrometer. Fast atom bombardment (FAB) mass spectra were run on a JEOL JMS-HX110 high resolution double-focusing mass spectrometer; *m*-nitrobenzyl alcohol was used as the FAB matrix. Elemental analyses were performed by Galbraith Laboratories, Inc., Knoxville, TN.

Routine ^1H and $^{13}C\{^1H\}$ NMR spectra were obtained at 300 and 75.5 MHz, respectively, on Varian GEMINI 300 or VXR-300 spectrometers. The ^1H NMR shifts are referenced to residual ^1H resonances in the deuterated solvents: acetone-d_6 (δ 2.04); benzene-d_6 (δ 7.15); $CDCl_3$ (δ 7.24); and CD_3NO_2 (δ 4.53). The ^{13}C shifts are referenced to those of the deuterated solvents: acetone-d_6 (δ 29.8); benzene-d_6 (δ 128.0); and $CDCl_3$ (δ 77.0). Peak multiplicities are abbreviated: s, singlet; d, doublet; t, triplet; q, quartet; dd, doublet of doublets; m, multiplet. Coupling constants (*J*) are reported in hertz. The ^7Li (116.57 MHz) and ^{23}Na (79.35 MHz) spectra were recorded on a Varian VXR-300 spectrometer and referenced to 0.30 M LiCl/MeOH and 3.0 M aqueous NaCl, respectively; no chemical shift corrections were made for bulk diamagnetic susceptibility differences between the sample and reference solvents. Two-dimensional ^1H ROESY[134] and ^6Li, ^1H HOESY[129] NMR experiments were performed on a Varian VXR-500 spectrometer.

All air-sensitive reactions were performed in oven-dried glassware using standard syringe/cannula techniques.[150] Gravity column chromatography was performed on E. Merck silica gel 60 (230–400 mesh) or Fisher neutral alumina (Brockman activity I, 80–200 mesh). Thin-layer chromatography was done on E. Merck plastic-backed plates (silica gel 60, F_{254}, 0.2 mm; aluminum oxide 60, type E, F_{254}, 0.2 mm).

Nitromethane (Fluka) and 1,2-dichlorobenzene (Aldrich) were used as received. Benzene, toluene, Et_2O, and THF were freshly distilled from Na/benzophenone ketyl under argon; 2-MeTHF was distilled from Na under argon. Absolute EtOH was dried according to Lund and Bjerrum.[151] Acetone was stirred for 24 h over B_2O_3 (5 wt%), and then filtered onto a fresh charge of B_2O_3 and distilled under argon.[152] DMF was stirred for 24 h over activated 3A molecular sieves (5 wt%), and then filtered onto a fresh charge of 3A sieves and distilled under reduced pressure.[152] Methylene chloride was refluxed over CaH_2 and distilled under argon.

Acetone-d_6 and benzene-d_6 were dried as described above for the nondeuterated solvents. Chloroform-*d* was passed through a short column of basic alumina immediately before use. Nitromethane-d_3 was refluxed over CaH_2 for 24 h, then decanted and allowed to stand over powdered 4A sieves (5 wt%) under argon for 12 h, and finally decanted onto fresh 4A sieves and distilled under reduced pressure.

The following salts were obtained from commercial sources and used as received: n-Bu_4NBF_4, $LiBF_4$, $NaBPh_4$, $RbBPh_4$, CsI (Aldrich); $LiBPh_4$•3glyme, $LiPF_6$ (Alfa); NaCl (EM Science); $Mg(ClO_4)_2$ (Fisher);

$MgBr_2$, LiCl, KCl, RbCl, NaI, KI (Strem). LiI (Aldrich) was twice recrystallized from acetone and dried in vacuo at 100 °C for two days. $LiClO_4$ (GFS Chemicals) was dried in vacuo at 180 °C for 30 h. The salts $LiBPh_4$,[153] $^6LiBPh_4$, $KBPh_4$,[153] $RbBPh_4$,[153] and $CsBPh_4$ [154] were prepared by reacting $NaBPh_4$ with the appropriate alkali metal chloride; sodium contamination (%) in the products was determined by metal analysis: $LiBPh_4$ (< 0.04%); $KBPh_4$ (0.079%); $RbBPh_4$ (<0.2%); $CsBPh_4$ (0.10%). $KB(4\text{-}ClPh)_4$ (Fluka) was used as received; metal analysis gave < 0.03% sodium content. The ^6LiCl (>96% ^6Li) used to prepare $^6LiBPh_4$ was a gift from Mr. J. F. Remenar in Professor D. B. Collum's group at Cornell University.

$BF_3{\bullet}Et_2O$ (Aldrich) was treated with dry Et_2O (2 wt%) to ensure an excess, and then distilled from CaH_2 under reduced pressure.[155] *n*-BuLi (Aldrich) was titrated with 2,5-dimethoxybenzyl alcohol immediately prior to use according to the procedure of Ronald.[156] $SOCl_2$ (Aldrich) was distilled from triphenylphosphite.[157]

Unless specified, all other commercial chemicals were used as supplied: *o*-anisidine, 2-bromoanisole, 18-crown-6, 1,3-dimethoxybenzene, 2,5-dimethoxybenzyl alcohol, diphenylamine, ethyl salicylate, 2-iodoanisole, 2-iodotoluene, MeOH (anhydrous), 2-methoxy-6-methylaniline, methyl 2-methoxybenzoate, 2-nitrophenol, *o*-toluidine, triphenylmethane (Aldrich); Mg pieces (Alfa); 2-nitroresorcinol, triphenylamine (Eastman Kodak); and Cu powder (Lancaster).

Syntheses

Tris(2-methoxyphenyl)amine (28). The synthesis of this compound has been described by Frye et al.[94] and more recently by Soulié et al.,[158] but neither report gave ^{13}C NMR data. A modified[97] synthesis and complete characterization details are as follows:

A mixture of *o*-anisidine (1.32 g, 10.7 mmol), 2-iodoanisole (6.27 g, 26.8 mmol), anhydrous K_2CO_3 (11.9 g, 86.1 mmol), 18-crown-6 (0.57 g, 2.16 mmol), Cu powder (2.73 g, 43.0 mmol), and 1,2-dichlorobenzene (20 mL) was refluxed under argon for 23 h. The hot mixture was filtered and the filtrate distilled under reduced pressure. The resulting residue was twice recrystallized from acetone to give **28** (1.58 g, 44%) as off-white crystals: mp 145–146.5 °C (lit.[94] mp 145–147 °C); ^1H NMR (300 MHz, $CDCl_3$) δ 7.04–6.97 (m, 3 H), 6.85–6.75 (m, 9 H), 3.54 (s, 9 H); $^{13}C\{^1H\}$ NMR ($CDCl_3$) δ 153.1, 137.8, 124.5, 123.7, 120.6, 112.6, 55.7.; EIMS m/z (relative intensity) 336 (M+1, 24), 335 (M^+, 100), 290 (16), 289 (72); FABHRMS calcd for $C_{21}H_{21}NO_3$ 335.1522, found 335.1534.

Tris(2-methylphenyl)amine (30). A mixture of *o*-toluidine (2.30 g, 21.5 mmol), 2-iodotoluene (11.7 g, 53.7 mmol), 18-crown-6 (1.15 g, 4.35 mmol), anhydrous K_2CO_3 (23.8 g, 172 mmol), Cu powder (5.47 g, 86.1 mmol), and 1,2-dichlorobenzene (40 mL) was refluxed under argon for 16 h. After cooling, the mixture was filtered through a thin layer (~2 cm) of silica gel. The inorganic solids were washed with hot $CHCl_3$ and the combined filtrates distilled under reduced pressure. The residue was twice recrystallized from 95% EtOH to give **30** (1.48 g, 24%) as yellow crystals: mp 104–105.5 °C (lit.[94] mp 104–106 °C); ^1H NMR (300 MHz, $CDCl_3$) δ

7.15–6.70 (m, 12 H), 1.88 (s, 9 H); $^{13}C\{^1H\}$ NMR (75.5 MHz, $CDCl_3$) δ 147.3, 133.2, 131.6, 126.5, 125.2, 123.6, 18.6.

Phenyl-*N,N*-bis(2-methoxyphenyl)amine (34). A mixture of aniline (1.99 g, 21.4 mmol), 2-iodoanisole (12.6 g, 53.8 mmol), anhydrous K_2CO_3 (23.8 g, 172 mmol), 18-crown-6 (1.16 g, 4.40 mmol), Cu powder (5.46 g, 86.0 mmol), and 1,2-dichlorobenzene (40 mL) was refluxed under argon for 24 h. The hot mixture was filtered and the filtrate distilled under reduced pressure. The resulting residue was twice recrystallized from 95% EtOH to give **34** (1.19 g, 18%) as pale-yellow crystals: mp 91.5–92 °C (lit.[159] mp 90 °C); ^1H NMR (300 MHz, $CDCl_3$) δ 7.18–7.07 (m, 6 H), 6.93–6.85 (m, 4 H), 6.80–6.75 (m, 1 H), 6.66–6.63 (m, 2 H), 3.65 (s, 6 H); $^{13}C\{^1H\}$ NMR (75.5 MHz, $CDCl_3$) δ 155.4, 148.3, 135.7, 128.7, 128.3, 125.9, 121.2, 119.1, 117.4, 112.9, 55.8; EIMS m/z (relative intensity) 306 (M+1, 19), 305 (M^+, 100), 274 (7), 260 (10), 259 (49), 182 (10); FABHRMS calcd for $C_{20}H_{19}NO_2$ 305.1417, found 305.1421.

Diphenyl-*N*-(2-methoxyphenyl)amine (35). A mixture of diphenylamine (4.04 g, 23.9 mmol), 2-iodoanisole (8.29 g, 35.4 mmol), anhydrous K_2CO_3 (13.1 g, 95.0 mmol), 18-crown-6 (0.63 g, 2.4 mmol), Cu powder (3.06 g, 48.1 mmol), and 1,2-dichlorobenzene (40 mL) was refluxed under argon for 14 h. The hot mixture was filtered and the filtrate distilled under reduced pressure. The resulting residue was twice recrystallized from 95% EtOH to give **35** (4.63 g, 70%) as white crystals: mp 74.5–75 °C (lit.[98] mp 74–75 °C); ^1H NMR (300 MHz, $CDCl_3$) δ 7.23–7.13 (m, 6 H), 7.01–6.87 (m, 8 H), 3.62 (s, 3 H); $^{13}C\{^1H\}$ NMR (75.5 MHz, $CDCl_3$) δ 156.1, 147.7, 135.5, 130.2, 128.8, 126.7, 121.6, 121.4, 113.3, 55.9 (remaining ^{13}C

resonance not observed); EIMS m/z (relative intensity) 276 (M+1, 23), 275 (M^+, 100), 260 (15), 259 (10), 244 (12), 182 (15); FABHRMS calcd for $C_{19}H_{17}NO$ 275.1311, found 275.1304.

Tris(2-methoxyphenyl)methane (36). Carbinol **48** (2.00 g, 5.72 mmol) was dissolved in refluxing 95% EtOH (125 mL) and treated with concentrated HCl (10 mL, 329 mmol). A deep purple color developed and then began to fade after ca. 2 min. The mixture was refluxed for 12 h and the colorless solution then cooled to room temperature. The product crystallized at –20 °C as a white solid (1.55 g, 81%): mp 136–137 °C (lit.[108] mp 136–137 °C); ^{1}H NMR (300 MHz, $CDCl_3$) δ 7.20–7.14 (m, 3 H), 6.86–6.70 (m, 9 H), 6.40 (s, broad, 1 H), 3.67 (s, 9 H); $^{13}C\{^1H\}$ NMR (75.5 MHz, $CDCl_3$) δ 157.3, 132.5, 129.6, 127.0, 119.9, 110.7, 55.8, 36.9; EIMS m/z (relative intensity) 335 (M+1, 25), 334 (M^+, 100), 319 (15), 303(36), 227 (9), 226 (10), 195 (9), 181 (9), 121 (55), 107 (17), 91 (24).

2-Iodo-3-methylanisole. 2-Methoxy-6-methylaniline (8.23 g, 60.0 mmol) was dissolved in concentrated H_2SO_4 (50 mL), cooled to 0–5 °C, and treated with a solution of $NaNO_2$ (4.28 g, 62.0 mmol) in H_2O (20 mL). When the addition was complete, the mixture was stirred for an additional 30 min at 0–5 °C, and then filtered through a plug of glass wool into a solution of KI (99.3 g, 0.60 mol) in H_2O (150 mL). The resulting brown mixture was heated on a steam bath until the evolution of N_2 ceased, and then Et_2O (200 mL) and 1 M aqueous Na_2SO_3 (20 mL) were successively added. The organic extracts were combined, washed with 2 M aqueous NaOH (4 x 100 mL), dried over Na_2SO_4, and evaporated to give a red/black solid. Chromatography over silica gel using CH_2Cl_2/hexanes (1:1, v/v)

afforded the iodide (4.08 g, 28%) as a white solid (R_f= 0.73): mp 43–43.5 °C (lit.[160] mp 49 °C); ^{1}H NMR (300 MHz, $CDCl_3$) δ 7.17 (t, 1 H, J = 8.0 Hz), 6.86 (d, 1 H, J = 8.2 Hz), 6.62 (d, 1 H, J = 8.3 Hz), 3.86 (s, 3 H), 2.46 (s, 3 H); ^{13}C{^{1}H} NMR (75.5 MHz, $CDCl_3$) δ 158.1, 143.4, 128.7, 122.4, 108.0, 93.1, 56.5, 28.8; EIMS m/z (relative intensity) 249 (M+1, 11), 248 (M^+, 100), 233 (18), 121 (3), 106 (14), 91 (15); FABHRMS calcd for C_8H_9IO 247.9699, found 247.9706.

Tris(2-methoxy-6-methylphenyl)borane (38). A solution of 2-iodo-3-methylanisole (1.97 g, 7.94 mmol) in dry Et_2O (10 mL) was added dropwise with stirring to Mg pieces (0.19 g, 8.0 mmol) in Et_2O (15 mL) under argon. When the addition was complete, the mixture was stirred for an additional 1 h, and cooled to 0–5 °C; freshly distilled BF_3•Et_2O (0.32 mL, 2.64 mmol) in Et_2O (10 mL) was then added dropwise. The mixture was refluxed for 20 h, cooled, and poured onto crushed ice (60 mL) containing 5% aqueous HCl (5 mL). The aqueous layer was separated and extracted with CH_2Cl_2 (4 x 50 mL). The organic extracts were combined, dried over Na_2SO_4, and evaporated to give a brownish-orange solid. Recrystallization of the crude product from 95% EtOH afforded **38** (0.60 g, 61%) as a white solid: mp 169.5–170 °C; ^{1}H NMR (300 MHz, $CDCl_3$) δ 7.13 (t, 3 H, J = 8.0 Hz), 6.69 (d, 3 H, J = 7.5 Hz), 6.63 (d, 3 H, J = 8.3 Hz), 3.41 (s, 9 H), 2.09 (s, 9 H); ^{13}C{^{1}H} NMR (75.5 MHz, $CDCl_3$) δ 161.2, 141.0, 129.4, 122.6, 108.9, 56.1, 21.2 (remaining ^{13}C resonance not observed); EIMS m/z (relative intensity) 375 (^{10B}M+2, 10), 374 (^{10B}M+1, 44), 373 ($^{10B}M^+$, 10), 253 (13), 252 (53), 251 (17), 238 (35), 237 (100), 236 (25), 223 (17), 222 (37), 221 (20), 208 (12), 207 (54), 206 (15), 205 (10), 195 (11), 193 (25), 192 (13), 191 (23), 180 (11), 179 (46), 178 (51), 166 (15), 165 (42), 152

(15), 133 (30), 132 (12), 117 (10), 105 (64), 104 (11), 103 (15), 91 (28); FABHRMS calcd for $C_{24}H_{27}BO_3$ 374.2054 (^{11}B), found 374.2060.

Colorless needles of **38** suitable for X-ray analysis were obtained by slowly evaporating a $CDCl_3$ solution in air at room temperature.

2,6-Dimethoxynitrobenzene. A mixture of 2-nitroresorcinol (15.0 g, 97.0 mmol), anhydrous K_2CO_3 (26.8 g, 194 mmol), CH_3I (13.5 mL, 217 mmol), and acetone (100 mL) was refluxed under argon for 10 h. The solvent was evaporated, H_2O (250 mL) added, and the mixture extracted with Et_2O (4 x 100 mL). The organic extracts were combined, washed with 2 M NaOH (3 x 100 mL), and dried over $MgSO_4$. Recrystallization from 95% EtOH afforded the nitro compound (10.11 g, 57%) as pale yellow needles: mp 129.5–130 °C (lit.[161] mp 129–130 °C); ^1H NMR (300 MHz, acetone-d_6) δ 7.44 (t, 1 H, J = 8.5 Hz), 6.85 (d, 2 H, J = 8.5 Hz), 3.90 (s, 6 H); $^{13}C\{^1H\}$ NMR (75.5 MHz, acetone-d_6) δ 152.5, 132.2, 120.5, 105.7, 57.0; EIMS m/z (relative intensity) 184 (M+1, 10), 183 (M^+, 100), 136 (44), 122 (12), 108 (11), 107 (48), 95 (20); FABHRMS calcd for $C_8H_9NO_4$ 183.0532, found 183.0535.

2,6-Dimethoxyaniline. A mixture of 2,6-dimethoxynitrobenzene (2.78 g, 15.2 mmol), activated carbon (600 mg, 50-200 mesh), $FeCl_3 \bullet 6H_2O$ (254 mg), and MeOH (50 mL) was refluxed with stirring for 15 min. Hydrazine hydrate (2.9 mL, 60.0 mmol) was then added in three portions over 30 min. The mixture was refluxed an additional 14 h, cooled, and evaporated. The resulting slurry was dissolved in CH_2Cl_2 and filtered. Chromatography over silica gel using CH_2Cl_2 gave the aniline (1.52 g, 65%) as a white solid: mp 76–77 °C (lit.[162] mp 75.5–77 °C); ^1H NMR (300 MHz,

$CDCl_3$) δ 6.61–6.51 (m, 3 H), 4.00 (s, broad, 2 H), 3.79 (s, 6 H); $^{13}C\{^1H\}$ NMR (75.5 MHz, $CDCl_3$) δ 147.9, 127.0, 116.7, 105.0, 56.0; EIMs m/z (relative intensity) 154 (M+1, 12), 153 (M^+, 63), 139 (10), 138 (100), 95 (49); FABHRMS calcd for $C_8H_{11}NO_2$ 153.0790, found 153.0794.

2,6-Dimethoxyiodobenzene. To a stirred solution of *n*-BuLi (48.0 mL, 0.12 mol, 2.5 M in hexanes) in dry THF (80 mL) at –5 °C under argon was added 1,3-dimethoxybenzene (13.8 g, 0.10 mol) in one portion. The mixture was allowed to warm to room temperature over 1 h, and was then cooled to –70 °C. A solution of I_2 (30.5 g, 0.12 mol) in dry THF (70 mL) was added dropwise with vigorous stirring and, in the latter part of the addition, the temperature was allowed to rise to –20 °C. When the addition was complete, the mixture was treated with $Na_2S_2O_3$ (10.0 g) in H_2O (250 mL). The aqueous layer was separated and extracted with Et_2O (3 x 100 mL). The organic extracts were combined, dried over Na_2SO_4, and evaporated to give a yellow/white solid. Recrystallization from 95% EtOH afforded the iodide (22.0 g, 84%) as white crystals: mp 103–104 °C (lit.[162] mp 102–103 °C); ^1H NMR (300 MHz, $CDCl_3$) δ 7.24 (t, 1 H, J = 8.3 Hz), 6.49 (d, 2 H, J = 8.3 Hz), 3.87 (s, 6 H); $^{13}C\{^1H\}$ NMR (75.5 MHz, $CDCl_3$) δ 159.5, 129.8, 104.1, 77.6, 56.5; EIMS m/z (relative intensity) 264 (M^+, 100), 249 (33), 234 (10), 221 (68), 206 (22), 132 (15), 122 (32); FABHRMS calcd for $C_8H_9IO_2$ 263.9648, found 263.9649.

Tris(2,6-dimethoxyphenyl)amine (39). A mixture of 2,6-dimethoxyaniline (0.51 g, 3.33 mmol), 2,6-dimethoxyiodobenzene (1.82 g, 6.89 mmol), anhydrous K_2CO_3 (3.65 g, 26.4 mmol), 18-crown-6 (0.18 g, 0.70 mmol), Cu powder (0.85 g, 13.3 mmol), and 1,2-dichlorobenzene

(6 mL) was refluxed under argon for 16 h. The cooled mixture was chromatographed over silica gel using hexanes/EtOAc (5:1, v/v), yielding an orange/white solid (R_f = 0.15). Trituration of the colored product with acetone afforded **39** (124 mg, 9%) as a white solid: mp 190–191 °C; IR (film from $CHCl_3$) 3000, 2929, 2834, 1582, 1492, 1472, 1430, 1295, 1250, 1165, 1108 cm^{-1}; ^1H NMR (300 MHz, $CDCl_3$) δ 6.87 (t, 3 H, J = 8.0 Hz), 6.50 (d, 6 H, J = 8.2 Hz), 3.43 (s, 18 H); $^{13}C\{^1H\}$ NMR (75.5 MHz, $CDCl_3$) δ 155.4, 129.8, 122.1, 107.3, 56.7; EIMS m/z (relative intensity) 426 (M+1, 29), 425 (M^+, 100), 379 (48), 333 (7), 213 (13); FABHRMS calcd for $C_{24}H_{27}NO_6$ 425.1839, found 425.1854.

Colorless needles of **39** suitable for X-ray analysis were obtained after two recrystallizations from acetone at –20 °C.

Cyclized amine 40 was obtained by the procedure described for **39**, except that the mixture was refluxed for 72 h. Chromatography over silica gel using hexanes/EtOAc (4:1, v/v) gave **40** (5%) as a beige solid (R_f = 0.05): ^1H NMR (300 MHz, $CDCl_3$) δ 7.11 (t, 1 H, J = 8.4 Hz), 6.76 (t, 2 H, J = 8.2 Hz), 6.52 (d, 2 H, J = 8.3 Hz), 6.44 (dd, 2 H, J = 8.2, 1.3 Hz), 6.31 (dd, 2 H, J = 8.3, 1.3 Hz), 3.79 (s, 6 H), 3.51 (s, 6 H); $^{13}C\{^1H\}$ NMR (75.5 MHz, $CDCl_3$) δ 159.8, 152.0, 150.1, 127.3, 126.0, 124.8, 123.1, 107.9, 106.5, 104.4, 56.0, 55.6; EIMS m/z (relative intensity) 380 (M+1, 27), 379 (M^+, 100), 333 (22), 287 (13), 226 (13), 189 (10); FABHRMS calcd for $C_{22}H_{21}NO_5$ 379.1420, found 379.1406.

1,2-Bis(2-nitrophenoxy)ethane. A solution of 2-nitrophenol (55.6 g, 0.40 mol) in dry DMF (200 mL) was added dropwise over 45 min to a mechanically stirred suspension of NaH (9.6 g, 0.40 mol) in DMF (200 mL)

under argon. The orange-red mixture was stirred for 4 h, and then 1,2-dichloroethane (15.8 mL, 0.20 mol) was added in one portion. The mixture was refluxed for 10 h and the cooled mixture poured into ice-cold H_2O (2 L). The precipitate was collected and washed successively with 2 M NaOH (3 x 100 mL), H_2O (5 x 200 mL), 95% EtOH (5 x 200 mL), and Et_2O (3 x 200 mL). The dinitro compound (30.44 g, 50%) was obtained as an off-white solid: mp 167–170 °C (lit.[163] mp 165–168 °C); ^{1}H NMR ($CDCl_3$) δ 7.81 (dd, 2 H, J = 8.1, 1.7 Hz), 7.58–7.52 (m, 2 H), 7.22 (dd, 2 H, J = 8.4, 1.2 Hz), 7.09–7.04 (m, 2 H), 4.52 (s, 4 H); ^{13}C{^{1}H} NMR ($CDCl_3$) δ 157.0, 151.9, 134.3, 125.6, 121.4, 115.9, 68.7; EIMS m/z (relative intensity) 305 (M+1, 13), 304 (M^+, 69), 167 (9), 166 (90), 123 (18), 122 (100).

1,2-Bis(2-aminophenoxy)ethane. Zinc dust (328 g, 5.0 mol) was added to a mechanically stirred suspension of 1,2-bis(2-nitrophenoxy)ethane (26.1 g, 85.6 mmol) in 78% EtOH (1.2 L), followed by a solution of $CaCl_2$ (12.0 g) in H_2O (20 mL). The mixture was refluxed for 6 h and then filtered through a coarse sintered glass funnel packed with Celite (3-cm) that was topped with a layer of glass wool. The metal sludge was washed with boiling 78% EtOH (200 mL), and the cooled filtrate was poured into H_2O (4 L). The product was collected and washed with H_2O (2 x 100 mL) to give the desired ethane (18.8 g, 90%) as a pearly-white solid: mp 130–132 °C (lit.[163] mp 127–130 °C); ^{1}H NMR ($CDCl_3$) δ 6.87–6.68 (m, 8 H), 4.35 (s, 4 H), 3.82 (s, broad, 4 H); ^{13}C{^{1}H} NMR ($CDCl_3$) δ 146.2, 136.8, 121.9, 118.3, 115.3, 112.5, 67.4; EIMS m/z (relative intensity) 245 (M+1, 20), 244 (M^+, 100), 136 (50), 135 (86), 120 (26), 109 (44), 108 (26).

1,2-Bis[{2-bis(2-methoxyphenyl)aminophenoxy}]ethane (45). A mixture of 1,2-bis(2-aminophenoxy)ethane (2.01 g, 8.22 mmol), 2-iodoanisole (9.64 g, 41.2 mmol), 18-crown-6 (0.91 g, 3.4 mmol), anhydrous K_2CO_3 (18.3 g, 132 mmol), Cu powder (4.20 g, 66.1 mmol), and 1,2-dichlorobenzene (80 mL) was refluxed under argon for 16 h. After cooling, the mixture was filtered through a thin layer (~2 cm) of silica gel. The inorganic solids were washed with hot CH_2Cl_2 and the combined filtrates distilled under reduced pressure. After column chromatography (neutral alumina, hexanes/CH_2Cl_2 (3:1)), the product was recrystallized from acetone and dried at ~60 °C under high vacuum for 24 h, affording **45** (2.24 g, 41%) as an off-white solid: mp 137–137.5 °C; IR (film from $CHCl_3$) 3061, 2934, 2834, 1588, 1497, 1455, 1319, 1267, 1248, 1181, 1119, 1048, 1028 cm^{-1}; ^1H NMR ($CDCl_3$) δ 7.08–6.63 (m, 24 H), 3.51 (s, 12 H), 3.38 (s, 4 H); $^{13}C\{^1H\}$ NMR ($CDCl_3$) δ 153.2, 151.6, 137.9, 137.6, 124.8, 124.0, 123.8, 123.1, 120.9, 120.8, 114.3, 112.9, 65.7, 55.8; EIMS m/z (relative intensity) 669 (M+1, 16), 668 (M^+, 46), 348 (15), 334 (31), 321 (10), 290 (17), 289 (100), 274 (10), 273 (12), 246 (18), 226 (11), 212 (11), 183 (21), 182 (35); FABHRMS calcd for $C_{42}H_{40}N_2O_6$ 668.2888, found 668.2869. Anal. Calcd for $C_{42}H_{40}N_2O_6$: C, 75.43; H, 6.03; N, 4.19. Found: C, 75.21; H, 6.34; N, 3.96.

Crystals of **45** suitable for X-ray analysis were obtained by treating a suspension of **45** in nitromethane with LiI (2 equiv). The ligand was solubilized after shaking the mixture for ~10 min. Slow evaporation of the solution at room temperature afforded free **45** as colorless crystals.

Tris(2-methoxyphenyl)methanol (48). A solution of 2-bromoanisole (23.1 g, 0.124 mol) in dry Et_2O (40 mL) was added dropwise to Mg pieces

(3.04 g, 0.125 mol) in dry Et_2O (40 mL) under argon. When the addition was complete (2 h), the mixture was stirred for an additional 30 min, and then a solution of methyl 2-methoxybenzoate (9.31 g, 0.056 mol) in dry benzene (120 mL) was added dropwise over 1 h. The mixture was refluxed for 22 h, cooled, and quenched with saturated aqueous NH_4Cl (400 mL). Benzene (500 mL) was added to dissolve the precipitate that had formed, and the aqueous layer was separated and extracted with benzene (3 x 150 mL). The organic layers were combined, dried over Na_2SO_4, filtered, and evaporated to give a yellow/white solid. The crude product was recrystallized from hexanes/benzene (1:1) to give carbinol **48** (12.69 g, 65%) as a white crystalline solid: mp 181–182 °C (lit.[108] mp 181.5–182.5 °C); IR 3532, 3071, 2996, 2938, 2836, 1597, 1582, 1489, 1462, 1435, 1285, 1244, 1184, 1157, 1026 cm^{-1}; ^1H NMR (300 MHz, benzene-d_6) δ 7.64 (dd, 3 H, J = 7.9, 1.8 Hz), 7.13–7.07 (m, 3 H), 6.91–6.85 (m, 3 H), 6.56 (d, 3 H, J = 7.3 Hz), 5.56 (s, 1 H), 3.02 (s, 9 H); $^{13}C\{^1H\}$ NMR (300 MHz, benzene-d_6) δ 158.0, 134.8, 130.5, 127.9, 120.3, 112.4, 80.7, 55.1; EIMS m/z (relative intensity) 351 (M+1, 4), 350 (M^+, 16), 244 (8), 243 (47), 215 (14), 136 (18), 135 (100), 121 (16); Anal. Calcd for $C_{22}H_{22}O_4$: C, 75.41; H, 6.33; O, 18.26. Found: C, 75.18; H, 6.36; O, 17.51.

Tris(2-methoxyphenyl)methyl chloride (49). A solution of **48** (250 mg, 0.71 mmol) in dry CH_2Cl_2 (2 mL) in a Schlenk flask was treated with $SOCl_2$ (0.5 mL, 6.85 mmol). The resulting deep purple solution was stirred for 16 h while protected by a $CaCl_2$ drying-tube. The mixture was evaporated under reduced pressure, and the resulting dark purple residue washed with small portions of dry Et_2O. The product was obtained as a

mixture consisting of a 31:1 ratio of **49** and **36** (see Figure 4.2); the product mixture was immediately used for the preparation of radical **47**.

The NMR data for pure **49** were obtained by shaking a solution of **48** (25 mg, 0.071 mmol) in dry benzene-d_6 (0.8 mL) with $SOCl_2$ (0.2 mL, 2.7 mmol) for 30 min in an NMR tube (see Figure 4.1):

49: ^{1}H NMR (300 MHz, benzene-d_6) δ 7.54 (d, broad, 3 H, J = 7.1 Hz), 7.11–7.05 (m, 3 H), 6.80–6.75 (m, 3 H), 6.56 (dd, 3 H, J = 8.2, 1.1 Hz), 3.12 (s, 9 H); ^{13}C{^{1}H} NMR (75.5 MHz, benzene-d_6) δ 158.1, 132.2, 131.4, 129.2, 119.7, 113.0, 55.2 (α-carbon resonance not observed).

However, evaporation of the volatiles resulted in hydrolysis to give variable amounts of carbinol **48**.

1,2-Bis[(2-carbethoxy)phenoxy]ethane. A solution of NaOEt was prepared by adding Na metal pieces (13.9 g, 0.60 mol, ~1-cm cubes) to anhydrous EtOH (350 mL) under argon. To the mechanically stirred solution was then added ethyl salicylate (99.8 g, 0.60 mol) in anhydrous EtOH (150 mL) dropwise over 1 h. The mixture (now containing a white precipitate) was stirred for an additional 30 min, and then 1,2-dichloroethane (29.64 g, 0.30 mol) was added in one portion. The mixture was refluxed for 18 h, cooled, poured into H_2O (1.2 L), and allowed to stand overnight. The product was collected and recrystallized from 70% EtOH, affording the diester (13.69 g, 13%) as colorless plates: mp 96.5–97 °C; IR 2981, 1723, 1599, 1590, 1495, 1446, 1368, 1291, 1251, 1167, 1143, 1083, 1058, 1019 cm^{-1}; ^{1}H NMR (300 MHz, $CDCl_3$) δ 7.76 (dd, 2 H, J = 7.7, 1.7 Hz), 7.46–7.41 (m, 2 H), 7.07–6.96 (m, 4 H), 4.43 (s, 4 H), 4.29 (q, 4 H, J = 7.1 Hz), 1.29 (t, 6 H, J = 7.1 Hz); ^{13}C{^{1}H} NMR (75.5 MHz, $CDCl_3$) δ 166.3, 158.1, 133.3, 131.5, 121.4, 120.9, 114.3, 67.9, 60.8, 14.2; EIMS m/z (relative

intensity) 359 (M+1, <0.1), 358 (M^+, <1), 313 (6), 193 (25), 192 (9), 166 (37), 165 (12), 151 (5), 147 (19), 121 (100), 120 (54), 119 (8), 93 (9), 92 (13); FABHRMS calcd for $C_{20}H_{22}O_6$ 358.1417, found 358.1422. Anal. Calcd for $C_{20}H_{22}O_6$: C, 75.63; H, 6.06. Found: C, 75.34; H, 6.21.

1,2-Bis[{2-bis(2-methoxyphenyl)hydroxymethylphenoxy}]ethane (50). A solution of 2-bromoanisole (11.5 g, 61.6 mmol) in dry Et_2O (20 mL) was added dropwise to Mg pieces (1.52 g, 62.4 mmol) in dry Et_2O (20 mL) under argon. When the addition was complete (2 h), the mixture was stirred for an additional 30 min, and then a solution of 1,2-bis[(2-carbethoxy)phenoxy]ethane (5.00 g, 14.0 mmol) in dry benzene (60 mL) was added dropwise over 45 min. The mixture was refluxed for 46 h, cooled, and quenched with saturated aqueous NH_4Cl (200 mL). The aqueous layer was separated and extracted with benzene (2 x 100 mL). The organic layers were combined, dried over Na_2SO_4, filtered, and evaporated to give a viscous yellow/white residue. Slow evaporation of a $CHCl_3$ solution of the crude product afforded **50** (6.38 g, 65%) as a white crystalline solid: mp 200–205 °C; IR 3503, 2936, 1584, 1487, 1462, 1287, 1238, 1181, 1113, 1024 cm^{-1}; ^1H NMR (300 MHz, benzene-d_6) δ 7.60 (dd, 6 H, J = 7.8, 1.7 Hz), 7.13–7.04 (m, 6 H), 6.89–6.81 (m, 6 H), 6.60–6.52 (m, 6 H), 6.15 (s, C*H*Cl_3), 5.52 (s, broad, 2 H), 3.45 (s, broad, 4 H), 3.00 (s, 12 H); $^{13}C\{^1H\}$ NMR (75.5 MHz, benzene-d_6) δ 158.0, 157.0, 135.3, 134.8, 130.6, 130.4, 128.1, 127.9, 120.5, 120.4, 113.6, 112.3, 80.3, 66.6, 55.0; EIMS m/z (relative intensity) 681 (4), 680 (M–H_2O, 8), 573 (5), 466 (3), 361 (5), 345 (9), 334 (10), 303 (20), 288 (17), 287 (78), 271 (21), 255 (11), 241 (17), 237 (13), 227 (17), 225 (16), 213 (21), 197 (16), 181 (14), 137 (14), 136 (19),

135 (100), 121 (93), 108 (11), 107 (52), 105 (17); Anal. Calcd for $C_{44}H_{42}O_8$: C, 75.63; H, 6.06; O, 18.31. Found: C, 75.34; H, 6.21; O, 17.70.

1,2-Bis[{2-bis(2-methoxyphenyl)chloromethylphenoxy}]ethane (51). A solution of diol **50** (60.8 mg, 0.087 mmol) in dry benzene (3.2 mL) in a Schlenk flask was treated with $SOCl_2$ (32μL, 0.44 mmol), and the mixture stirred in the *closed* vessel for 24 h. The yellow supernatant was removed via syringe from the white precipitate that had formed, and the solid was washed successively with small portions of benzene/$SOCl_2$ (100:1, v/v) and dry benzene. The product was obtained as a mixture consisting of **51** (>95%) and incompletely reacted **50** (<5%) (see Figure 4.4); the product mixture was immediately used for the generation of biradical **46**.

The NMR data for pure **51** were obtained by shaking a solution of **50** (25 mg, 0.071 mmol) in dry benzene-d_6 (0.8 mL) with $SOCl_2$ (0.2 mL, 2.7 mmol) for 30 min in an NMR tube (see Figure 4.3):

51: ^{1}H NMR (300 MHz, benzene-d_6) δ 7.49 (apparent d, broad, 6 H, J = 7.7 Hz), 7.09–7.01 (m, 6 H), 6.78–6.69 (m, 6 H), 6.57–6.51 (m, 6 H), 6.32 (s, C*H*Cl_3), 3.48 (s, broad, 4 H), 3.12 (s, broad, 12 H); ^{13}C{^{1}H} NMR (75.5 MHz, benzene-d_6) δ 158.1, 156.9, 132.3, 132.1, 131.6, 131.3, 129.4, 129.3, 127.9, 119.8, 114.0, 113.0, 66.5, 55.2 (α-carbon resonance not observed).

However, evaporation of the volatiles resulted in hydrolysis to give variable amounts of carbinol **50**.

1,2-Bis[{2-bis(2-methoxyphenyl)methanophenoxy}]ethane (52). A suspension of diol **50** (1.00 g, 1.43 mmol) in dry Et_2O (10 mL) containing a few granules of anhydrous $CaCl_2$ was saturated with anhydrous HCl gas.

The deep purple mixture was stoppered and allowed to stand overnight. The supernatant (now brownish-orange in color) was removed via syinge under argon, and the remaining solid residue was washed with dry Et_2O. The combined Et_2O layers were stored under argon and, after ca. 8 h, an orange-red solid precipitated. The product was filtered and washed with Et_2O to give **52** (7.2 mg, 0.8%) as a pale orange solid; ^1H NMR (300 MHz, $CDCl_3$) δ 7.20–7.07 (m, 6 H), 6.90–6.65 (m, 18 H), 6.44 (m, 2 H), 3.71 (s, 4 H), 3.59 (s, 12 H); $^{13}C\{^1H\}$ NMR (75.5 MHz, $CDCl_3$) δ 157.4, 156.4, 133.7, 132.3, 129.9, 129.2, 127.1, 126.9, 120.3, 119.9, 112.4, 110.6, 66.6, 55.6, 37.1; EIMS m/z (relative intensity) 668 (M+2, <1), 667 (M+1, <1), 666 (M^+, 2), 560 (<1), 559 (3), 558 (7), 441 (<1), 440 (3), 439 (11), 288 (18), 287 (75), 271 (10), 227 (11), 213 (16), 181 (32), 135 (44), 121 (100), 107 (53); FABHRMS calcd for $C_{44}H_{42}O_6$ 666.2983, found 666.3026.

Generation of Tris(2-methoxyphenyl)methyl (47) and 1,2-Bis[{2-bis(2-methoxyphenyl)methylphenoxy}]ethane (46)

A Schlenk flask containing either **49** (~0.26 mmol) or **51** (~0.13 mmol) under vacuum was transferred to a nitrogen-filled dry-box. Silver powder (470 mg, 4.36 mmol, Alfa, 99.95%, -100 mesh) was added, and the flask transferred to a Schlenk line and evacuated. The flask was back-filled with argon and evacuated again. This was repeated three times, and then a volume (25 mL) of an appropriate solvent (2-MeTHF, benzene, toluene, or $CHCl_3$) was added under argon. Stirring the mixture under argon for several minutes produced a brilliant, yellow-orange solution of **47** or **46**. Typically the mixture was stirred for 2 h before samples were prepared for ESR studies.

Semi-Empirical Calculations

Geometry optimizations were carried out using standard AM1[120] and MNDO[164] procedures as implemented in the SPARTAN computer program (SPARTAN version 3.1, Copyright 1994 Wavefunction, Inc.).

Stoichiometry Determinations for LiI Complexes

For the LiI complexes, stoichiometries were determined using ^1H and ^7Li NMR. As an example, the procedure is described below for the **28**•LiI complex:

A tube containing a reference sample of $LiBPh_4$•3glyme in $CDCl_3$ was coaxially mounted in a 5-mm NMR tube containing **28** and excess LiI (ca. 5 equiv) in $CDCl_3$. LiI is insoluble in $CDCl_3$ (by ^7Li NMR) in the absence of added ligand. The **28**•xLiI:$LiBPh_4$•3glyme ratio was determined from the respective OCH_3 ^1H integrals, and a LiI:$LiBPh_4$ ratio was obtained from the respective ^7Li integrals. The stoichiometry (x) is the ratio of the ^7Li to ^1H ratios. The **38**•LiI and **45**•xLiI stoichiometries were similarly determined.

NMR Titration Experiments

Samples were prepared at **28**/M^+ mole ratios from 0 to 9 by mixing appropriate volumes (μL syringe) of **28**/CD_3NO_2 and M^+/CD_3NO_2 stock solutions in an NMR tube, and diluting with CD_3NO_2 to the desired final volume (0.7 mL); the metal ion concentration was held constant at

5.0 x 10^{-3} M throughout. All samples were prepared in a dry-box under a N_2 atmosphere, and the NMR spectra were obtained immediately after sample preparation. Formation constants (K_f's) were obtained from the variation of chemical shifts with the concentration of **28** by means of a nonlinear least-squares curve-fitting program (KINFIT[165]). The ^1H and $^7Li/^{23}Na$ shifts were used in multiple-data-set fits to equations that assumed (1) formation of only a 1:1 complex, and (2) formation of both 1:1 and 2:1 ligand/M^+ complexes. The equilibria are given below:

$$A + M^+ \underset{}{\overset{K_1}{\rightleftharpoons}} A{\bullet}M^+ \overset{K_2}{\rightleftharpoons} A_2{\bullet}M^+$$

where A is the amine ligand **28**, M^+ is the appropriate alkali metal ion (Li^+ or Na^+), $A{\bullet}M^+$ is the 1:1 complex between the amine and the metal ion, $A_2{\bullet}M^+$ is the 2:1 complex between the amine and the metal ion, and K_1 and K_2 are the formation constants for the 1:1 and 2:1 complexes, respectively.

The equations describing case (1) are as follows:

$$\begin{aligned}\delta_{obs}(M^+) = \; & \{(K_1[A]_T + K_1[M^+]_T + 1) - (K_1{}^2[A]_T{}^2 + K_1{}^2[M^+]_T{}^2 \\ & - 2K_1{}^2[A]_T[M^+]_T + 2K_1[A]_T + 2K_1[M^+]_T + 1)^{1/2} / 2K_1[M^+]_T\} \\ & \{\delta_{1:1}(M^+) - \delta_f(M^+)\} + \delta_f(M^+)\end{aligned}$$

$$\begin{aligned}\delta_{obs}(^1H) = \; & \{(K_1[A]_T + K_1[M^+]_T + 1) - (K_1{}^2[A]_T{}^2 + K_1{}^2[M^+]_T{}^2 \\ & - 2K_1{}^2[A]_T[M^+]_T + 2K_1[A]_T + 2K_1[M^+]_T + 1)^{1/2} / 2K_1[A]_T\} \\ & \{\delta_{1:1}(^1H) - \delta_f(^1H)\} + \delta_f(^1H)\end{aligned}$$

where $\delta_{obs}(M^+)$ is the observed alkali metal chemical shift, $[A]_T$ is the total amine concentration, $[M^+]_T$ is the total metal ion concentration, $\delta_{1:1}(M^+)$ is the alkali metal chemical shift for the 1:1 ($A{\bullet}M^+$) complex, $\delta_f(M^+)$ is the alkali metal chemical shift for the free (solvated) metal ion, $\delta_{1:1}(^1H)$ is the OCH_3 proton chemical shift for the 1:1 ($A{\bullet}M^+$) complex, $\delta_f(^1H)$ is the OCH_3 proton chemical shift for the free amine ligand, and K_1 and K_2 are as defined above.

The equations describing case (2) are as follows:

$$\begin{aligned}\delta_{obs}(M^+) = \; & \{\delta_f(M^+) / [1 + K_1[A]_T + K_1K_2[A]_T^2]\} \\ & + \{\delta_{1:1}(M^+) / [1 + (1 / K_1[A]_T) + K_2[A]_T]\} \\ & + \{\delta_{2:1}(M^+) / [1 + (1 / K_2[A]_T) + (1 / K_1K_2[A]_T^2)]\}\end{aligned}$$

$$\begin{aligned}\delta_{obs}(^1H) = \; & \{\delta_{1:1}(^1H) - \delta_f(^1H)\} \{[M^+]_T / [A]_T(1 + (1 / K_1[A]_T) \\ & + K_2[A]_T)\} + \{\delta_{2:1}(^1H) - \delta_f(^1H)\} \\ & \{2[M^+]_T / [A]_T(1 + (1 / K_2[A]_T) + (1 / K_1K_2[A]_T^2))\} + \delta_f(^1H)\end{aligned}$$

where $\delta_{2:1}(M^+)$ and $\delta_{2:1}(^1H)$ are the alkali metal chemical shift and the OCH_3 proton chemical shift, respectively, for the 2:1 ($A_2{\bullet}M^+$) complex; the remaining parameters are as defined above.

A visual comparison of the two curve-fits was used to determine the complex stoichiometry and, in each case, only the curve-fits obtained using the equations given for case (1) showed good agreement with the plots obtained from the experimental data. The results are summarized in Table 2.1.

NMR Data for Metal Complexes

Typically, NMR samples were prepared by adding a $CDCl_3$ solution of the ligand (0.03 M) to the appropriate alkali metal salt. All of the salts used are insoluble in $CDCl_3$ (by NMR) in the absence of added ligand. After shaking for ~10 min, the NMR spectra were recorded. Complexes of NaB(4-ClPh)$_4$ were prepared by treating $CDCl_3$ solutions of the respective $NaBPh_4$ complexes with KB(4-ClPh)$_4$. After shaking for 10 min, the $KBPh_4$ precipitate was removed by filtration. The ^{13}C chemical shift assignments for the BAr_4^- counterions are primarily based on known[166] ^{11}B–^{13}C coupling constants.

28•LiI: ^1H NMR δ 7.23–7.16 (m, 6 H), 7.05–6.9 (m, 6 H), 4.02 (s, 9 H); $^{13}C\{^1H\}$ NMR δ 152.9, 135.7, 127.3, 126.9, 121.9, 112.1, 58.3; ^7Li NMR δ 2.11 ($\Delta\nu_{1/2}$ = 1.0 Hz).

28•LiBPh$_4$: ^1H NMR δ 7.62–7.51 (m, 8 H), 7.24–7.17 (m, 4 H), 7.11–6.85 (m, 20 H), 3.45 (s, 9 H); $^{13}C\{^1H\}$ NMR δ 164.0 (q, $^1J_{BC}$ = 49.3 Hz), 152.5, 135.9 ($^2J_{BC}$ unresolved), 135.5, 127.7, 127.2, 126.1 ($^3J_{BC}$ = 2.9 Hz) , 122.7, 122.2 ($^4J_{BC}$ unresolved), 112.4, 56.7; ^7Li NMR δ –0.08 ($\Delta\nu_{1/2}$ = 41 Hz).

28$_2$•NaBPh$_4$: ^1H NMR δ 7.44–7.36 (m, 8 H), 7.19–7.11 (m, 6 H), 7.04–6.97 (m, 8 H), 6.94–6.85 (m, 16 H), 6.71 (dd, 6 H, J = 8.0, 1.0 Hz), 3.14 (s, 18 H); $^{13}C\{^1H\}$ NMR δ 163.9 (q, $^1J_{BC}$ = 49.3 Hz), 151.9, 137.1, 136.0 ($^2J_{BC}$ unresolved), 126.1, 125.6 ($^3J_{BC}$ unresolved), 124.8, 122.3, 121.8 ($^4J_{BC}$ unresolved), 113.4, 56.3; ^{23}Na NMR δ –11.9 ($\Delta\nu_{1/2}$ = 240 Hz).

28_2•NaB(4-ClPh)$_4$: ^{1}H NMR δ 7.23–7.08 (m, 14 H), 6.96 (d, 8 H, J = 8.4 Hz), 6.91–6.83 (m, 12 H), 6.72 (dd, 6 H, J = 8.1, 1.8 Hz), 3.24 (s, 18 H); ^{13}C{^{1}H} NMR δ 160.9 (q, $^1J_{BC}$ = 49.7 Hz), 152.1, 137.3, 137.2 ($^2J_{BC}$ unresolved), 127.9, 125.6 ($^3J_{BC}$ unresolved), 124.8, 122.1 ($^4J_{BC}$ unresolved), 113.3, 56.2 (remaining ^{13}C resonance not observed); ^{23}Na NMR δ –10.3 ($\Delta\nu_{1/2}$ = 200 Hz).

34•LiI: ^{1}H NMR δ 7.31–7.17 (m, 6 H), 7.07–6.99 (m, 5 H), 6.73 (d, 2 H, J = 8.0 Hz), 4.01 (s, 6 H); ^{13}C{^{1}H} NMR δ 153.5, 147.2, 134.9, 129.5, 128.8, 128.3, 123.7, 123.1, 119.9, 112.5, 57.9; ^{7}Li NMR δ 2.74 ($\Delta\nu_{1/2}$ = 2.8 Hz).

34•LiBPh$_4$: ^{1}H NMR δ 7.54–7.44 (m, broad, 8 H), 7.31–7.12 (m, 6 H), 7.08–6.93 (m, 12 H), 6.89–6.80 (m, 5 H), 6.50–6.45 (m, 2 H), 3.44 (s, 6 H); ^{13}C{^{1}H} NMR δ 163.8 (q, 1:1:1:1, J_{BC} = 49.2 Hz), 153.5, 147.0, 138.5, 135.9 (J_{BC} unresolved), 129.2, 128.4, 128.0, 126.0 (J_{BC} unresolved), 123.4, 122.3, 122.1 (J_{BC} unresolved), 118.1, 113.5, 57.1; ^{7}Li NMR δ –2.43 ($\Delta\nu_{1/2}$ = 8.2 Hz).

38•LiI: ^{1}H NMR δ 7.26 (t, 3 H, J = 7.8 Hz), 6.95–6.86 (m, 6 H), 3.49 (s, 9 H), 2.13 (s, 9 H); ^{13}C{^{1}H} NMR δ 158.3, 140.1, 136.7, 131.2, 125.6, 113.3, 60.6, 21.1; ^{7}Li NMR δ 0.97 ($\Delta\nu_{1/2}$ = 1.6 Hz).

39•2LiI: ^{1}H NMR δ 7.22 (t, 3 H, J = 8.0 Hz), 6.85 (d, 6 H, J = 8.2 Hz), 3.75 (s, 18 H); ^{13}C and ^{7}Li NMR data were not obtained.

45•2LiI: ^{1}H NMR δ 7.29–6.83 (m, 24 H), 4.04 (s, 4 H), 4.01 (s,

12 H); $^{13}C\{^1H\}$ NMR δ 152.9, 150.7, 136.7, 135.3, 127.7, 127.2, 127.1, 125.3, 122.6, 122.1, 114.6, 112.4, 64.9, 58.3; ^7Li NMR δ 1.85 ($\Delta\nu_{1/2}$ = 2.0 Hz).

45•LiBPh$_4$: ^1H NMR δ 7.40–7.32 (m, 8 H), 7.21–7.15 (m, 4 H), 7.10–7.04 (m, 2 H), 6.96–6.77 (m, 28 H), 6.57 (dd, 2 H, J = 7.1, 1.1 Hz), 3.38 (s, 12 H), 3.21 (s, 4 H); $^{13}C\{^1H\}$ NMR δ 164.2 (q, $^1J_{BC}$ = 49.3 Hz), 152.4, 150.8, 137.6, 136.3, 136.2 ($^2J_{BC}$ unresolved), 126.5, 126.0, 125.6, 125.4 ($^3J_{BC}$ = 2.4 Hz), 124.4, 122.9, 122.4, 121.5 ($^4J_{BC}$ unresolved), 114.5, 113.1, 67.8, 56.2; ^7Li NMR δ 0.15 ($\Delta\nu_{1/2}$ = 4.0 Hz).

45•NaBPh$_4$: ^1H NMR δ 7.40–7.31 (m, 8 H), 7.30–6.63 (m, 34 H), 6.48 (dd, 2 H, J = 8.0, 1.2 Hz), 3.23 (m, 2 H), 3.14 (s, 6 H), 2.95 (m, 2 H), 2.88 (s, 6 H); $^{13}C\{^1H\}$ NMR δ 164.1 (q, $^1J_{BC}$ = 49.4 Hz), 153.1, 151.6, 149.5, 138.3, 136.3, 136.1 ($^2J_{BC}$ unresolved), 134.3, 128.9, 127.9, 126.7, 126.3, 125.7, 125.4 ($^3J_{BC}$ = 2.8 Hz), 122.5, 122.2, 122.0, 121.9, 121.5 ($^4J_{BC}$ unresolved), 112.0, 111.8, 111.7, 65.1, 55.4, 55.2; ^{23}Na NMR δ –5.5 ($\Delta\nu_{1/2}$ = 260 Hz).

45•NaB(4-ClPh)$_4$: ^1H NMR δ 7.24–7.07 (m, 14 H), 6.97–6.79 (m, 22 H), 6.70 (dd, 2 H, J = 7.8, 1.5 Hz), 6.61 (dd, 2 H, J = 8.0, 1.2 Hz), 3.47 (s, br, 2 H), 3.39 (s, br, 2 H), 3.23 (s, 6 H), 2.95 (s, 6 H); $^{13}C\{^1H\}$ NMR δ 160.8 (q, $^1J_{BC}$ = 49.8 Hz), 153.0, 151.6, 149.4, 138.4, 137.2 ($^2J_{BC}$ unresolved), 136.3, 134.2, 128.8, 128.0, 127.9, 126.9, 126.5, 125.8, 125.7 ($^3J_{BC}$ = 2.7 Hz), 122.7 ($^4J_{BC}$ unresolved), 122.3, 122.2, 111.9, 111.8, 111.7, 65.0, 55.5, 55.3 (remaining ^{13}C resonance not observed); ^{23}Na NMR δ –5.3 ($\Delta\nu_{1/2}$ = 240 Hz).

45•KB(4-ClPh)$_4$: ^{1}H NMR δ 7.23–7.05 (m, 14 H), 7.00–6.68 (m, 24 H), 6.58 (dd, 2 H, J = 8.0, 1.2 Hz), 3.40 (s, 6 H), 3.13 (s, 6 H), 3.23 (s, 4 H); ^{13}C{^{1}H} NMR δ 160.9 (q, $^1J_{BC}$ = 49.6 Hz), 151.7, 149.4, 137.7, 137.2 ($^2J_{BC}$ unresolved), 136.7, 136.2, 127.9, 126.5, 126.2, 126.0, 125.7 ($^3J_{BC}$ = 2.7 Hz), 125.5, 125.2, 123.6, 123.3, 123.0, 122.7 ($^4J_{BC}$ unresolved), 114.7, 114.5, 112.5, 65.7, 56.6, 56.5 (remaining ^{13}C resonance not observed).

Saturation Spin Transfer (SST) Measurements

The SST technique[132] was used to obtain rate constants for methoxy group site-exchange (k_{ex}) in **45**•NaBPh$_4$, **45**•NaB(4-ClPh)$_4$, and **45**•KB(4-ClPh)$_4$. Experiments were carried out on 0.03 M $CDCl_3$ solutions of the complexes at 293 K by delivering a selective 180° pulse on the higher frequency methoxy proton signal, followed by a nonselective 90° pulse after increasingly longer delay times. Treatment of the change of intensities[132] of the methoxy signals as a function of time, using the Kaleidagraph™ program (version 2.1.4, Copyright 1992 Abelbeck Software), afforded exchange rate constants; the reported standard deviations are those given by the curve-fitting program. The $\Delta G^{\ddagger}$ values were calculated from the Eyring equation assuming a transmission coefficient of unity.

Preparation of Crystalline Complexes

28$_2$•NaBPh$_4$. A suspension of **28** (107.0 mg, 0.32 mmol) in nitromethane (5 mL) was treated with NaBPh$_4$ (55.5 mg, 0.16 mmol). A clear solution resulted after shaking the mixture for ~2 min. Slow

evaporation of this solution at room temperature afforded **28**$_2$•$NaBPh_4$ (101.6 mg, 63%) as colorless crystals: mp 193–194.5 °C (dec); ^{1}H NMR ($CDCl_3$) δ 7.44–7.36 (m, 8 H), 7.19–7.11 (m, 6 H), 7.04–6.97 (m, 8 H), 6.94–6.85 (m, 16 H), 6.71 (dd, 6 H, J = 8.0, 1.5 Hz), 3.24 (s, 18 H); FABMS m/z 693 (M^+). Anal. Calcd for $C_{66}H_{62}BN_2NaO_6$: C, 78.25; H, 6.17; N, 2.76; Na, 2.27. Found: C, 78.47; H, 6.23; N, 2.66; Na, 2.12.

45•NaBPh$_4$. A solution of **45** (100 mg, 0.15 mmol) in $CHCl_3$ (5 mL) was treated with $NaBPh_4$ (513 mg, 1.5 mmol). After shaking for 10 min, the mixture was filtered to remove excess $NaBPh_4$. Evaporation of the filtrate afforded a viscous oil that solidified to white microcystals on trituration with nitromethane. Recrystallization from nitromethane gave **45**•$NaBPh_4$ (64 mg, 42%) as colorless cubes that were suitable for X-ray analysis: mp 231–232 °C; ^{1}H NMR ($CDCl_3$) δ 7.40–7.31 (m, 8 H), 7.30–6.63 (m, 34 H), 6.48 (dd, 2 H, J = 8.0, 1.2 Hz), 3.23 (m, 2 H), 3.14 (s, 6 H), 2.95 (m, 2 H), 2.88 (s, 6 H). Anal. Calcd for $C_{66}H_{60}BN_2NaO_6$: C, 78.41; H, 5.98; N, 2.77; Na, 2.27. Found: C, 78.07; H, 6.33; N, 2.46; Na, 2.31.

45•NaB(4-ClPh)$_4$. A suspension of **45** (32.1 mg, 0.05 mmol) in nitromethane (1 mL) was treated with a solution of $NaBPh_4$ (16.4 mg, 0.05 mmol) in nitromethane (1 mL). After shaking for 10 min, the mixture was filtered through a plug of glass wool into a solution of KB(4-ClPh)$_4$ (23.7 mg, 0.05 mmol) in nitromethane (0.5 mL). The mixture was shaken for 10 min, during which time a fine, white solid ($KBPh_4$) precipitated. The resulting suspension was centrifuged, and the supernatant was carefully removed and slowly evaporated at room temperature; **45**•NaB(4-ClPh)$_4$ (26.3 mg, 46%) was obtained as colorless cubes that were suitable for X-ray

analysis: mp 179–181 °C; ^{1}H NMR ($CDCl_3$) δ 7.24–7.07 (m, 14 H), 6.97–6.79 (m, 22 H), 6.70 (dd, 2 H, J = 7.8, 1.5 Hz), 6.61 (dd, 2 H, J = 8.0, 1.2 Hz), 3.47 (s, broad, 2 H), 3.39 (s, broad, 2 H), 3.23 (s, 6 H), 2.95 (s, 6 H). Anal. Calcd for $C_{66}H_{56}BCl_4N_2NaO_6$: C, 69.01; H, 4.91; N, 2.44; Na, 2.00. Found: C, 68.33; H, 4.83; N, 2.33; Na, 2.24.

45•KB(4-ClPh)$_4$•CH$_3$NO$_2$. A solution of **45** (200 mg, 0.30 mmol) in $CHCl_3$ (10 mL) was treated with KB(4-ClPh)$_4$ (345 mg, 0.70 mmol). After shaking for 10 min, the mixture was filtered to remove excess KB(4-ClPh)$_4$. Evaporation of the filtrate afforded a viscous oil that solidified overnight to a waxy residue. Recrystallization of this residue by slowly evaporating a nitromethane solution (ca. 1.5 mL) at room temperature yielded **45**•KB(4-ClPh)$_4$•CH_3NO_2 (111 mg, 30%) as colorless crystals that lose CH_3NO_2 on standing: mp 177–178 °C; ^{1}H NMR ($CDCl_3$) δ 7.23–7.05 (m, 14 H), 7.00–6.68 (m, 24 H), 6.58 (dd, 2 H, J = 8.0, 1.2 Hz), 4.31 (s, CH_3NO$_2$), 3.40 (s, 6 H), 3.13 (s, 6 H), 3.23 (s, 4 H). Anal. Calcd for $C_{66}H_{56}BCl_4N_2KO_6$•CH_3NO_2: C, 65.64; H, 4.85; N, 3.43; K, 3.19. Anal. Calcd for $C_{66}H_{56}BCl_4N_2KO_6$•0.5CH_3NO_2: C, 66.82; H, 4.85; N, 2.93; K, 3.27. Found: C, 67.26; H, 4.93; N, 2.30; K, 3.52.

X-ray Crystallography

Crystal data for **39**, **38**, and **26**•I_3 are given in Table 2.3, while crystal data for **28**$_2$•NaBPh$_4$, **45**•NaBPh$_4$, **45**•NaB(4-ClPh)$_4$, **45**•KB(4-ClPh)$_4$•CH_3NO_2, and **45** are presented in Table 3.7. Intensity data were collected at room temperature on an Enraf-Nonius CAD4 diffractometer with graphite monochromated Mo K_α radiation. The measured intensities

were corrected for Lorentz and polarization effects; in the case of **38**, an empirical absorption correction[167] was applied. The structures were solved by direct methods (SHELXS-86[168]) and refined by full-matrix least-squares procedures using the MolEN[169] package of programs. Non-hydrogen atoms were refined anisotropically. Hydrogen atoms were located in the succeeding difference Fourier syntheses and added to the structure factor calculations, but their positions were not refined.

All of the crystal data were obtained and analyzed at Purdue University in Professor B. E. Kahr's group.

39: A colorless needle of $C_{24}H_{27}NO_6$ having approximate dimensions 0.36 x 0.21 x 0.20 mm was mounted on a glass fiber. A total of 2602 reflections ($+h$, $+k$, $\pm l$) were collected in the range $4° < 2\theta < 55°$ with 1203 having $I_o > 3\sigma(I_o)$ being used in the refinement (142 variables). Final $R = 0.057$ and $R_w = 0.076$.

38: A colorless needle of $C_{24}H_{27}BO_3$ having approximate dimensions 0.30 x 0.34 x 0.36 mm was mounted on a glass fiber. A total of 3872 reflections ($\pm h$, $-k$, $+l$) were collected in the range $4° < 2\theta < 50°$ with 1223 having $I_o > 3\sigma(I_o)$ being used in the refinement (253 variables). Final $R = 0.079$ and $R_w = 0.093$.

26•I$_3$: A colorless needle of $C_{25}H_{27}I_3O_6$ having approximate dimensions 0.32 x 0.13 x 0.05 mm was mounted on a glass fiber. A total of 1886 reflections ($\pm h$, $+k$, $+l$) were collected in the range $4° < 2\theta < 45°$ with 1082 having $I_o > 3\sigma(I_o)$ being used in the refinement (156 variables). Final $R = 0.057$ and $R_w = 0.067$.

28_2•NaBPh$_4$: A colorless cube of $C_{66}H_{62}BN_2NaO_6$ having approximate dimensions 0.26 x 0.22 x 0.22 mm was mounted on a glass fiber. A total of 9814 reflections ($\pm h$, $+k$, $+l$) were collected in the range $4° < 2\theta < 50°$ with 2577 having $I_o > 3\sigma(I_o)$ being used in the refinement (560 variables). Final $R = 0.056$ and $R_w = 0.057$. The maximum and minimum peaks in the final difference Fourier map corresponded to 0.22 and 0.10 e/Å^3, respectively.

45•NaBPh$_4$: A clear needle of $C_{66}H_{60}BN_2NaO_6$ having approximate dimensions 0.30 x 0.25 x 0.20 mm was mounted on a glass fiber. A total of 12544 reflections ($\pm h$, $\pm k$, $+l$) were collected in the range $4° < 2\theta < 55°$ with 4100 having $I_o > 3\sigma(I_o)$ being used in the refinement (560 variables). Final $R = 0.108$ and $R_w = 0.132$. The high R-values are a consequence of unresolved disorder in the BPh_4^- counterion. Coordinates of the ligand were quickly convergent and the atomic displacement parameters were ordinary. The maximum and minimum peaks in the final difference Fourier map corresponded to 1.10 and –0.09 e/Å^3, respectively.

45•NaB(4-ClPh)$_4$: A colorless cube of $C_{66}H_{56}BCl_4N_2NaO_6$ having approximate dimensions 0.60 x 0.50 x 0.20 mm was mounted on a glass fiber. A total of 9381 reflections ($\pm h$, $-k$, $-l$) were collected in the range $5° < 2\theta < 47°$ with 3210 having $I_o > 3\sigma(I_o)$ being used in the refinement (586 variables). Final $R = 0.051$ and $R_w = 0.056$. The maximum and minimum peaks in the final difference Fourier map corresponded to 0.37 and 0.23 e/Å^3, respectively.

45•KB(4-ClPh)$_4$•CH$_3$NO$_2$: A colorless cube of $C_{67}H_{59}BCl_4KN_3O_8$ having approximate dimensions 0.30 x 0.30 x 0.10 mm was mounted on a glass fiber. A total of 5182 reflections ($\pm h$, $-k$, $+l$) were collected in the range $5° < 2\theta < 47°$ with 2054 having $I_o > 3\sigma(I_o)$ being used in the refinement (430 variables). Final $R = 0.055$ and $R_w = 0.061$. The maximum and minimum peaks in the final difference Fourier map corresponded to 0.22 and –0.07 e/Å^3, respectively.

45: A colorless crystal of $C_{42}H_{40}N_2O_6$ having approximate dimensions 0.41 x 0.23 x 0.14 mm was mounted on a glass fiber. A total of 8103 reflections ($\pm h$, $\pm k$, $+l$) were collected in the range $4° < 2\theta < 55°$ with 2068 having $I_o > 2\sigma(I_o)$ being used in the refinement (451 variables). Final $R = 0.102$ and $R_w = 0.101$. The maximum and minimum peaks in the final difference Fourier map corresponded to 0.43 and –0.29 e/Å^3, respectively.

ESR Studies

ESR spectra were obtained with a Varian E4 X-band spectrometer equipped with a variable-temperature unit. The temperature was controlled by passing N_2 gas through cooling coils which were immersed in liquid nitrogen. Quartz ESR tubes (Wilmad, 4-mm O. D.) were connected to a Schlenk line via a Cajon Ultra-Torr® reducing union (3/8"→1/4" O. D.). The ESR tubes were modified with quartz→Pyrex graded seals (1/4" O. D.) so they could be attached to the Cajon fitting. The opposite end of the Cajon adapter was connected to a glass "Y" assembly (3/8" O. D.); one end of this assembly was connected to the Schlenk line, while the other end was sealed with a rubber septum to allow for solution transfers.

A solution of radical **47** or biradical **46**, generated as described above, was filtered through a glass frit assembly under anaerobic conditons to remove Ag metal and AgCl. Aliquots of the colored solution were transferred via cannula under argon into quartz ESR tubes containing solid metal salts; the samples were degassed (three freeze–pump–thaw cycles) and sealed under vacuum. For samples prepared using a $CHCl_3$/acetone (7:1, v/v) solvent mixture, the salts were dissolved in acetone, added to the ESR tubes, and degassed (five freeze–pump–thaw cycles); the solution of **47** or **46** was then transferred, the samples degassed (three freeze–pump–thaw cycles) and sealed under vacuum.

The simulated ESR spectrum of monoradical **47** (Figure 4.5a) was generated using the ESRa program written by A. K. Rappé and C. J. Casewit, Calleo Scientific Software, Colorado State University.

Table 2.4A. Atomic Positional and Isotropic Thermal Parameters for **39**

Atom	x	y	z	B(Å^2)
O12	0.4453(3)	0.4239(2)	0.0341(3)	4.94(7)
O16	0.3270(3)	0.3281(2)	0.4192(3)	5.18(7)
O22	0.4028(3)	0.2764(2)	0.0246(3)	5.49(8)
N1	1/2	0.3433(2)	1/4	2.98(9)
C11	0.3855(3)	0.3780(2)	0.2283(4)	3.03(8)
C12	0.3578(4)	0.4197(2)	0.1178(4)	3.70(9)
C13	0.2463(4)	0.4549(2)	0.0985(5)	4.6(1)
C14	0.1632(4)	0.4479(2)	0.1859(5)	4.8(1)
C15	0.1863(4)	0.4063(2)	0.2944(5)	4.6(1)
C16	0.2977(4)	0.3717(2)	0.3167(4)	3.69(9)
C17	0.4043(5)	0.4413(3)	–0.1018(5)	6.9(1)
C18	0.2688(6)	0.3345(3)	0.5346(5)	7.7(2)
C21	1/2	0.2743(3)	1/4	3.5(1)
C22	0.4500(4)	0.2399(2)	0.1338(5)	4.44(9)
C23	0.4492(5)	0.1724(2)	0.1352(6)	6.4(1)
C24	1/2	0.1412(3)	1/4	8.0(2)
C25	0.3815(6)	0.2454(3)	–0.1053(5)	7.4(1)

Table 2.5A. Atomic Positional and Isotropic Thermal Parameters for **38**

Atom	x	y	z	B(Å^2)
O12	0.1825(6)	0.8160(3)	0.5443(4)	6.1(1)
O26	0.1636(6)	0.7154(4)	0.1892(4)	7.7(2)
O36	0.3029(7)	0.6174(4)	0.3648(5)	9.2(2)
C11	0.0694(8)	0.7152(4)	0.4487(5)	4.3(2)
C12	0.0932(8)	0.7452(5)	0.5386(5)	4.3(2)
C13	0.032(1)	0.7100(5)	0.6129(5)	5.9(2)
C14	–0.054(1)	0.6403(6)	0.5980(6)	7.1(3)
C15	–0.0819(2)	0.6065(5)	0.5124(6)	6.4(2)
C16	–0.0255(8)	0.6451(1)	0.4358(8)	5.0(2)
C17	–0.0568(2)	0.6072(5)	0.3450(6)	6.0(2)
C18	0.222(1)	0.8501(6)	0.6309(6)	7.4(3)
C21	0.0512(8)	0.8070(5)	0.2888(5)	4.7(2)
C22	–0.0493(8)	0.8703(5)	0.3042(6)	5.3(2)
C23	–0.1282(2)	0.9063(5)	0.2310(6)	6.9(2)
C24	–0.1077(9)	0.8767(6)	0.1440(6)	8.2(3)
C25	–0.013(1)	0.8149(6)	0.1252(6)	7.8(3)
C26	0.0661(9)	0.7803(5)	0.1980(6)	5.7(2)
C27	–0.0676(9)	0.9047(6)	0.3989(7)	6.8(3)
C28	0.191(1)	0.6855(8)	0.1018(7)	9.7(3)
C31	0.3104(8)	0.7646(5)	0.3647(5)	5.4(2)
C32	0.3852(8)	0.8451(6)	0.3653(6)	6.4(2)
C33	0.5322(9)	0.8374(6)	0.3649(6)	6.6(2)
C34	0.6058(9)	0.7572(6)	0.3663(6)	7.1(3)
C35	0.5325(8)	0.6816(5)	0.3655(6)	5.7(2)
C36	0.3888(8)	0.6890(5)	0.3672(5)	4.9(2)
C37	0.320(1)	0.9275(7)	0.3668(7)	9.7(3)
C38	0.3651(1)	0.5406(7)	0.3646(9)	11.5(4)
B	0.1462(9)	0.7609(5)	0.3684(6)	3.8(2)

Table 2.6A. Atomic Positional and Isotropic Thermal Parameters for **26**•I_3

Atom	x	y	z	B(Å^2)
O12	0.103(1)	0.9865(9)	0.3881(6)	3.2(2)
O22	–0.210(1)	0.6709(8)	0.1801(6)	2.4(2)
O26	0.301(1)	0.9148(9)	0.1718(5)	2.2(2)
C11	0.000	0.855(2)	1/4	1.7(4)
C12	0.000	0.981(2)	1/4	1.9(4)
C13	0.051(2)	1.174(2)	0.321(1)	2.3(3)
C14	0.000	1.232(2)	1/4	4.4(6)
C21	0.052(2)	0.786(1)	0.1827(7)	1.8(3)
C22	–0.047(2)	0.682(1)	0.1569(8)	1.9(3)
C23	0.023(2)	0.603(1)	0.1022(9)	2.8(3)
C24	0.186(2)	0.627(1)	0.0746(9)	3.4(4)
C25	0.2482(2)	0.730(1)	0.0985(8)	2.6(3)
C26	0.214(2)	0.812(1)	0.1493(8)	2.0(3)
C121	0.178(2)	1.051(2)	0.4604(9)	4.8(4)
C221	–0.309(2)	0.563(2)	0.160(1)	4.4(5)
C261	0.480(2)	0.934(1)	0.1494(9)	2.9(4)
I1	1/2	0.2790(2)	1/4	3.74(3)
I2	0.6223(2)	0.2826(1)	0.42273(7)	4.83(3)

Table 3.2A. Atomic Positional and Isotropic Thermal Parameters for $\mathbf{28}_2$•$NaBPh_4$

Atom	x	y	z	B(Å^2)
Na	0.6284(3)	0.11796(7)	0.3148(2)	3.66(7)
O1	0.8117(4)	0.0837(1)	0.2611(3)	3.5(1)
O2	0.5673(4)	0.0700(1)	0.4340(3)	4.7(1)
O3	0.4255(4)	0.1035(1)	0.2059(4)	4.2(1)
O4	0.5206(4)	0.1667(1)	0.3975(3)	4.1(1)
O5	0.6478(4)	0.1476(1)	0.1369(3)	3.8(1)
O6	0.8025(4)	0.1364(1)	0.4463(3)	4.1(1)
N1	0.5928(5)	0.0497(1)	0.2535(4)	2.7(1)
N2	0.7144(5)	0.1845(1)	0.3048(4)	3.0(1)
C1	0.6514(6)	0.0506(2)	0.1657(5)	2.9(2)
C2	0.5984(7)	0.0366(2)	0.0782(5)	4.0(2)
C3	0.6634(7)	0.0378(2)	–0.0026(5)	4.8(2)
C4	0.7833(7)	0.0518(2)	0.0077(5)	4.6(2)
C5	0.8375(6)	0.0663(2)	0.0956(5)	3.8(2)
C6	0.7701(6)	0.0674(2)	0.1743(4)	2.7(2)
C7	0.6628(6)	0.0307(2)	0.3351(5)	3.2(2)
C8	0.6440(6)	0.0412(2)	0.4291(5)	3.6(2)
C9	0.7058(8)	0.0238(2)	0.5108(5)	5.2(2)
C01	0.9414(7)	0.0921(2)	0.2829(6)	5.5(2)
C02	0.5166(8)	0.0759(3)	0.5219(6)	7.5(3)
C03	0.3409(8)	0.1316(2)	0.1723(6)	5.5(2)
C04	0.4989(8)	0.1755(2)	0.4954(6)	5.8(2)
C05	0.5958(7)	0.1367(2)	0.0401(6)	5.0(2)
C06	0.8583(7)	0.1113(2)	0.5179(6)	5.1(2)
C10	0.7891(8)	–0.0034(2)	0.4983(6)	6.0(2)
C11	0.8102(8)	–0.0034(2)	0.4063(6)	5.3(2)
C12	0.7461(7)	0.0035(2)	0.3247(5)	4.2(2)
C13	0.4592(6)	0.0427(2)	0.2400(5)	3.1(2)
C14	0.3734(6)	0.0704(2)	0.2153(5)	3.6(2)
C15	0.2453(6)	0.0639(2)	0.2004(5)	4.3(2)
C16	0.2013(7)	0.0293(2)	0.2097(6)	4.9(2)
C17	0.2852(7)	0.0027(2)	0.2366(5)	4.1(2)

Table 3.2A. (*Continued*)

Atom	x	y	z	B(Å^2)
C18	0.4137(7)	0.0085(2)	0.2512(5)	4.0(2)
C19	0.5937(6)	0.2013(2)	0.2730(5)	3.3(2)
C20	0.4990(6)	0.1934(2)	0.3290(5)	3.3(2)
C21	0.3850(7)	0.2114(2)	0.3106(6)	4.3(2)
C22	0.3641(7)	0.2360(2)	0.2354(6)	5.1(2)
C23	0.4566(7)	0.2417(2)	0.1777(6)	4.6(2)
C24	0.5707(7)	0.2250(2)	0.1960(5)	4.0(2)
C25	0.8011(6)	0.1810(2)	0.2341(5)	3.2(2)
C26	0.7670(6)	0.1616(2)	0.1473(5)	3.4(2)
C27	0.8511(7)	0.1572(2)	0.0805(5)	4.0(2)
C28	0.9718(7)	0.1712(2)	0.1018(5)	4.9(2)
C29	1.0083(7)	0.1898(2)	0.1879(6)	4.9(2)
C30	0.9235(6)	0.1949(2)	0.2539(5)	3.8(2)
C31	0.7672(6)	0.1958(2)	0.4015(5)	3.4(2)
C32	0.7682(7)	0.2319(2)	0.4253(5)	4.5(2)
C33	0.8146(7)	0.2433(2)	0.5196(6)	4.8(2)
C34	0.8585(7)	0.2187(2)	0.5891(5)	5.2(2)
C35	0.8555(7)	0.1829(2)	0.5666(5)	4.4(2)
C36	0.8102(6)	0.1716(2)	0.4735(5)	3.3(2)
C40	0.5734(6)	–0.1339(2)	0.2274(5)	3.4(2)
C41	0.4998(7)	–0.1031(2)	0.2178(6)	4.7(2)
C42	0.3677(8)	–0.1035(2)	0.2148(6)	5.6(2)
C43	0.3078(7)	–0.1349(2)	0.2236(6)	5.4(2)
C44	0.3744(7)	–0.1658(2)	0.2359(6)	5.1(2)
C45	0.5054(7)	–0.1655(2)	0.2377(6)	4.7(2)
C50	0.7743(6)	–0.1399(2)	0.3556(5)	3.0(2)
C51	0.7659(7)	–0.1115(2)	0.4204(5)	3.7(2)
C52	0.7968(7)	–0.1142(2)	0.5219(5)	4.1(2)
C53	0.8360(7)	–0.1464(2)	0.5631(5)	4.0(2)
C54	0.8455(7)	–0.1748(2)	0.5032(5)	4.0(2)
C55	0.8144(6)	–0.1719(2)	0.4025(5)	3.6(2)
C60	0.7878(6)	–0.0987(2)	0.1952(5)	3.4(2)

Table 3.2A. (*Continued*)

Atom	x	y	z	B(Å^2)
C61	0.7351(7)	–0.0828(2)	0.1078(6)	4.8(2)
C62	0.7898(8)	–0.0534(2)	0.0660(6)	5.6(2)
C63	0.9003(8)	–0.0409(2)	0.1119(6)	5.5(2)
C64	0.9582(8)	–0.0546(2)	0.1973(6)	5.8(2)
C65	0.9026(7)	–0.0843(2)	0.2386(6)	4.9(2)
C70	0.7816(6)	–0.1675(2)	0.1762(5)	3.5(2)
C71	0.9101(8)	–0.1754(2)	0.1915(6)	5.6(2)
C72	0.9644(8)	–0.2027(2)	0.1392(6)	5.8(2)
C73	0.8907(7)	–0.2207(2)	0.0706(6)	5.5(2)
C74	0.7655(8)	–0.1869(2)	0.1027(6)	6.0(2)
C75	0.7117(7)	–0.1348(2)	0.237796)	5.0(2)
B	0.7274(8)	–0.1348(2)	0.2377(6)	3.3(2)

Table 3.3A. Atomic Positional and Isotropic Thermal Parameters for **45**•$NaBPh_4$

Atom	x	y	z	B(Å^2)
Na	0.1828(3)	0.2488(2)	0.1393(2)	3.65(8)
O1	0.2355(5)	0.2209(4)	–0.0176(4)	4.0(1)
O2	0.1348(5)	0.0842(4)	0.1551(4)	4.7(2)
O3	0.3527(5)	0.2510(4)	0.2315(4)	4.3(2)
O4	0.1675(5)	0.3158(5)	0.2995(4)	4.9(2)
O5	0.2356(5)	0.4136(4)	0.1425(4)	4.5(2)
O6	–0.0048(5)	0.2144(4)	0.0690(4)	4.7(2)
N1	0.3260(5)	0.1218(4)	0.0816(4)	2.9(2)
N2	0.0334(6)	0.3742(5)	0.1986(5)	3.5(2)
C1	0.2962(6)	0.0773(6)	–0.0098(5)	3.3(2)
C2	0.2536(7)	0.1309(6)	–0.0609(5)	3.3(2)
C3	0.2338(7)	0.0911(7)	–0.1503(6)	4.4(2)
C4	0.2488(8)	–0.0028(7)	–0.1865(6)	5.1(3)
C5	0.2824(8)	–0.0571(7)	–0.1368(6)	4.8(3)
C6	0.3072(7)	–0.0164(6)	–0.0485(6)	3.8(2)
C7	0.3228(7)	0.0589(6)	0.1367(5)	3.4(2)
C8	0.2212(8)	0.0378(6)	0.1708(6)	4.3(2)
C9	0.217(1)	–0.0263(7)	0.2205(7)	6.8(3)
C01	0.1931(9)	0.2273(7)	–0.0695(6)	5.2(3)
C02	0.0342(8)	0.0669(7)	0.1952(7)	5.7(3)
C03	0.3587(8)	0.3137(7)	0.3169(6)	5.1(3)
C04	0.2496(9)	0.2927(8)	0.3531(6)	5.7(3)
C05	0.3398(8)	0.4349(7)	0.1087(7)	5.3(3)
C06	–0.0264(9)	0.1261(8)	0.0029(8)	6.3(3)
C10	0.313(1)	–0.0671(7)	0.2380(8)	7.3(3)
C11	0.4095(9)	–0.0432(8)	0.2065(7)	6.5(3)
C12	0.4143(8)	0.0192(6)	0.1549(6)	4.3(2)
C13	0.4240(6)	0.1883(5)	0.0972(5)	2.9(2)
C14	0.4387(7)	0.2538(6)	0.1792(6)	3.5(2)
C15	0.5323(8)	0.3173(7)	0.2009(6)	4.4(2)
C16	0.6102(8)	0.3165(7)	0.1370(7)	4.9(2)
C17	0.5955(7)	0.2539(7)	0.0563(6)	4.5(2)

Table 3.3A. (*Continued*)

Atom	x	y	z	B(Å^2)
C18	0.5021(7)	0.1879(6)	0.0362(5)	3.5(2)
C19	–0.0148(7)	0.3273(6)	0.2582(5)	3.5(2)
C20	0.0571(8)	0.2997(7)	0.3138(6)	4.2(2)
C21	0.0169(9)	0.2579(7)	0.3765(6)	5.4(3)
C22	–0.0932(9)	0.2403(8)	0.3826(6)	6.0(3)
C23	–0.1668(9)	0.2651(8)	0.3250(7)	6.1(3)
C24	–0.1258(8)	0.3097(7)	0.2638(6)	4.8(3)
C25	0.0973(7)	0.4633(6)	0.2397(6)	3.9(2)
C26	0.2004(8)	0.4828(6)	0.2094(6)	4.2(2)
C27	0.2614(9)	0.5683(7)	0.2462(7)	5.4(3)
C28	0.221(1)	0.6305(8)	0.3136(8)	7.1(4)
C29	0.120(1)	0.6127(8)	0.3464(8)	7.3(4)
C30	0.0594(9)	0.5282(7)	0.3082(7)	5.9(3)
C31	–0.0328(7)	0.3734(6)	0.1220(6)	3.9(2)
C32	–0.0535(7)	0.2900(6)	0.0546(6)	4.1(2)
C33	–0.1153(8)	0.2872(8)	–0.0205(7)	5.4(3)
C34	–0.154(1)	0.3669(9)	–0.0298(7)	7.4(3)
C35	–0.135(1)	0.4478(8)	0.0344(8)	8.1(3)
C36	–0.0748(9)	0.4529(7)	0.1092(8)	5.9(3)
C40	0.3854(7)	0.3199(6)	–0.2709(6)	3.6(2)
C41	0.3692(8)	0.4048(6)	–0.2107(6)	4.3(2)
C42	0.4144(8)	0.4313(7)	–0.1254(6)	4.7(2)
C43	0.4772(8)	0.3727(7)	–0.0985(6)	4.8(2)
C44	0.4971(9)	0.2901(7)	–0.1532(7)	5.2(2)
C45	0.4509(8)	0.2641(7)	–0.2385(6)	4.8(2)
C50	0.2970(8)	0.3784(6)	–0.4027(6)	4.2(2)
C51	0.1926(8)	0.3936(7)	–0.4288(6)	4.7(2)
C52	0.1762(9)	0.4708(8)	–0.4618(7)	6.1(3)
C53	0.263(1)	0.5304(8)	–0.4665(8)	6.9(3)
C54	0.368(1)	0.5215(8)	–0.4404(7)	6.5(3)
C55	0.3823(9)	0.4457(8)	–0.4089(7)	5.7(3)
C60	0.212(1)	0.2208(8)	–0.3632(7)	6.4(3)

Table 3.3A. (*Continued*)

Atom	x	y	z	B(Å^2)
C61	0.132(1)	0.2477(8)	–0.3080(8)	7.1(3)
C62	0.029(1)	0.195(1)	–0.303(1)	9.8(4)
C63	0.020(2)	0.114(2)	–0.356(1)	15.7(7)
C64	0.103(3)	0.057(2)	–0.395(2)	25(1)
C65	0.205(2)	0.130(2)	–0.407(2)	18.9(9)
C70	0.4051(9)	0.2274(8)	–0.4390(7)	5.7(3)
C71	0.367(2)	0.177(1)	–0.523(1)	13.4(6)
C72	0.547(2)	0.154(2)	–0.575(1)	16.3(7)
C73	0.446(2)	0.137(2)	–0.598(2)	19.0(9)
C74	0.578(2)	0.216(1)	–0.513(1)	14.8(7)
C75	0.499(2)	0.253(1)	–0.454(1)	13.1(6)
B	0.3250(9)	0.2850(8)	–0.3708(7)	4.0(2)

Table 3.4A. Atomic Positional and Isotropic Thermal Parameters for **45**•NaB(4-ClPh)$_4$

Atom	x	y	z	B(Å^2)
Cl1	0.1393(2)	1.0598(1)	0.1141(1)	8.25(6)
Cl2	0.7463(1)	0.7248(1)	0.12256(9)	7.07(6)
Cl3	0.4344(2)	0.8111(1)	0.49922(9)	7.86(6)
Cl4	0.0732(1)	0.5520(1)	0.14773(9)	6.75(5)
Na	0.6030(2)	0.2837(1)	0.1196(1)	3.72(6)
O1	0.5289(3)	0.3724(2)	0.0522(2)	4.8(1)
O2	0.5386(3)	0.3036(2)	0.2160(2)	4.3(1)
O3	0.7589(3)	0.3380(2)	0.1625(2)	4.9(1)
O4	0.7246(3)	0.1959(2)	0.1603(2)	4.5(1)
O5	0.6952(3)	0.2607(2)	0.0306(2)	5.1(1)
O6	0.4407(3)	0.2253(2)	0.1038(2)	4.5(1)
N1	0.6024(3)	0.4191(2)	0.1565(2)	2.9(1)
N2	0.6017(3)	0.1493(2)	0.0789(2)	3.2(1)
C1	0.5112(4)	0.4489(3)	0.1332(3)	3.2(2)
C2	0.4755(4)	0.4254(3)	0.0779(3)	3.7(2)
C3	0.3899(4)	0.4534(4)	0.0536(3)	5.0(2)
C4	0.3378(4)	0.5025(4)	0.0840(3)	5.6(2)
C5	0.3712(4)	0.5248(4)	0.1378(3)	6.0(2)
C6	0.4582(4)	0.4984(3)	0.1627(3)	4.6(2)
C7	0.6111(4)	0.4171(3)	0.2202(3)	3.3(1)
C8	0.5739(4)	0.3590(3)	0.2491(3)	3.5(2)
C9	0.5774(4)	0.3594(4)	0.3111(3)	4.8(2)
C10	0.6177(5)	0.4170(4)	0.3405(3)	5.9(2)
C11	0.6561(5)	0.4723(4)	0.3115(3)	6.4(2)
C12	0.6522(5)	0.4729(4)	0.2517(3)	5.1(2)
C13	0.6893(4)	0.4448(3)	0.1292(2)	3.2(1)
C14	0.7723(4)	0.4016(3)	0.1333(3)	4.1(2)
C15	0.8581(4)	0.4216(4)	0.1104(3)	4.9(2)
C16	0.8628(4)	0.4842(4)	0.0803(3)	5.9(2)
C17	0.7827(5)	0.5274(4)	0.0749(3)	5.4(2)
C18	0.6959(4)	0.5079(3)	0.1003(3)	4.4(2)
C19	0.5987(4)	0.1167(3)	0.1356(3)	3.5(2)

Table 3.4A. (*Continued*)

Atom	x	y	z	B(Å^2)
C20	0.6671(4)	0.1401(3)	0.1788(3)	3.7(2)
C21	0.6730(4)	0.1110(4)	0.2337(3)	4.6(2)
C22	0.6082(5)	0.0591(4)	0.2478(3)	5.4(2)
C23	0.5361(5)	0.0373(3)	0.2068(3)	5.2(2)
C24	0.5325(4)	0.0658(3)	0.1509(3)	4.2(2)
C25	0.6929(4)	0.1386(3)	0.0505(3)	3.5(2)
C26	0.7391(4)	0.1956(3)	0.0247(3)	3.9(2)
C27	0.8260(4)	0.1862(4)	–0.0027(3)	5.1(2)
C28	0.8669(5)	0.1187(4)	–0.0036(3)	6.3(2)
C29	0.8241(5)	0.0628(4)	0.0222(3)	6.0(2)
C30	0.7374(4)	0.0727(3)	0.0495(3)	4.5(2)
C31	0.5135(4)	0.1434(3)	0.0416(3)	3.6(2)
C32	0.4307(4)	0.1808(3)	0.0566(3)	3.7(2)
C33	0.3457(4)	0.1740(4)	0.0228(3)	5.1(2)
C34	0.3434(5)	0.1310(4)	–0.0273(3)	6.1(2)
C35	0.4254(5)	0.0965(4)	–0.0428(3)	5.6(2)
C36	0.5115(5)	0.1010(3)	–0.0076(3)	4.3(2)
C50	0.3002(4)	0.8720(3)	0.2015(3)	3.6(1)
C51	0.2117(4)	0.8989(3)	0.2211(3)	4.4(2)
C52	0.1616(5)	0.9553(4)	0.1947(3)	5.0(2)
C53	0.2015(5)	0.9889(4)	0.1483(3)	5.0(2)
C54	0.2868(5)	0.9656(4)	0.1259(3)	5.0(2)
C55	0.3352(5)	0.9073(3)	0.1528(3)	4.7(2)
C60	0.4521(4)	0.7790(3)	0.2004(3)	3.4(1)
C61	0.5305(4)	0.8272(3)	0.2010(3)	4.1(1)
C62	0.6199(4)	0.8115(3)	0.1767(3)	4.2(2)
C63	0.6337(4)	0.7467(3)	0.1518(3)	4.4(2)
C64	0.5616(5)	0.6974(4)	0.1510(3)	5.0(2)
C65	0.4723(4)	0.7142(3)	0.1743(3)	4.6(2)
C70	0.3506(4)	0.8638(3)	0.3351(3)	4.3(2)
C71	0.3712(4)	0.8050(3)	0.3006(3)	3.5(1)
C72	0.4162(4)	0.7486(3)	0.3327(3)	3.7(1)

Table 3.4A. (*Continued*)

Atom	x	y	z	B(Å^2)
C73	0.4351(4)	0.7487(3)	0.3932(3)	4.0(1)
C74	0.4112(4)	0.8087(3)	0.4231(3)	4.1(1)
C75	0.3708(5)	0.8659(4)	0.3958(3)	4.9(2)
C80	0.2693(4)	0.7346(3)	0.2138(3)	3.4(1)
C81	0.2174(4)	0.7362(3)	0.1596(3)	4.4(2)
C82	0.1554(4)	0.6807(3)	0.1407(3)	4.6(2)
C83	0.1455(4)	0.6230(3)	0.1737(3)	4.0(1)
C84	0.1905(4)	0.6182(3)	0.2282(3)	4.5(2)
C85	0.2515(4)	0.6742(3)	0.2466(3)	3.9(1)
C01	0.4968(6)	0.3497(4)	–0.0050(3)	6.5(2)
C02	0.4980(5)	0.2448(3)	0.2463(3)	4.9(2)
C03	0.8385(4)	0.2883(4)	0.1678(3)	5.6(2)
C04	0.7990(5)	0.2237(4)	0.1982(3)	5.6(2)
C05	0.7362(6)	0.3186(4)	0.0001(3)	6.9(2)
C06	0.3565(4)	0.2636(4)	0.1195(3)	5.7(2)
B	0.3475(5)	0.7992(4)	0.2296(3)	3.4(2)

Table 3.5A. Atomic Positional and Isotropic Thermal Parameters for **45**•KB(4-ClPh)$_4$•CH_3NO_2

Atom	x	y	z	B(Å^2)
K1	0.9349(2)	0.0178(2)	0.6953(2)	4.79(7)
Cl1	0.08070	–0.5538(4)	0.94150	8.1(1)
Cl2	0.8384(3)	–0.6852(3)	1.0548(2)	6.6(1)
Cl3	0.4063(3)	–1.1071(3)	0.6807(2)	7.7(1)
Cl4	0.6423(4)	–0.3077(3)	0.6285(2)	8.0(1)
O1	0.7955(5)	–0.0671(7)	0.7744(4)	4.9(2)
O2	1.0090(7)	–0.1840(7)	0.6774(4)	6.8(3)
O3	1.0984(5)	0.0381(6)	0.7868(4)	4.5(2)
O4	1.0958(5)	0.1260(7)	0.6513(4)	5.4(2)
O5	0.8740(6)	0.2264(7)	0.7333(4)	5.2(2)
O6	0.8332(6)	0.0116(7)	0.5680(4)	5.7(2)
O(S1)	0.371(1)	0.241(1)	0.5496(7)	13.2(4)
O(S2)	0.275(1)	0.342(2)	0.6031(9)	17.7(6)
N1	0.9806(6)	–0.1323(7)	0.8150(5)	3.4(2)
N2	0.9297(6)	0.2036(7)	0.5964(4)	3.2(2)
N(S)	0.351(1)	0.324(1)	0.5756(8)	11.2(4)
C1	0.8999(8)	–0.2044(9)	0.8247(6)	3.6(2)
C2	0.8044(9)	–0.172(1)	0.8038(6)	4.2(3)
C3	0.7246(9)	–0.243(1)	0.8130(7)	5.1(3)
C4	0.7417(9)	–0.340(1)	0.8393(7)	5.7(3)
C5	0.8272(9)	–0.376(1)	0.8610(7)	5.4(3)
C6	0.9114(9)	–0.307(1)	0.8548(6)	5.2(3)
C7	1.0689(8)	–0.1841(9)	0.7951(6)	3.5(2)
C8	1.0783(9)	–0.214(1)	0.7241(6)	5.4(3)
C9	1.1619(9)	–0.273(1)	0.7029(7)	5.8(3)
C(S)	0.418(1)	0.409(2)	0.583(1)	11.4(6)
C10	1.231(1)	–0.297(1)	0.7509(8)	7.0(4)
C11	1.225(1)	–0.271(1)	0.8208(8)	8.1(4)
C12	1.142(1)	–0.210(1)	0.8418(7)	6.2(3)
C13	0.9942(8)	–0.0450(9)	0.8667(6)	3.4(2)
C14	1.0550(8)	0.040(1)	0.8520(6)	3.9(3)

Table 3.5A. (*Continued*)

Atom	x	y	z	B(Å^2)
C15	1.0691(9)	0.125(1)	0.9026(6)	4.8(3)
C16	1.0162(9)	0.125(1)	0.9629(7)	5.0(3)
C17	0.9537(9)	0.044(1)	0.9771(7)	4.8(3)
C18	0.9415(9)	–0.044(1)	0.9288(6)	4.3(3)
C19	1.0002(8)	0.1600(9)	0.5502(6)	3.6(2)
C20	1.0880(8)	0.122(1)	0.5775(6)	4.1(3)
C21	1.1618(8)	0.084(1)	0.5355(6)	4.5(3)
C22	1.1452(9)	0.081(1)	0.4654(7)	6.1(3)
C23	1.061(1)	0.115(1)	0.4343(7)	6.5(4)
C24	0.9844(9)	0.157(1)	0.4772(7)	5.5(3)
C25	0.9583(8)	0.2958(9)	0.6371(6)	3.5(2)
C26	0.9277(9)	0.310(1)	0.7056(6)	4.5(3)
C27	0.953(1)	0.404(1)	0.7455(7)	6.8(4)
C28	1.013(1)	0.481(1)	0.7144(8)	7.7(4)
C29	1.044(1)	0.466(1)	0.6493(9)	8.2(4)
C30	1.017(1)	0.375(1)	0.6076(7)	6.2(3)
C31	0.8292(8)	0.2020(9)	0.5732(6)	3.6(2)
C32	0.7796(8)	0.105(1)	0.5587(6)	4.2(3)
C33	0.6812(9)	0.106(1)	0.5405(7)	5.4(3)
C34	0.632(1)	0.203(1)	0.5352(7)	6.1(3)
C35	0.679(1)	0.299(1)	0.5461(8)	6.9(4)
C36	0.7783(9)	0.297(1)	0.5666(7)	4.9(3)
C50	0.3878(8)	–0.6353(9)	0.8661(6)	3.6(3)
C51	0.3070(9)	–0.625(1)	0.8209(6)	4.5(3)
C52	0.2137(9)	–0.598(1)	0.8405(7)	5.3(3)
C53	0.2012(9)	–0.584(1)	0.9140(7)	5.3(3)
C54	0.274(1)	–0.593(1)	0.9610(7)	5.7(3)
C55	0.3717(9)	–0.615(1)	0.9368(6)	4.8(3)
C60	0.5801(8)	–0.6773(9)	0.8955(6)	3.5(3)
C61	0.6310(8)	–0.7726(9)	0.9143(6)	3.9(3)
C62	0.7096(9)	–0.774(1)	0.9640(6)	4.4(3)
C63	0.7384(8)	–0.681(1)	0.9956(6)	4.2(3)

Table 3.5A. (*Continued*)

Atom	x	y	z	B(Å^2)
C64	0.6909(8)	–0.586(1)	0.9829(6)	4.1(3)
C65	0.6128(8)	–0.584(1)	0.9333(6)	4.6(3)
C70	0.4786(8)	–0.7829(9)	0.7914(6)	3.6(3)
C71	0.4981(9)	–0.808(1)	0.7231(6)	4.9(3)
C72	0.4815(9)	–0.905(1)	0.6857(6)	5.0(3)
C73	0.4378(9)	–0.983(1)	0.7252(6)	4.3(3)
C74	0.4177(9)	–0.973(1)	0.7937(7)	4.8(3)
C75	0.4369(9)	0.8659(4)	0.3958(3)	4.9(2)
C80	0.5304(8)	–0.5731(9)	0.7788(6)	3.5(3)
C81	0.4825(9)	–0.473(1)	0.7688(7)	4.9(3)
C82	0.5166(9)	–0.390(1)	0.7231(7)	5.4(3)
C83	0.6016(9)	–0.410(1)	0.6862(6)	4.4(3)
C84	0.6547(9)	–0.506(1)	0.6971(6)	5.0(3)
C85	0.6163(8)	–0.583(1)	0.7421(6)	4.4(3)
C01	0.6987(9)	–0.030(1)	0.7517(8)	7.0(4)
C02	1.019(2)	–0.210(2)	0.611(1)	29.9(8)
C03	1.1625(8)	0.123(1)	0.7666(7)	5.6(4)
C04	1.1848(8)	0.101(1)	0.6896(7)	6.1(4)
C05	0.844(1)	0.232(1)	0.8063(6)	6.6(4)
C06	0.803(1)	–0.084(1)	0.533(1)	13.4(7)
B	0.495(1)	–0.665(1)	0.8316(7)	3.6(3)

Table 3.6A. Atomic Positional and Isotropic Thermal Parameters for **45**

Atom	x	y	z	B(Å^2)
O1	0.5913(9)	–0.0880(6)	0.5966(5)	3.8(2)
O2	0.774(1)	0.0751(5)	0.8657(5)	4.2(2)
O3	0.3805(9)	0.1617(5)	0.7580(4)	3.4(2)
O4	0.2454(9)	0.3734(5)	0.7979(4)	3.1(2)
O5	–0.163(1)	0.2347(5)	0.6912(5)	3.8(2)
O6	0.084(1)	0.3656(6)	0.5528(5)	4.2(2)
N1	0.485(1)	–0.0108(6)	0.7676(5)	2.8(2)
N2	–0.041(1)	0.4192(6)	0.7176(5)	2.9(2)
C01	0.647(2)	–0.122(1)	0.5101(8)	5.3(4)
C1	0.369(1)	–0.0565(7)	0.6932(6)	2.3(3)
C02	0.892(2)	0.124(1)	0.937(1)	9.3(6)
C2	0.422(1)	–0.0913(7)	0.6053(7)	2.7(3)
C03	0.236(1)	0.1910(8)	0.7235(7)	3.7(3)
C3	0.307(1)	–0.1327(8)	0.5335(8)	3.8(3)
C04	0.266(2)	0.2858(8)	0.7142(7)	3.9(3)
C4	0.136(2)	–0.1319(9)	0.5459(8)	4.5(4)
C05	–0.214(2)	0.1342(9)	0.6784(9)	5.3(4)
C5	0.089(2)	–0.0947(8)	0.6326(8)	4.2(4)
C06	0.150(2)	0.343(1)	0.4699(8)	5.6(4)
C6	0.197(1)	–0.0580(8)	0.7055(7)	3.7(3)
C7	0.613(1)	–0.0721(7)	0.7801(7)	3.0(3)
C8	0.759(1)	–0.0291(8)	0.8302(7)	3.5(3)
C9	0.883(2)	–0.0894(9)	0.8423(7)	4.5(3)
C10	0.859(2)	–0.1930(9)	0.8024(8)	5.4(4)
C11	0.719(2)	–0.2365(8)	0.7512(8)	4.7(3)
C12	0.593(2)	–0.1779(8)	0.7387(8)	4.2(3)
C13	0.429(1)	0.0704(7)	0.8478(6)	2.1(2)
C14	0.372(1)	0.1578(8)	0.8405(7)	2.9(3)
C15	0.315(1)	0.2370(8)	0.9158(7)	3.4(3)
C16	0.315(1)	0.2317(9)	0.9964(7)	3.7(3)
C17	0.371(2)	0.1461(9)	1.0019(7)	3.9(3)
C18	0.425(1)	0.0675(8)	0.9286(6)	3.2(3)

Table 3.6A. (*Continued*)

Atom	x	y	z	B(Å^2)
C19	0.104(1)	0.4860(8)	0.7444(7)	2.6(3)
C20	0.241(1)	0.4625(8)	0.7866(7)	3.0(3)
C21	0.375(1)	0.5292(9)	0.8213(7)	3.6(3)
C22	0.381(2)	0.6180(9)	0.8101(9)	4.9(4)
C23	0.248(2)	0.6388(8)	0.7664(9)	4.5(4)
C24	0.113(2)	0.5740(8)	0.7336(8)	4.0(3)
C25	–0.115(1)	0.4049(7)	0.7897(6)	2.6(3)
C26	–0.179(1)	0.3122(8)	0.7761(7)	3.4(3)
C27	–0.258(1)	0.2966(8)	0.8424(8)	4.1(3)
C28	–0.266(2)	0.3792(9)	0.9257(7)	4.6(4)
C29	–0.199(2)	0.4727(9)	0.9417(8)	4.9(4)
C30	–0.124(1)	0.4858(8)	0.8750(7)	3.6(3)
C31	–0.146(1)	0.4157(7)	0.6448(6)	2.3(3)
C32	–0.081(1)	0.3872(7)	0.5614(7)	3.2(3)
C33	–0.185(2)	0.3827(8)	0.4905(8)	4.3(3)
C34	–0.355(2)	0.4033(9)	0.5027(7)	4.9(4)
C35	–0.414(2)	0.428(1)	0.5857(9)	5.8(4)
C36	–0.312(1)	0.4352(8)	0.6556(8)	3.7(3)

REFERENCES

1. Lindsey, J. S. *New J. Chem.* **1991**, *5*, 153–180.

2. Rajca, A. *Chem. Rev.* **1994**, *94*, 871–893.

3. Baxter, P.; Lehn, J.-M.; DeCian, A.; Fischer, J. *Angew. Chem., Int. Ed. Engl.* **1993**, *32*, 69–72.

4. Caspar, D. L. D.; Klug, A. *Cold Spring Harbor Symp. Quant. Biol.* **1962**, *27*, 1–24.

5. Timasheff, S. N. In *Protein-Protein Interactions*; Frieden, C., Nichols, L. W., Eds.; Wiley: New York, 1981; pp 315–336.

6. Klug, A. *Angew. Chem., Int. Ed. Engl.* **1983**, *22*, 565–582.

7. (a) Etter, M. C.; Frankenbach, G. M. *Chem. Mater.* **1989**, *1*, 1–10. (b) Etter, M. C.; Frankenbach, G. M.; Adsmond, D. A. *Mol. Cryst. Liq. Cryst.* **1990**, *187*, 25–39. (c) Prasad, P. N.; Williams, D. J. *Introduction to Nonlinear Optical Effects in Molecules and Polymers*; Wiley: New York, 1991. (d) Etter, M. C.; Huang, K. S.; Frankenbach, G. M.; Adsmond, D. A. In *Materials for Nonlinear Optics: Chemical Perspectives*; Marder, S. R., Sohn, J. E., Stucky, G. D., Eds.; American Chemical Society: Washington, DC, 1991; Vol. 455, pp 446–456. (e) Russell, V. A.; Etter, M. C.; Ward, M. D. *Chem. Mater.* **1994**, *6*, 1206–1217.

8. (a) Torrance, J. B. *Acc. Chem. Res.* **1979**, *12*, 79–86. (b) Wudl, F. *Acc. Chem. Res.* **1984**, *17*, 227–232. (c) Williams, J. M.; Beno, M. A.; Wang, H. H.; Leung, P. C. W.; Emge, T. J.; Geiser, U.; Carlson, K. D. *Acc. Chem. Res.* **1985**, *18*, 261–267. (d) Fagan, P. J.; Ward, M. D.; Calabrese, J. C. *J. Am. Chem. Soc.* **1989**, *111*, 1689–1719. (e) Ward, M. D.; Fagan, P. J.; Calabrese, J. C.; Johnson, D. C. *J. Am. Chem. Soc.* **1989**, *111*, 1719–1732.

9. (a) Torrance, J. B.; Oostra, S.; Nazzal, A. *Synth. Met.* **1987**, *19*, 709–714. (b) Miller, J. S.; Epstein, A. J.; Reiff, W. M. *Acc. Chem. Res.* **1988**, *21*, 114–120. (c) Miller, J. S.; Glazhofer, D. T.; Calabrese, J. C.; Epstein, A. J. *J. Chem. Soc., Chem. Commun.* **1988**, 322–323. (d) Miller, J. S.; Epstein, A. J. *Angew. Chem., Int. Ed. Engl.* **1994**, *33*, 385–415.

10. (a) Desiraju, G. R. *Crystal Engineering: The Design of Organic Solids*; Materials Science Monographs, Vol. 54; Elsevier: New York, 1989. (b) Wright, J. D. *Molecular Crystals*, 2nd ed.; Cambridge University Press: Cambridge, NY, 1995.

11. Sarma, J. A. R. P.; Desiraju, G. R. *Acc. Chem. Res.* **1986**, *19*, 222–228.

12. (a) Diederich, F. *Angew. Chem., Int. Ed. Engl.* **1988**, *27*, 362–386. (b) Hamilton, A. D.; Pant, N.; Muehldorf, A. *Pure Appl. Chem.* **1988**, *60*, 533–538. (c) Zimmerman, S. C.; Wu, W. *J. Am. Chem. Soc.* **1989**, *111*, 8054–8055. (d) Rebek, J., Jr. *Angew. Chem., Int. Ed. Engl.* **1990**, *29*, 245–255. (e) Ebmeyer, F.; Rebek, J.,

Jr. *Angew. Chem., Int. Ed. Engl.* **1990**, *29*, 1148–1150. (f) Wyler, R.; de Mendoza, J.; Rebek, J., Jr. *Angew. Chem., Int. Ed. Engl.* **1993**, *32*, 1699–1701.

13. (a) Vinogradov, S. N.; Linnel, R. H. *Hydrogen Bonding*; Van Nostrand Reinhold: New York, 1971. (b) Joesten, M. D.; Schaad, L. J. *Hydrogen Bonding*; M. Dekker: New York, 1974. (c) Jeffrey, G. A.; Saenger, W. *Hydrogen Bonding in Biological Structures*; Springer-Verlag: Berlin, 1991.

14. (a) Etter, M. C. *Acc. Chem. Res.* **1990**, *23*, 120–126. (b) Etter, M. C. *J. Phys. Chem.* **1991**, *95*, 4601–4610. (c) Reutzel, S. M.; Etter, M. C. *J. Phys. Org. Chem.* **1992**, *5*, 44–54. (d) Etter, M. C.; MacDonald, J. C.; Wanke, R. A. *J. Phys. Org. Chem.* **1992**, *5*, 191–200.

15. (a) Leiserowitz, L. *Acta Crystallogr., Sect. B: Struct. Crystallogr. Cryst. Chem.* **1976**, *B32*, 775–802. (b) Leiserowitz, L. *Acta Crystallogr., Sect. B: Struct. Crystallogr. Cryst. Chem.* **1977**, *B33*, 2719–2733. (c) Leiserowitz, L.; Tuval, M. *Acta Crystallogr., Sect. B: Struct. Crystallogr. Cryst. Chem.* **1978**, *B34*, 1230–1247. (d) Weinstein, S.; Leiserowitz, L. *Acta Crystallogr., Sect. B: Struct. Crystallogr. Cryst. Chem.* **1980**, *B36*, 1406–1418. (e) Weinstein, S.; Leiserowitz, L.; Gil-Av, E. *J. Am. Chem. Soc.* **1980**, *102*, 2768–2772.

16. (a) Taylor, R.; Kennard, O. *J. Am. Chem. Soc.* **1982**, *104*, 5063–5070. (b) Taylor, R.; Kennard, O. *Acc. Chem. Res.* **1984**, *17*, 320–326.

17. (a) Zhao, X.; Chang, Y.-L.; Fowler, F. W.; Lauher, J. W. *J. Am. Chem. Soc.* **1990**, *112*, 6627–6634. (b) Fan, E.; Vicent, C.; Geib, S. J.; Hamilton, A. D. *Chem. Mater.* **1994**, *6*, 1113–1117. (c) MacDonald, J. C.; Whitesides, G. M. *Chem. Rev.* **1994**, *94*, 2383–2420. (d) Whitesides, G. M.; Mathias, J. P.; Seto, C. T.; Chin, D. N.; Mammen, M.; Gordon, D. M.; *Acc. Chem. Res.* **1995**, *28*, 37–44.

18. (a) Hernandez, E.; Mas, M.; Molins, E.; Rovira, C.; Veciana, J. *Angew. Chem., Int. Ed. Engl.* **1993**, *32*, 882–884. (b) Cirujeda, J.; Ochando, L. E.; Amigó, J. M.; Rovira, C.; Rius, J.; Veciana, J. *Angew. Chem., Int. Ed. Engl.* **1995**, *32*, 55–57. (c) Cirujeda, J.; Mas, M.; Molins, E.; de Panthou, F. L.; Laugier, J.; Park, J. G.; Paulsen, C.; Rey, P.; Rovira, C.; Veciana, J. *J. Chem. Soc., Chem. Commun.* **1995**, 709–710.

19. Simard, M.; Su, D.; Wuest, J. D. *J. Am. Chem. Soc.* **1991**, *113*, 4696–4698.

20. Martell, A. E.; Calvin, M. *Chemistry of the Metal Chelate Compounds*; Prentice-Hall: New York, 1952.

21. Pedersen, C. J. *Angew. Chem., Int. Ed. Engl.* **1988**, *27*, 1021–1027.

22. Lehn, J.-M. *Acc. Chem. Res.* **1978**, *11*, 49–57.

23. Cram, D. J. *Angew. Chem., Int. Ed. Engl.* **1986**, *25*, 1039–1057.

24. Lehn, J.-M. In *Struct. Bonding*, **1973**, *16*, 1–69.

25. Seiler, P.; Dobler, M.; Dunitz, J. D. *Acta Crystallogr., Sect. B: Struct. Crystallogr. Cryst. Chem.*, **1974**, *B30*, 2744–2745.

26. van Remoortere, F. P.; Boer, F. P. *Inorg. Chem.* **1974**, *13*, 2071–2078.

27. Boer, F. P.; Neuman, M. A.; van Remoortere, F. P.; Steiner, E. C. *Inorg. Chem.* **1974**, *13*, 2826–2834.

28. Feneau-Dupont, P. J.; Arte, E.; Declercq, J. P.; Germain, G.; Van Meerssche, M. *Acta Crystallogr., Sect. B: Struct. Crystallogr. Cryst. Chem.*, **1979**, *B35*, 1217–1220.

29. Mallinson, P. R.; Truter, M. R. *J. Chem. Soc., Perkin Trans. II* **1972**, 1818–1823.

30. Hughes, D. L. *J. Chem. Soc., Dalton Trans.* **1975**, 2374–2378.

31. (a) Fenton, D. E.; Mercer, M.; Poonia, N. S.; Truter, M. R. *J. Chem. Soc., Chem. Commun.* **1972**, 66–67. (b) Mercer, M.; Truter, M. R. *J. Chem. Soc., Dalton Trans.* **1973**, 2469–2473.

32. Owen, J. D.; Truter, M. R. *J. Chem. Soc., Dalton Trans.* **1979**, 1831–1835.

33. (a) Groh, S. E. *Isr. J. Chem.* **1976/77**, *15*, 277–307. (b) Drew, M. G. B.; Rodgers, A.; McCann, M.; Nelson, S. M. *J. Chem. Soc., Chem. Commun.* **1978**, 415–416. (c) Coughlin, P. K.; Dewan, J. C.; Lippard, S. J.; Watanabe, E. I.; Lehn, J.-M. *J. Am. Chem. Soc.* **1979**, *101*, 265–266. (d) Agnus, Y.; Louis, R.; Weiss, R. *J. Am. Chem. Soc.* **1979**, *101*, 3381–3384.

34. Parsons, D. G.; Truter, M. R.; Wingfield, J. N. *Inorg. Chim. Acta* **1975**, *14*, 45–48.

35. Lehn, J.-M.; Pine, S. H.; Watanabe, E. I.; Willard, A. K. *J. Am. Chem. Soc.* **1977**, *99*, 6766–6768.

36. (a) Melinger, M.; Fischer, J.; Weiss, R. *Angew. Chem., Int. Ed. Engl.* **1973**, *12*, 771. (b) Wiest, R.; Weiss, R. *J. Chem. Soc., Chem. Commun.* **1973**, 678–679. (c) Fischer, J.; Mellinger, M.; Weiss, R. *Inorg. Chim. Acta* **1977**, *21*, 259–263.

37. Lehn, J.-M. *Pure Appl. Chem.* **1980**, *52*, 2441–2459.

38. Lehn, J.-M. *Angew. Chem., Int. Ed. Engl.* **1990**, *29*, 1304–1319.

39. Lehn, J.-M.; Rigault, A.; Siegel, J.; Harrowfield, J.; Chevrier, B.; Moras, D. *Proc. Natl. Acad. Sci. USA*, **1987**, 2565–2569.

40. (a) Constable, E. C.; Ward, M. D. *J. Am. Chem. Soc.* **1990**, *112*, 1256–1258. (b) Constable, E. C. *Tetrahedron* **1992**, *48*, 10013–10059.

41. (a) Lehn, J.-M.; Rigault, A. *Angew. Chem., Int. Ed. Engl.* **1988**, *27*, 1095–1097. (b) Garrett, T. M.; Koert, U.; Lehn, J.-M.; Rigault, A.; Meyer, D.; Fischer, J. *J. Chem. Soc., Chem. Commun.* **1990**, 557–558.

42. Krämer, R.; Lehn, J.-M.; DeCian, A.; Fischer, J. *Angew. Chem., Int. Ed. Engl.* **1993**, *32*, 703–706.

43. Leize, A.; Van Dorsselaer, A.; Krämer, R.; Lehn, J.-M. *J. Chem. Soc., Chem. Commun.* **1993**, 990–993.

44. Baxter, P. N. W.; Lehn, J.-M.; Fischer, J.; Youinou, M.-T. *Angew. Chem., Int. Ed. Engl.* **1994**, *33*, 2284–2287.

45. Hanan, G. S.; Arana, C. R.; Lehn, J.-M.; Fenske, D. *Angew. Chem., Int. Ed. Engl.* **1995**, *34*, 1122–1124.

46. (a) Dewar, M. J. S.; Talati, A. M. *J. Am. Chem. Soc.* **1963**, *85*, 1874. (b) Dewar, M. J. S.; Talati, A. M. *J. Am. Chem. Soc.* **1964**, *86*, 1592–1595.

47. (a) Fox, M. A.; Chandler, D. A.; Wang, P. *Macromolecules* **1991**, *24*, 4626–4636. (b) Fox, M. A.; Chandler, D. A.; Kyba, E. P. *J. Coord. Chem.* **1992**, *25*, 1–19.

48. Fox, M. A.; Chandler, D. A. *Adv. Mater.* **1991**, *3*, 381–384.

49. Flurry, R. L., Jr. *Quantum Chemistry: An Introduction*; Prentice-Hall: Englewood Cliffs, New Jersey, 1983.

50. Michl, J; Bonacic-Koutecky, V. *Electronic Aspects of Organic Photochemistry*; Wiley: New York, 1990.

51. Salem, L. *Electrons in Chemical Reactions: First Principles*; Wiley: New York, 1982.

52. Veciana, J.; Vidal, J.; Jullian, N. *Mol. Cryst. Liq. Cryst.* **1989**, *176*, 443–450.

53. Kollmar, C.; Kahn, O. *Acc. Chem. Res.* **1993**, *26*, 259–265.

54. Kollmar, H.; Staemmler, V. *Theor. Chim. Acta* **1978**, *48*, 223–239.

55. (a) Dowd, P.; Chang, W.; Paik, Y. H. *J. Am. Chem. Soc.* **1986**, *108*, 7416–7417. (b) Roth, W. R.; Kowalczik, U.; Maier, G.; Reisenauer, H. P.; Sustmann, R.;

Müller, W. *Angew. Chem., Int. Ed. Engl.* **1987**, *26*, 1285–1287. (c) Du, P.; Borden, W. T. *J. Am. Chem. Soc.* **1987**, *109*, 930–931.

56. (a) Dowd, P. *J. Am. Chem. Soc.* **1966**, *88*, 2587–2589. (b) Baseman, R. J.; Pratt, D. W.; Chow, M.; Dowd, P. *J. Am. Chem. Soc.* **1976**, *98*, 5726–5727.

57. Dixon, D. A.; Dunning, T. H., Jr.; Eades, R. A.; Kleier, D. A. *J. Am. Chem. Soc.* **1981**, *103*, 2878–2880.

58. Hudson, B. S.; Kohler, B. E.; Schulten, K. In *Excited States*; Lim, E. C., Ed.; Academic Press: New York, 1982, Vol. 6, pp 54–55.

59. (a) Migirdicyan, E.; Baudet, J. *J. Am. Chem. Soc.* **1975**, *97*, 7400–7404. (b) Platz, M. S. In *Diradicals*; Borden, W. T., Ed.; Wiley: New York, 1982, pp 195–258. (c) Rule, M.; Matlin, A. R.; Seeger, D. E.; Hilinski, E. F.; Dougherty, D. A.; Berson, J. A. *Tetrahedron* **1982**, *38*, 787–798. (d) Wright, B. B.; Platz, M. S. *J. Am. Chem. Soc.* **1983**, *105*, 628–630. (e) Goodman, J.; Berson, J. A. *J. Am. Chem. Soc.* **1985**, *107*, 5409–5424. (f) Berson, J. A. In *The Chemistry of Quinoid Compounds*; Patai, S., Rappaport, Z., Eds.; Wiley: New York, 1988; Vol. 2, Chapter 10.

60. (a) Kato, S.; Morokuma, K.; Feller, D.; Davidson, E. R.; Borden, W. T. *J. Am. Chem. Soc.* **1983**, *105*, 1791–1795. (b) Fort, R. C., Jr.; Getty, S. J.; Hrovat, D. A.; Lahti, P. M.; Borden, W. T. *J. Am. Chem. Soc.* **1992**, *114*, 7549–7552.

61. (a) Flynn, C. R.; Michl, J. *J. Am. Chem. Soc.* **1974**, *96*, 3280–3288. (b) Trahanovsky, W. S.; Chou, C.-H.; Fischer, D. R.; Gerstein, B. C. *J. Am. Chem. Soc.* **1988**, *110*, 6579–6581.

62. Williams, D. J.; Pearson, J. M.; Levy, M. *J. Am. Chem. Soc.* **1970**, *92*, 1436–1438.

63. Polycarbenes with spins up to $S = 9$ have been prepared. See: (a) Fujita, I.; Teki, Y.; Takui, T.; Kinoshita, T.; Itoh, K.; Miko, F.; Sawaki, Y.; Iwamura, H. Izuoka, A.; Sugawara, T. *J. Am. Chem. Soc.* **1990**, *112*, 4074–4075. (b) Nakamura, N.; Inoue, K.; Iwamura, H.; Fujioka, T.; Sawaki, Y. *J. Am. Chem. Soc.* **1992**, *114*, 1484–1485. (c) Iwamura, H.; Koga, N. *Acc. Chem. Res.* **1993**, *26*, 346–351. (d) Nakamura, N.; Inoue, K.; Iwamura, H. *Angew. Chem., Int. Ed. Engl.* **1993**, *32*, 872–874.

64. Schlenk, W.; Brauns, M. *Chem. Ber.* **1915**, *48*, 661–669; 716–728.

65. (a) Kothe, G.; Denkel, K.-H.; Sümmermann, W. *Angew. Chem., Int. Ed. Engl.* **1970**, *9*, 906–907. (b) Lockhurst, G. R.; Pedulli, G. F.; Tiecco, M. *J. Chem. Soc. B* **1971**, 329–334.

66. (a) Lankamp, H.; Nauta, W. Th.; MacLean, C. *Tetrahedron Lett.* **1968**, 249–254. (b) For a review on the "hexaphenylethane riddle", see: McBride, J. M. *Tetrahedron* **1974**, *30*, 2009–2022.

67. (a) Neumann, W. P.; Uzick, W.; Zarkadis, A. K. *J. Am. Chem. Soc.* **1986**, *108*, 3762–3770. (b) Dünnebacke, D.; Neumann, W. P.; Penenory, A.; Stewen, U. *Chem. Ber.* **1989**, *122*, 533–535. (c) Neumann, W. P.; Penenory, A.; Stewen, U.; Lehnig, M. *J. Am. Chem. Soc.* **1989**, *111*, 5845–5851.

68. (a) Veciana, J.; Rovira, C.; Crespo, M. I.; Armet, O.; Domingo, V. M.; Palacio, F. *J. Am. Chem. Soc.* **1991**, *113*, 2552–2561. (b) Rajca, A.; Utamapanya, S.; Xu, J. *J. Am. Chem. Soc.* **1991**, *113*, 9235–9241. (c) Rajca, A.; Utamapanya, S. *J. Org. Chem.* **1992**, *57*, 1760–1767.

69. Rajca, A.; Utamapanya, S.; Smithhisler, D. *J. Org. Chem.* **1993**, *58*, 5650–5652.

70. (a) Jarrett, H. S.; Sloan, G. J.; Vaughn, W. R. *J. Chem. Phys.* **1956**, *25*, 697–701. (b) Sloan, G. J.; Vaughn, W. R. *J. Org. Chem.* **1957**, *22*, 750–761. (c) Montgomery, L. K.; Huffman, J. C.; Jurczak, E. A.; Grendze, M. P. *J. Am. Chem. Soc.* **1986**, *108*, 6004–6011.

71. For an excellent discussion of the "diradical paradox" associated with **19**, see ref 59b.

72. Schmidt, R.; Brauer, H.-D. *Angew. Chem., Int. Ed. Engl.* **1971**, *10*, 506–507.

73. Silverman, S. K.; Dougherty, D. A. *J. Phys. Chem.* **1993**, *97*, 13273–13283.

74. (a) Pranata, J.; Dougherty, D. A. *J. Phys. Org. Chem.* **1989**, *2*, 161–176. (b) Goldberg, A. H.; Dougherty, D. A. *J. Am. Chem. Soc.* **1983**, *105*, 284–290.

75. Hoffmann, R. *Acc. Chem. Res.* **1971**, *4*, 1–9.

76. Dougherty, D. A. *Acc. Chem. Res.* **1991**, *24*, 88–94.

77. (a) Sinn, E. *Coord. Chem. Rev.* **1970**, *5*, 313–347. (b) Hay, P. J.; Thibeault, J. C.; Hoffmann, R. *J. Am. Chem. Soc.* **1975**, *97*, 4884–4899.

78. Kahn, O.; Tola, P.; Galy, J.; Coudanne, H. *J. Am. Chem. Soc.* **1978**, *100*, 3931–3933.

79. Kahn, O.; Galy, J.; Journaux, Y.; Jaud, J.; Morgenstern-Badarau, I. *J. Am. Chem. Soc.* **1982**, *104*, 2165–2176.

80. (a) Kahn, O. *Comments Inorg. Chem.* **1984**, *3*, 105–132. (b) Kahn, O. *Angew. Chem., Int. Ed. Engl.* **1985**, *24*, 834–850.

81. Caneschi, A.; Gatteschi, D.; Sessoli, R. *Acc. Chem. Res.* **1989**, *22*, 392–398.

82. (a) Eaton, S. S.; Eaton, G. R. *Coord. Chem. Rev.* **1978**, *26*, 207–262. (b) Eaton, S. S.; Eaton, G. R. *Coord. Chem. Rev.* **1988**, *83*, 29–72.

83. Porter, L. C.; Dickman, M. H.; Doedens, R. J. *Inorg. Chem.* **1988**, *27*, 1548–1552.

84. Gatteschi, D.; Laugier, J.; Rey, P.; Zanchini, C. *Inorg. Chem.* **1987**, *26*, 938–943.

85. Dickman, M. H.; Porter, L. C.; Doedens, R. J. *Inorg. Chem.* **1986**, *25*, 2595–2599.

86. Benelli, C.; Gatteschi, D.; Zanchini, C.; Doedens, R. J.; Dickman, M. H.; Porter, L. C. *Inorg. Chem.* **1986**, *25*, 3453–3457.

87. Sabacky, M. J.; Johnson, C. S., Jr.; Smith, R. G.; Gutowsky, H. S.; Martin, J. C. *J. Am. Chem. Soc.* **1967**, *89*, 2054–2058.

88. (a) Vögtle, F.; Weber, E. *Angew. Chem., Int. Ed. Engl.* **1979**, *18*, 753–776. (b) Weber, E.; Vögtle, F. *Top. Current Chem.* **1981**, *98*, 1–41. (c) Hilgenfeld, R.; Saenger, W. In *Host Guest Complex Chemistry—Macrocycles—Synthesis, Structures, Applications*; Vögtle, F.; Weber, E., Eds.; Springer-Verlag: Berlin, 1985, pp 43–124.

89. Kahr, B.; Jackson, J. E.; Ward, D. L.; Jang, S.-H.; Blount, J. F. *Acta Crystallogr., Sect. B: Struct. Sci.* **1992**, *B48*, 324–329.

90. Mislow, K. *Acc. Chem. Res.* **1976**, *9*, 26–33.

91. By analogy to the crown ethers, we propose the name "tripod ether" for the propeller-like tris(*o*-alkoxyaryl)-Z compounds, where Z may be any sp^2 or sp^3 hybridized element.

92. Artz, S. P.; Cram, D. J. *J. Am. Chem. Soc.* **1984**, *106*, 2160–2171.

93. Force-field calculations suggest a racemization barrier of ca. 10 kcal/mol (Jackson, J. E., unpublished results).

94. Frye, C. L.; Vincent, G. A.; Hauschildt, G. L. *J. Am. Chem. Soc.* **1966**, *88*, 2727–2730.

95. Muller, E.; Burgi, H.-B. *Acta Crystallogr., Sect. C: Struct. Commun.* **1989**, *C45*, 1400–1403.

96. Barriers of ca. 12–13 kcal/mol have been determined for compounds closely related to **28**. See: Hellwinkel, D.; Melan, M.; Degel, C. R. *Tetrahedron* **1973**, *29*, 1895–1907.

97. Gauthier, S.; Fréchet, J. M. J. *Synthesis* **1987**, 383–385.

98. Nelson, R. F.; Adams, R, N. *J. Am. Chem. Soc.* **1968**, *90*, 3925–3930.

99. Loveland, J. W.; Dimeler, G. R. *Anal. Chem.* **1961**, *33*, 1196–1201.

100. Seo, E. T.; Nelson, R. F.; Fritsch, J. M.; Marcoux, L. S.; Leedy, D. W.; Adams, R. N. *J. Am. Chem. Soc.* **1966**, *88*, 3498–3503.

101. Dollish, F. R.; Hall, W. K. *J. Phys. Chem.* **1965**, *59*, 2127–2129.

102. Fleischmann, M.; Pletcher, D. *Tetrahedron Lett.* **1968**, 6255–6258.

103. Stickley, K. R.; Blackstock, S. C. *J. Am. Chem. Soc.* **1995**, *116*, 11576–11577.

104. Vogtle, F.; Weber, E. In *The Chemistry of the Ether Linkage*; Patai, S., Ed.; Supplement E; Wiley: London, 1981, part 1, p 59.

105. Gutmann, V. *Chimia* **1977**, *31*, 1–7.

106. Cahen, Y. M.; Handy, P. R.; Roach, E. T.; Popov, A. I. *J. Phys. Chem.* **1975**, *79*, 80–85.

107. Greenberg, M. S.; Bodner, R. L.; Popov, A. I. *J. Phys. Chem.* **1973**, *77*, 2449–2454.

108. Lund, H.; *J. Am. Chem. Soc.* **1927**, *49*, 1346–1360.

109. Brown, H. C.; Dodson, V. H. *J. Am. Chem. Soc.* **1957**, *79*, 2302–2306.

110. (a) Heimann, U.; Herzhoff, M.; Vögtle, F. *Chem. Ber.* **1979**, *112*, 1392–1399. (b) Jang, S.-H.; Lee, H.-I.; McCracken, J.; Jackson, J. E. *J. Am. Chem. Soc.* **1993**, *115*, 12623–12624.

111. Lehn, J.-M. *Angew. Chem., Int. Ed. Engl.* **1988**, *27*, 89–112.

112. Dostal, S.; Stoudt, S. J.; Fanwick, P.; Sereatan, W. F.; Kahr, B.; Jackson, J. E. *Organometallics* **1993**, *12*, 2284–2291.

113. Hayes, K. S.; Nagumo, M.; Blount, J. F.; Mislow, K. *J. Am. Chem. Soc.* **1980**, *102*, 2273–2276.

114. Martin, J. C.; Smith, R. G. J. *Am. Chem. Soc.* **1964**, *86*, 2252-2256.

115. Blount, J. F.; Finocciaro, P.; Gust, D.; Mislow, K. *J. Am. Chem. Soc.* **1973**, *95*, 7019-7029.

116. Olmstead, M. M.; Power, P. P. J. *Am. Chem. Soc.* **1986**, *108*, 4235-4236.

117. Bartlett, R. A.; Power, P. P. *Organometallics* **1985**, *5*, 1916-1917.

118. Kahr, B.; Van Engen, D.; Gopalan, P.*Chem. Mat.* **1993**, *5*, 729-732

119. Brown, G. M.; Freeman, G. R.; Walter, R. I. *J. Am. Chem. Soc.* **1977**, *99*, 6910-6915.

120. AM1 method: Dewar, M. J. S.; Zoebisch, E. G.; Healy, E. F.; Stewart, J. J. P. *J. Am. Chem. Soc.* **1985**, *107*, 3902-3909.

121. Jang, S.-H.; Gopalan, P.; Jackson, J. E.; Kahr, B. *Angew. Chem., Int. Ed. Engl.*, **1994**, *33*, 775–777.

122. Jang, S.-H.; Bertsch, R. A.; Jackson, J. E.; Kahr, B. *Mol. Cryst. Liq. Cryst.* **1992**, *211*, 289–303.

123. (a) Vögtle, F.; Müller, W. M.; Wehner, W.; Buhleier, E. *Angew. Chem., Int. Ed. Engl.* **1977**, *16*, 548–549; (b) Vögtle, F.; Müller, W. M.; Buhleier, E.; Wehner, W. *Chem. Ber.* **1979**, *112*, 899–907; (c) Tümmler, B.; Maass, G.; Vögtle, F.; Sieger, H.; Heimann, U.; Weber, E. *J. Am. Chem. Soc.* **1979**, *101*, 2588–2598. For reviews, see: (d) Vögtle, F.; Weber, E. *Angew. Chem., Int. Ed. Engl.* **1979**, *18*, 753–776; (e) Vogtle, F. *Chimia* **1979**, *33*, 239–251.

124. Green, D. P.; Reich, H. J. *J. Am. Chem. Soc.* **1989**, *111*, 8729–8731.

125. In acetone, which is a better solvating medium than $CDCl_3$, the ion pair formation constant for LiI is reported to be 145. See: Savedoff, L. G. *J. Am. Chem. Soc.* **1966**, *88*, 664–667.

126. Brownstein, S. K.; Plouffe, P.-Y.; Bensimon, C.; Tse, J. *Inorg. Chem.* **1994**, *33*, 354–358.

127. Gilkerson, W. R.; Jackson, M. D. *J. Am. Chem. Soc.* **1982**, *104*, 1218–1223.

128. Bauer, W. *Magn. Reson. Chem.* **1991**, *29*, 494–499.

129. (a) Bauer, W.; Schleyer, P. v. R. *Magn. Reson. Chem.* **1988**, *26*, 827–833. (b) Hoffmann, D.; Bauer, W.; Schleyer, P. v. R. *J. Chem. Soc., Chem. Commun.* **1990**, 208–211. (c) Bauer, W.; Lochmann, L. *J. Am. Chem. Soc.* **1992**, *114*, 7482–7489. (d) Hilmersson, G.; Davisson, Ö. *J. Organomet. Chem.* **1995**, *489*, 175–179. (e) Hilmersson, G.; Davisson, Ö. *Organometallics* **1995**, *14*, 912–918.

130. Erlich, R. H.; Popov, A. I. *J. Am. Chem. Soc.* **1971**, *93*, 5620–5623.

131. Kintzinger, J. P.; Lehn, J.-M. *J. Am. Chem. Soc.* **1974**, *96*, 3313–3314.

132. Dahlquist, F. W.; Longmuir, K. J.; Du Vernet, R. B. *J. Magn. Reson.* **1975**, *17*, 406–410.

133. In THF, which is a better solvating medium than $CDCl_3$, the ion pair formation constants for $LiBPh_4$ and $NaBPh_4$ at 25 °C are reported to be 1.26 x 10^4 and 1.23 x 10^4, respectively. See: Comyn, J.; Dainton, F. S.; Ivin, K. J. *Electrochim. Acta* **1968**, *13*, 1851–1860.

134. (a) Bothner-By, A. A.; Stephens, R. L.; Lee, J.-M.; Warren, C. D.; Jeanholz, R. W. *J. Am. Chem. Soc.* **1984**, *106*, 811–813. (b) Bax, A.; Davis, D. G. *J. Magn. Reson.* **1985**, *63*, 207–213.

135. Moras, D.; Weiss, R. *Acta Crystallogr., Sect. B: Struct. Crystallogr. Cryst. Chem.* **1973**, *B29*, 396–399.

136. Tehan, F. J.; Barnett, B. L.; Dye, J. L. *J. Am. Chem. Soc.* **1974**, *96*, 7203–7208.

137. (a) Adolphson, D. G.; Corbett, J. D.; Merryman, D. J. *J. Am. Chem. Soc.* **1976**, *98*, 7234–7239; (b) Teller, R. G.; Finke, R. G.; Collman, J. P.; Chin, H. B.; Bau, R. *J. Am. Chem. Soc.* **1977**, *99*, 1104–1111.

138. Moras, D.; Metz, B.; Weiss, R. *Acta Crystallogr., Sect. B: Struct. Crystallogr. Cryst. Chem.* **1973**, *B29*, 383–388.

139. Stoudt, S. J.; Gopalan, P.; Kahr, B.; Jackson, J. E. *Struct. Chem.* **1994**, *5*, 335–340.

140. The rotational barrier in anisole is a matter of recent debate. Estimates from both theory and experiment are converging on a value of 2–3 kcal mol^{-1} for the perpendicular transition state. See: (a) Spellmeyer, D. C.; Grootenhuis, P. D. J.; Miller, M. D.; Kuyper, L. F.; Kollman, P. A. *J. Phys. Chem.* **1990**, *94*, 4483–4491. (b) Vincent, M. A.; Hillier, I. A. *Chem. Phys.* **1990**, *140*, 35–40.

141. (a) Cox, B. G.; Knop, D.; Schneider, H. *J. Phys. Chem.* **1980**, *84*, 320–323; (b) Cox, B. G.; Van Truong, Ng.; Garcia-Rosas, J.; Schneider, H. *J. Phys. Chem.* **1984**, *88*, 996–1001; (c) Buschmann, H.-J. *Chem. Ber.* **1985**, *118*, 3408–3412.

142. For a more complete compendium of binding data, see: Izatt, R. M.; Pawlak, K.; Bradshaw, J. S.; Bruening, R. L. *Chem. Rev.* **1991**, *91*, 1721–2085.

143. The anisyl group is an intrinsically poor ligand, as determined by its weakness in hydrogen bonding. See: (a) Arnett, E. M.; Joris, L.; Mitchell, E.; Murty, T. S. S. R.; Schleyer, P. v. R. *J. Am. Chem. Soc.* **1970**, *92*, 2365–2377. (b) Mitsky, J.; Joris, L.; Taft, R. W. *J. Am. Chem. Soc.* **1972**, *94*, 3442–3445.

144. Triphenylamine itself forms exceedingly unstable adducts with Lewis acids. See: Kemmitt, R. D. W.; Nuttall, R. H.; Sharp, D. W. A. *J. Chem. Soc.* **1960**, 46–50.

145. For example, see: (a) Gomberg, M.; Nishida, D. *J. Am. Chem. Soc.* **1923**, *45*, 190–207. (b) Gomberg, M.; Buchler, C. C. *J. Am. Chem. Soc.* **1923**, *45*, 207–222. (c) Gomberg, M.; Forrester, G. C. *J. Am. Chem. Soc.* **1925**, *47*, 2373–2391. (d) Bent, H. E.; Dorfman, M.; Bruce, W. F. *J. Am. Chem. Soc.* **1932**, *54*, 3250–3258. (e) Bachmann, W. E.; Kloetzel, M. C. *J. Org. Chem.* **1935**, *2*, 356–375. (f) Marvel, C. S.; Whitson, J.; Johnston, H. W. *J. Am. Chem. Soc.* **1944**, *66*, 415–417. (g) Bowden, S. T. *J. Chem. Soc.* **1957**, 4235–4239. (h) Bowden, S. T.; Zalichi, D. T. *J. Chem. Soc.* **1957**, 4240–4243. (i) Zarkadis, A. K.; Neumann, W. P.; Marx, R.; Uzick, W. *Chem. Ber.* **1985**, *118*, 450–456.

146. Ishizu, K.; Mukai, K.; Shibayama, A.; Kondo, K. *Bull. Chem. Soc. Jpn.* **1977**, *50*, 2269–2271.

147. Compound **49** has been used as a hydride abstraction reagent. See: Huszthy, P.; Lempert, K.; Simig, G.; Tamás, J. H.-V.; Almásy, A. *J. Chem.Research (S)* **1985**, 228–229.

148. Tukada, H. *J. Chem. Soc., Chem. Commun.* **1994**, 2293–2294.

149. (a) Broser, W.; Kurreck, H.; Niemeier, W. *Tetrahedron* **1976**, *32*, 1183–1187. Also see: (b) Hinrichs, K.; Kurreck, H.; Niemeier, W. *Tetrahedron* **1974**, *30*, 315–320. (c) Kurreck, H.; Niemeier, W. *Tetrahedron Lett.* **1974**, 3523–3526. (d) Broser, W.; Kurreck, H.; Plato, M. *Tetrahedron* **1975**, *31*, 1769–1779.

150. Shriver, D. F.; Drezdzon, M. A. *The Manipulation of Air-Sensitive Compounds*, 2nd ed.; Wiley: New York, 1986.

151. Lund, H.; Bjerrum, J. *Ber.* **1931**, *64*, 210–213.

152. (a) Burfield, D. R.; Gan, G.-H.; Smithers, R. H. *J. Appl. Chem. Biotechnol.* **1978**, *28*, 23–30. (b) Burfield, D. R.; Smithers, R. H. *J. Org. Chem.* **1978**, *43*, 3966–3968.

153. Bhattacharyya, D. N.; Lee, C. L.; Szwarc, M. *J. Phys. Chem.* **1965**, *69*, 608–611.

154. DeWitte, W. J.; Liu, L.; Mei, E.; Dye, J. L.; Popov, A. I. *J. Solution Chem.* **1977**, *6*, 337–348.

155. Furniss, B. S.; Hannaford, A. J.; Smith, P. W. G.; Tatchell, A. R. *Vogel's Textbook of Practical Organic Chemistry*, 5th ed.; Wiley: New York, 1989, p 421.

156. Winkle, M. R.; Lansinger, J. M.; Ronald, R. C. *J. Chem. Soc., Chem. Commun.* **1980**, 87–88.

157. Perrin, D. D.; Armarego, W. L. F. *Purification of Laboratory Chemicals*, 3rd ed.; Pergamon: New York, 1988.

158. Soulié, C.; Bassoul, P.; Simon, J. *New J. Chem.* **1993**, *17*, 787–791.

159. Flad, G.; Demerseman, P.; Royer, R. *Bull. Soc. Chim. Fr.* **1976**, *11–12*, 1823–1824.

160. Sugii, Y.; Shindo, H.; *J. Pharm. Soc. Jpn.* **1934**, *54*, 829–844.

161. VanArendonk, A. M.; Cupery, M. E.; Adams, R. *J. Am. Chem. Soc.* **1933**, *55*, 4225–4230.

162. Lofgren, N. M.; Takman, B. *Acta Chem. Scand.* **1952**, *6*, 1016–1019.

163. Angelici, R. J.; Quick, M. H.; Kraus, G. A.; Plummer, D. T. *Inorg. Chem.* **1982**, *21*, 2178–2184.

164. MNDO method: (a) Dewar, M. J. S.; Thiel, W. *J. Am. Chem. Soc.* **1977**, *99*, 4899–4907. (b) Dewar, M. J. S.; Thiel, W. *J. Am. Chem. Soc.* **1977**, *99*, 4907–4917.

165. Dye, J. L.; Nicely, V. A. *J. Chem. Ed.* **1971**, *48*, 443–448.

166. (a) Weigert, F. J.; Roberts, J. D. *J. Am. Chem. Soc.* **1969**, *91*, 4940–4941. (b) Odom, J.; Hall, L. W.; Ellis, P. D. *Org. Magn. Reson.* **1974**, *6*, 360–361.

167. Walker, N.; Stuart, D. *Acta Crystallogr., Sect. A: Cryst. Phys. Diffr. Theor. Gen. Crystallogr.* **1983**, *A39*, 158–166.

168. Sheldrick, G. M., Institut für Anorganische Chemie der Universität Göttingen, FRG, 1986.

169. MolEN, An Interactive Structure Solution Procedure, Enraf-Nonius, Delft, The Netherlands (1990).